NASA CR-174773
R84-925830-33

National Aeronautics and Space Administration

HOT SECTION VIEWING SYSTEM

by

William W. Morey

UNITED TECHNOLOGIES RESEARCH CENTER

prepared for

NATIONAL AERONAUTICS AND SPACE ADMINISTRATION

NASA Lewis Research Center
Contract NAS 3 - 23156

FOREWORD

The Hot Section Viewing System Program was initiated in September of 1981 as a 24 month program for the development and testing of a prototype combustion viewing system. The program was extended 3 months to allow for digital image analysis of video data. Two more extensions totaling an additional 8 months were granted at no cost to NASA to allow for an engine test of the viewing system at Pratt & Whitney's Wilgoos test facility.

A large number of people at the Research Center contributed to the program. Major contributions were made by Ed McComb who designed the prototype actuator and probes, Arnold Wilson helped design and fabricate the optics interface board and also was responsible for the assembly and operation of the system, Tom Rosfjord assisted with the rig testing, and Jim Dunphy and Francois Mottier provided assistance with the digital image analysis. Randy Hershberger of Pratt & Whitney provided the needed assistance for the engine tests.

TABLE OF CONTENTS

TABLE OF CONTENTS (Cont'd)

SUMMARY

The Hot Section Viewing System Program was a program for the development and testing of a new type of instrument that would allow one to monitor and record images inside a fully operating gas turbine combustor. The program ran through planned phases of conceptual design, preliminary test program to resolve problem areas, design and fabrication, bench testing, high pressure rig testing, analysis, and an additional test on a jet engine at Pratt & Whitney.

Coherent fiber optics were used to transfer the image from inside the combustor to a nearby instrumentation pallet that contained video and film cameras. Besides taking an image out of the combustor, illumination was provided from either an arc lamp or pulsed laser source that was coupled to large diameter fiber optics and transported to the distal end of the viewing device in the combustor. The viewing device itself was a 12.7 mm diameter, water cooled probe that could be traversed in and out of the combustor and rotated 330° with an external actuator mounted to the combustor case. The actuator, cameras and illumination were remotely controlled. Water cooling was used to protect the probe and optics and a gas purge was used to keep the exposed viewing surfaces clean. Two probes were designed - one to cover narrow fields of view, the other to cover wide fields of view. In addition, two interchangeable lenses were designed for each probe. The probes were also interchangeable with the actuator unit.

During laboratory testing we experimented with probe cooling and gas purge designs, measured optical distortion, and demonstrated the use of pulsed laser illumination to allow one to record images in the presence of luminous flame. Stereoscopic viewing was also examined as a design approach, but not used for the final probe design.

The prototype viewing system was tested on a high pressure combustor at UTRC's jet burner test facility. Video and film camera pictures were taken inside and outside the combustor liner. Images were recorded of the combusting flame and of liner louvers and air mixing holes. Several images were processed with digital image analysis techniques for image enhancement, intensity profiles, and contour plots. The viewing system was also tested on the igniter port of a PW 2037 engine where views were recorded of fuel nozzles under full engine power.

While some more development may be required, especially in the pulsed laser illumination system, we feel that the viewing probe can be an aid in the future design of more durable combustors. The system can be used for observation of such things as liner damage during operation, location of combustor flames, fuel spray, coking deposits, flame transients, hot liner spots, first stage turbine vanes during operation, luminous flame temperature, and flame turbulence and instabilities. The viewing system could also open up new techniques for visualizing problems and effects inside combustors.

1.0 INTRODUCTION

1.1 Background - For several years now, optical viewing systems have been used in aircraft engine and engine test rigs. Viewing systems have been developed for monitoring blade tip clearances, knife edge seal positions and turbine vane clearances, and for inspection of blade and vane damage on engines when they are not in operation (refs. 1, 2). Also, optical pyrometers have been developed and used to measure turbine blade temperatures (ref. 3). The idea of using coherent fiber optic viewing devices, or fiberscopes, to view the inside of operating gas turbine combustors was suggested over four years ago in response to several existing problems on the durability of combustor liners and turbine vanes. With new advances in engine design requiring efficient combustion and operation at higher temperatures, combustor design and durability become even more critical. All aspects of combustor design are not fully understood; and the viewing probe can prove useful in helping to understand the operation and failure modes for future combustor designs.

A previous program at the Research Center, sponsored in part by the Naval Air Systems Command (NASC), demonstrated the feasibility of operating a fiberscope in the hostile environment of a gas turbine combustor (ref. 4). During this program, the location and shape of the luminious combustor flame was recorded. The flame motion or evolution was examined by taking motion pictures at 5000 frames per second. Flame fluctuation frequencies and optical spectra were also studied. Work recently completed under a follow-on program with NASC demonstrated the ability to measure a flame temperature and emissivity with a fiber optic probe viewing the luminous flame (ref. 5). It is thus possible to generate flame temperatures and density contours from image data. The measured temperatures in this case, however, are weighted to maximum temperatures over the ray pathlength of the view angle.

Besides flame dynamics, another important use of a viewing probe is to inspect the inside or outside surface of the combustor liner for overheating, crack damage, and formation of hard carbon deposits. The probe could tell when and under what conditions these problems occur and follow the course of their development. Examination of other components in the combustor such as fuel nozzles, flameholders, and spray patterns, may also be achieved with proper probe placement and articulation. The fiberscope as a combustor viewing instrument, then, can be used as a research tool to study and understand the operation of gas turbine combustors.

Another use of a combustor viewing instrument would be to monitor, over a long term, combustor image patterns and spectra as a signature. The relation and sensitivity of combustor or engine malfunctions to changes in flame signature would have to be determined. The combustor monitoring probe would have different design considerations as compared to the research probe.

1.2 Program Objectives and Approach - The objectives of this program were to develop, test, and analyze a prototype instrument for viewing the interior of a high pressure gas turbine combustor during full operation of the combustor. The instrument was to provide best quality images from different views in the combustor so that visual records of premature liner failure could be obtained. The program was divided into several phases including analysis, preliminary testing, prototype design, fabrication, bench testing, combustor rig testing, and data analysis. A final test was also made on a commercial jet engine.

The most difficult problem with the development of a combustor viewing system is the design of a probe with certain size constraints that will withstand the hostile environment in a gas turbine combustor. The probe must withstand high temperatures and pressures, a soot ladened and highly oxidizing gas environment, and in addition be subjected to intense mechanical vibrations and high speed gas flows associated with a gas turbine combustor. The accumulation of soot deposits on the viewing optics must also be prevented. For this program a water cooled probe was designed that could be inserted directly into the combustion zone. The probe could be articulated with remote controls so that the view inside the combustor is scanned.

The initial analysis phase of the program explored and evaluated a large number of different design and imaging concepts that may have application to combustor viewing. In the next phase of the program preliminary testing and development took place on several concepts to resolve problem areas such as material choice, cooling design, and type of illumination. Computer techniques for image enhancement and analysis of combustor images were also examined. A prototype viewing system was then designed and fabricated based on the experience gained from the previous analysis and preliminary test phases. After bench testing and correcting minor problems, the prototype system was tested in a high pressure combustor rig at the Research Center's jet burner test stand facility. Film and video data were taken during the combustor tests. The video data was analyzed using digital analysis techniques.

The material for the following sections of this report are presented in a topical format. In the next section, Section 2.0, we will discuss the optical design including the viewing optics, imaging fibers, camera interface optics, and illumination optics. In the following section, Section 3.0, we will discuss the mechanical design of the probe and actuator unit. This discussion will include: thermal loading, temperature and stress analysis, probe and actuator design features, and the results of the tests that relate to mechanical design. Section 4.0 discusses the problems and test results of viewing inside combustors. Optical distortion, illumination for viewing through flames, digital image analysis, and wide latitude photography are some of the topics discussed. In Section 5.0, we will describe the high pressure combustor test facility and the

ten test runs made on the high pressure rig at the Research Center. Section 6.0 describes the engine tests performed at the Wilgoos Laboratory of Pratt and Whitney on an experimental PW2037 engine. A discussion of the results of the program and the conclusions are given in Sections 7.0 and 8.0.

2.0 OPTICAL DESIGN

2.1 Objectives and Approach - The principal objectives of the optical design are to (1) transmit clear images from an operating combustor to the outside world, (2) couple the images to video and film camera instruments, (3) provide illumination light at the distal end of the probe, and (4) encompass a range of viewing fields with interchangeable optics. We were especially concerned with being able to view combustor liner surfaces. The best resolution was to be 0.25 mm. A fast lens speed was also desired in order to transmit sufficient light under marginal conditions. The illumination was to provide light for viewing when the combustor was off and also to assist in viewing liner surfaces when the combustor was in operation. A scan of the view was also provided by mechanical actuation which will be described in Section 3.0. We also wanted the probe to have as small a diameter as was reasonably possible so that we would not significantly alter the combustor or perturb the combustion process. These objectives, then, guided the optical design.

In order to keep the probe diameter small and still be able to transmit clear images we used a fused coherent bundle of fibers, called an image conduit, to carry the image from the distal end of the probe to the outside of the combustor pressure vessel. The image conduit consists of about 70,000 glass fibers and is 3.2 mm in diameter. The individual glass fibers were 10 μm in diameter. A 3 meter long coherent flexible bundle of fibers was butt coupled to the image conduit to transfer the image away from the combustor vessel to nearby recording cameras. Besides allowing a minimum size for the viewing probe, use of the image conduit allows operation to temperatures of 500°C; and if damage occurs to the probe in the hostile combustor environment, the more expensive 3 meter flexible bundle would be spared.

The optical system, then, consists of a viewing lens at the distal end of the probe that forms an image of the scene on the end of the image conduit. The image is transferred outside the combustor pressrue vessel with the conduit and then carried 3 meters further with a flexible fiber bundle to recordiong cameras. Another set of lenses enlarges the image from the proximal end of the fiber bundle for the film and video cameras. In addition, there are two large core fibers that deliver illumination light from an arc lamp or laser to the distal end of the probe.

The field-of-view (FOV), resolution, depth-of-field (DOF), and viewing distance of the probe are interrelated and depend on the diameter of the image conduit, the focal length of of the viewing lens, and pixel (individual imaging fiber) size. Figure 1 shows the resolvable separation between two objects in the object plane versus FOV for 3 different object distances from the lens. This result was based on a resolution limit of 20 μm in the image plane at the conduit, using an ideal lens. The best resolution of an imaging fiber system is

FIG. 1 RESOLUTION IN OBJECT PLANE

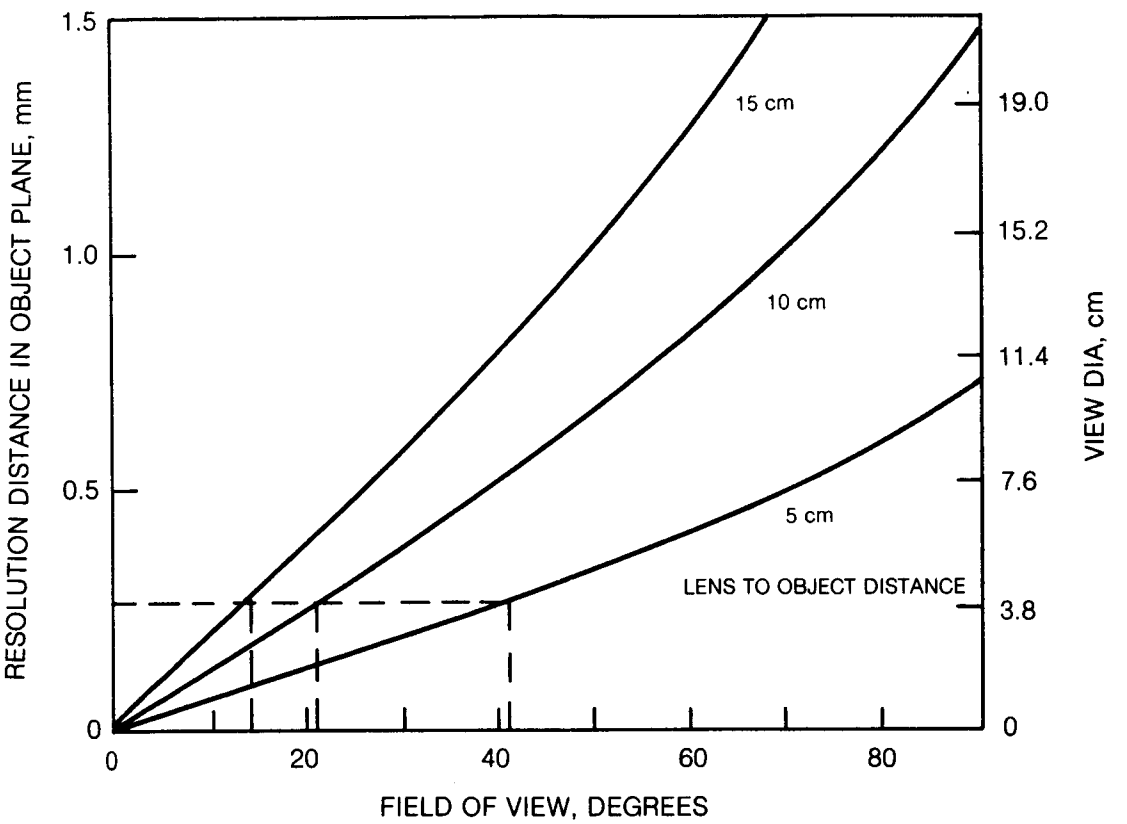

84–7–78–1

about twice the diameter of the individual fibers (ref. 6), and in our case is 20 μm. Since we have a fixed number of imaging fibers or pixels, a large FOV will have a much coarser resolution than a smaller FOV as shown in Fig. 1. To resolve 0.25 mm, for example, we need a FOV of about 21° for an object at 10 cm and 42° for an object at 5 cm.

Figure 2 shows the DOF or range over which an object remains in focus. At a 90° FOV the DOF can extend from a few centimeters to infinity. On the other hand, with a narrow FOV like 20°, the DOF shrinks to a couple centimenters or less. In addition to a change in the DOF, the wide FOV's require short focal length lenses and the narrow FOV's longer focal length lenses. Thus, in order to cover a range of viewing fields and keep the probe diameter small, we were required to build two probes.

Figure 3 shows a schematic of the wide field probe, distal end cross section. The probe is enlarged four times in the schematic. The view is turned at 45° to the probe axis so that a 90° FOV could cover the entire view inside the combustor with probe rotation. In the wide field probe the image conduit was bent at 45°, cut, ground and polished in a special fixture. The viewing lenses were mounted in a threaded lens holder as shown in the figure. Due to the dimensional limitations of the lens focal length, the smallest FOV that could be used with this design is about 40°. The largest FOV depends on the lens design and aperture, and would probably be limited to about 120° with the desired separation between the aperture and lens for purge gas flow.

A narrow field probe was constructed to cover the FOVs under 40°. This probe schematic is shown in Fig. 4. In this case we used a mirror to turn the view. The turning mirror arrangement requires a large aperture which in our case limited the maximum FOV to about 40°. Any smaller FOV could be used, of course. A direction of view 60° to the probe axis was arbitrarily chosen for the narrow angle probe. Probe rotation allows us to scan the view 360°.

Two viewing lenses were designed and made for each probe. A 90° and a 60° FOV lens were designed for the wide field probe, and a 30° and 15° FOV lens were designed for the narrow field probe. The four lens designs and viewing tests made with the lenses will be discussed in the next section.

2.2 Viewing Lenses

2.2.1 Introduction - The basic objective of the viewing lens design was to design a two element lens that was telecentric, had a speed of F/2 to F/5.6, and whose modulation transfer function was as good or better than the imaging fiber systems. In a telecentric lens the ray bundles converge normally onto the face of the fiber bundles. The fiber imaging systems have an equivalent F number of about 1 and could handle faster optics. Providing good quality lens at the viewing end and at the camera interfaces with speeds faster than about F/4 becomes

FIG. 2 DEPTH OF FIELD TO PRODUCE A 10 μm BLUR

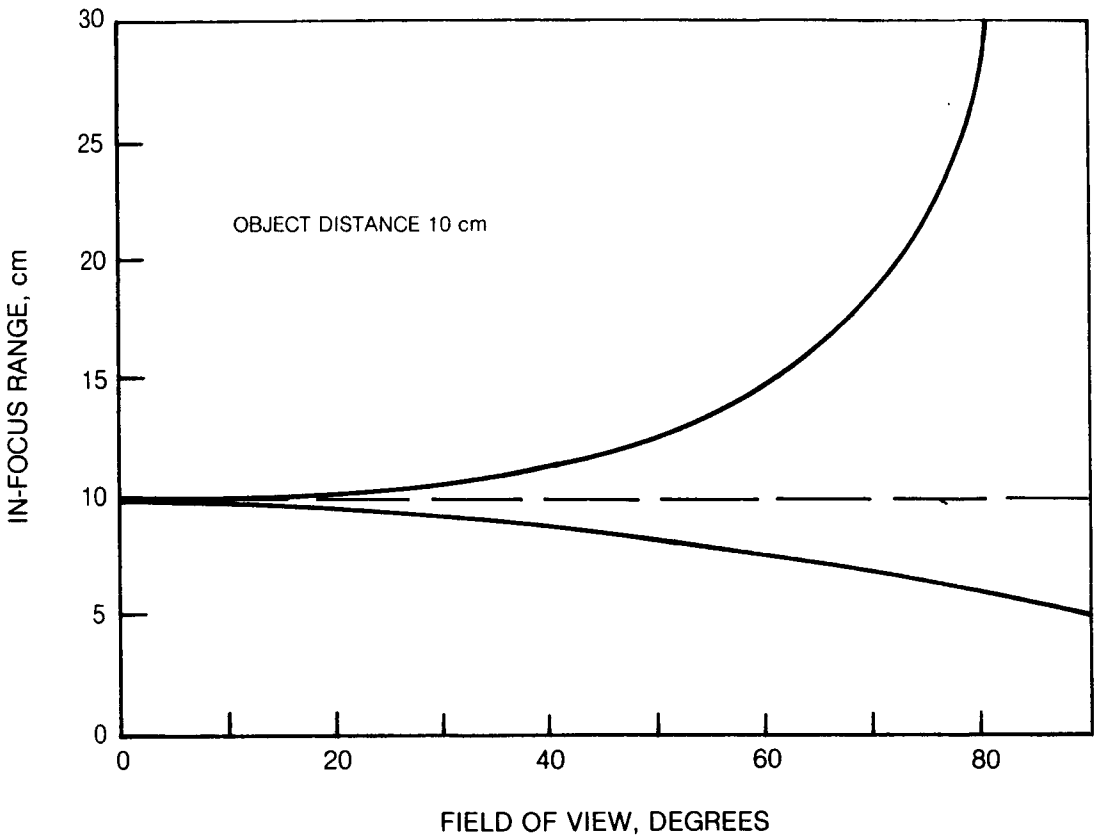

84–7–78–2

FIG. 3 WIDE FIELD PROBE

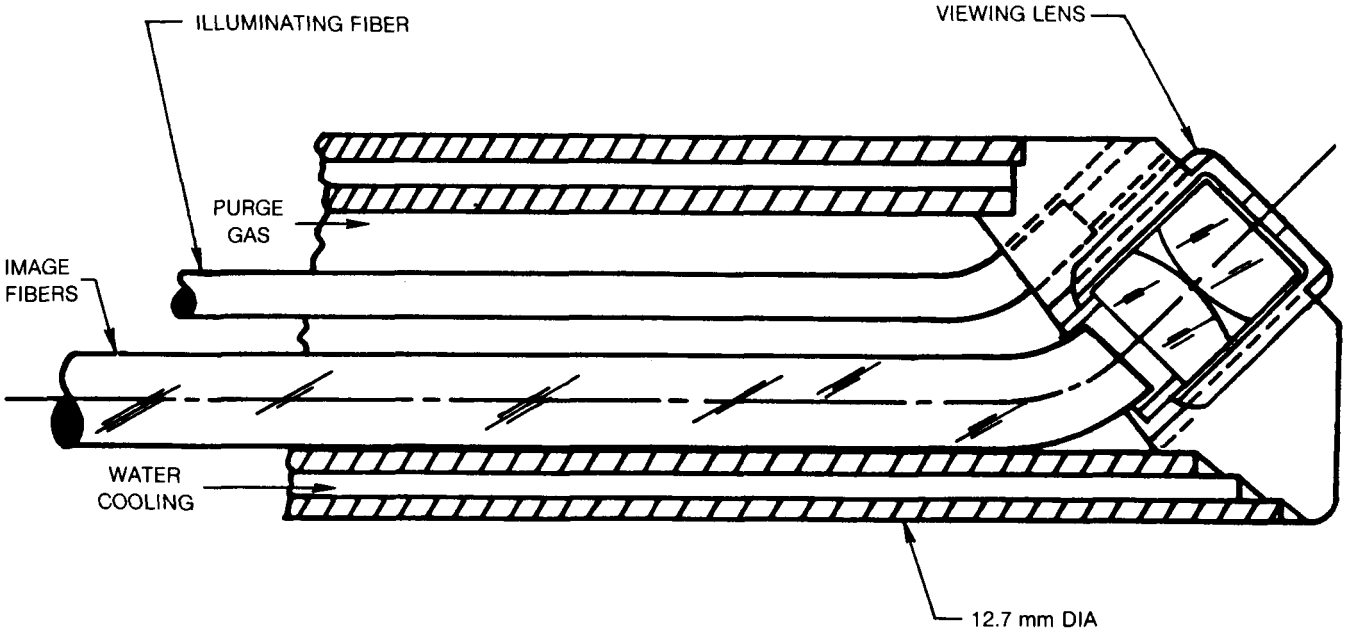

84–7–78–3

FIG. 4 NARROW FIELD PROBE

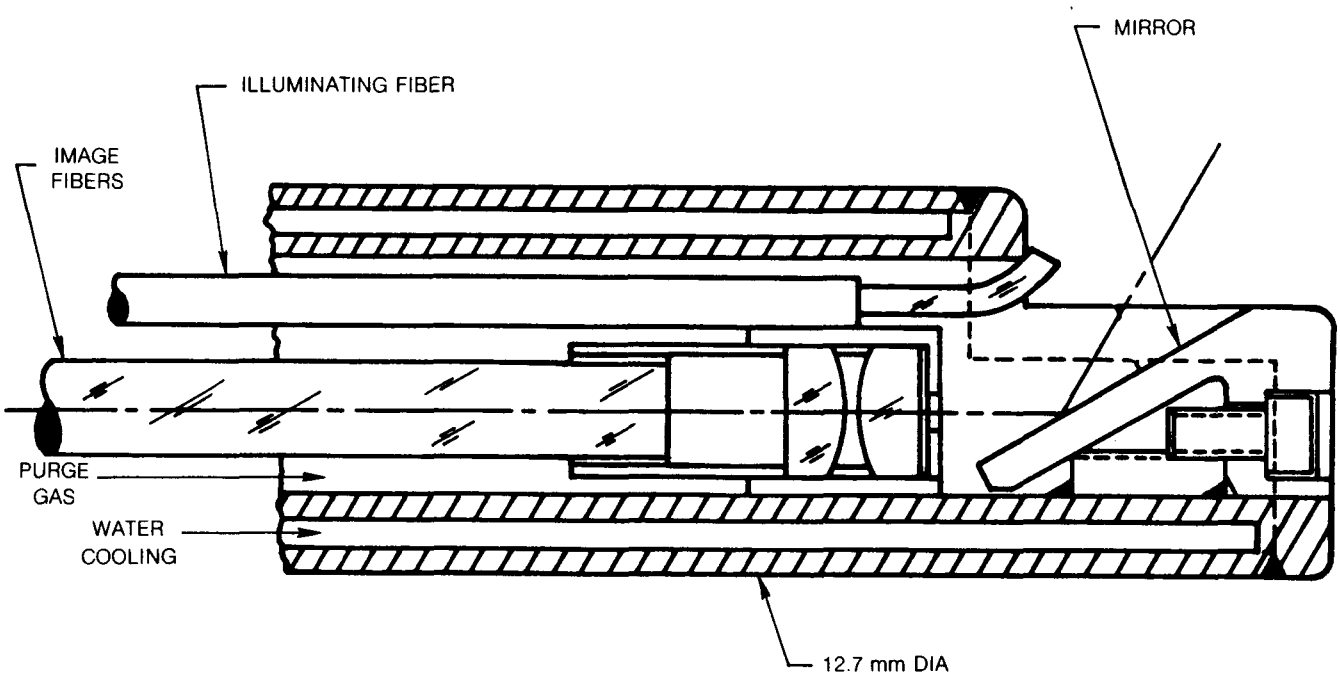

84-7-78-4

difficult. The fast lens system is desirable for use when the light levels are low or when high speed framing cameras are being used. It takes a 1/1000 sec or less to catch the flame motion.

An OSLO II ray tracing program was used to minimize focal spot diameter and compute the modulation transfer function (MTF). With the MTF we could measure the lens design performance for sagital and transverse focal planes, for polychromatic and monochromatic light, for different F numbers, and at different field angles.

The lens designs were made for sapphire lenses. Sapphire has the advantage of very high temperature operation and has a high index of refraction which is useful for the wide angle design. A thermal analysis (discussed in Section 3.0), however, gave lens temperatures less than 50°C. As a consequence, standard glass lenses could be used in place of the sapphire lenses which were very expensive ($555 to $875 ea). For the wide angle, 90° FOV lens, we used sapphire, but standard glass lenses that had nearly equivalent focal lengths were used for the smaller FOVs.

2.2.2 90° FOV Lens - A ray trace with radius and thickness data is shown in Fig. 5 for the 90° FOV lens. The dimensions are scaled upwards 21.4 times. Actual lens diameters are 4.4 mm. Three ray directions plotted in Fig. 5 are at full field angles, on axis, and at an intermediate field angle. The object plane was 100 mm away to the left hand side. An effective focal length of the lens was 2.17 mm. The data in Fig. 5 and in the other ray trace figures are in mm.

The lens aperture shown in Fig. 5 where the ray bundles pass through the first lens surface is .84 mm diameter. This aperture gives an effective F/no. of 2.6. The aperture was designed on the lens surface. To allow for purge gas flow out the aperture the lens was actually recessed about .25 mm from the aperture and increased to a 1.0 mm diameter.

The MTF for the 90° FOV lens at full field angle and F/5.6 (i.e., smaller aperture) is shown in Fig. 6. For comparison, the MTF for an image conduit with 10 μm fiber elements is shown with the broken line. This result was taken from Kapany (ref. 6). The lens MTFs are shown for transverse and sagittal image planes and for monochromatic and polychromatic light. We see that for monochromatic light the lens has only a small amount astigmatism, but there is greater stigmatism with white light along with chromatic aberration. The lens responds reasonably well but not as well as the image conduit at the full field angles. On axis, of course, the lens responds as well as the conduit.

A comparison of the lens performance for different aperture diameters or equivalent F/numbers is shown in Fig. 7. These results are for full field angle. Reducing the aperture improves the spatial frequency response for the particular components but the stigmatism increases.

FIG. 5 90 DEG LENS

21.4X MAGNIFICATION

EFL 2.17 mm

SURF	RADIUS	THICKNESS 100.0000	GLASS	APERTURE	REMARKS OBJECT
1	0.000	0.000	AIR	2.200	STOP ENTR. PUPIL
2	0.000	3.000	1.7683	2.200	
3	– 3.333	0.100	AIR	2.200	DUMMY SURF
4	3.333	2.119	1.7683	2.200	
5	–55.782	0.981	AIR	2.200	
6	0.000	1.000	AIR	2.200	DUMMY SURF
7	0.000	0.000	AIR	2.200	DUMMY SURF

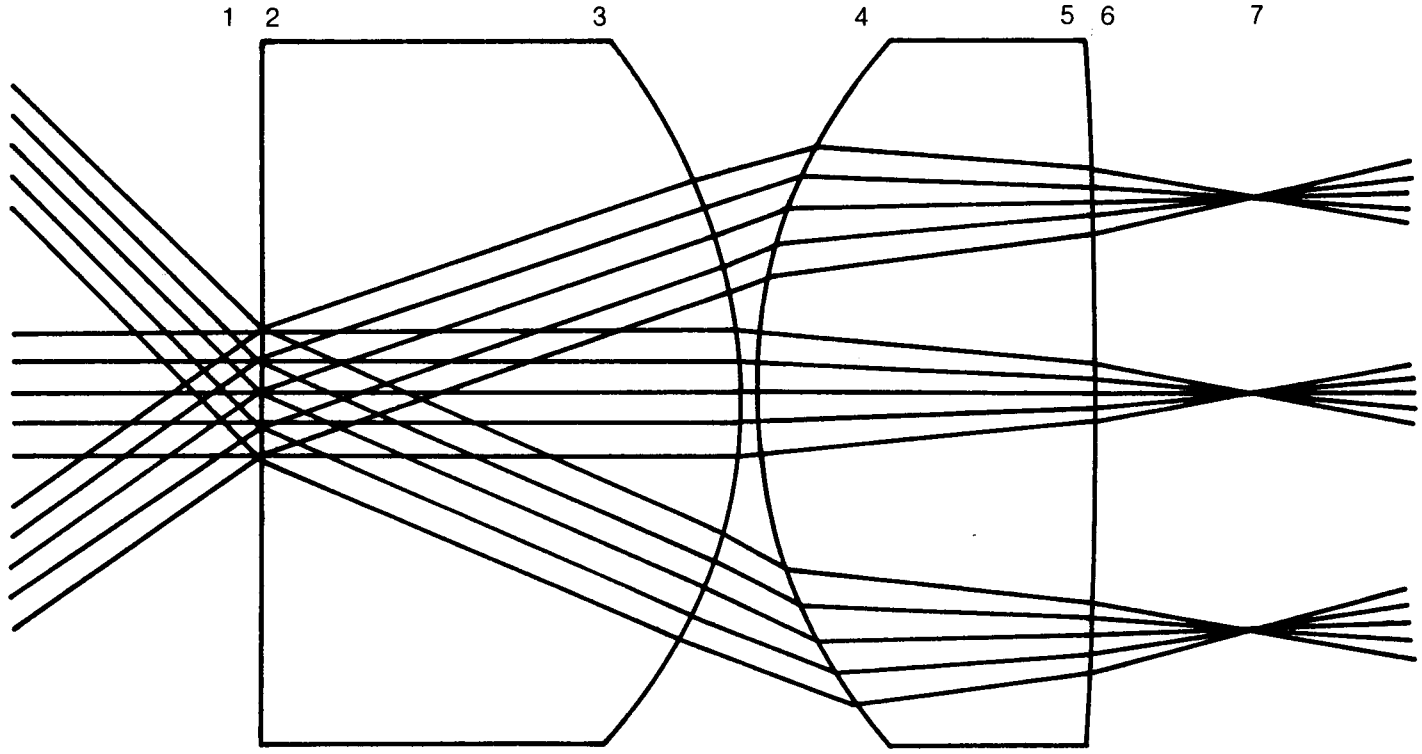

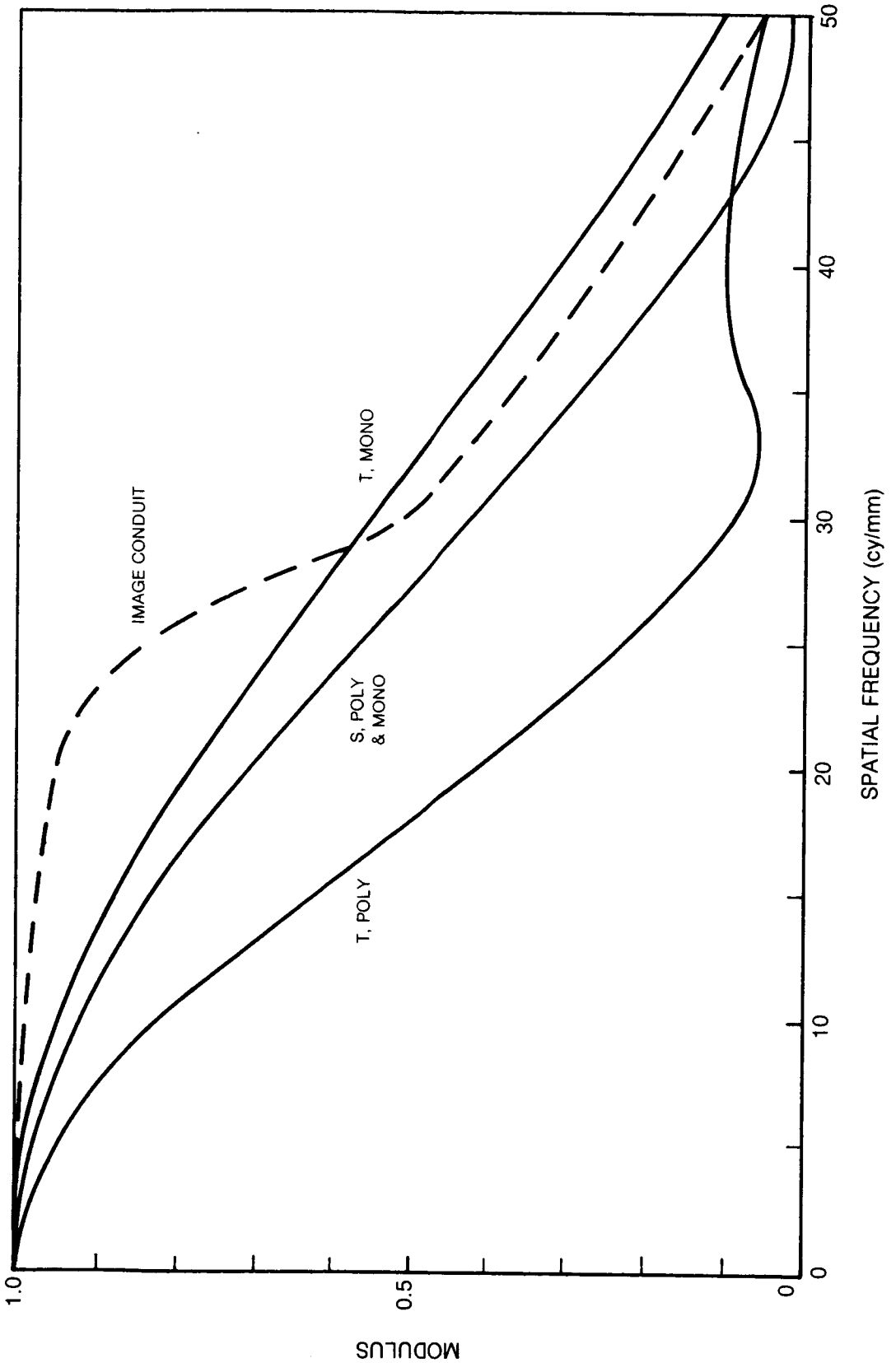

FIG. 6 MTF FOR 90° LENS AT FULL ANGLE, F/5.6

82-3-90-8

FIG. 7

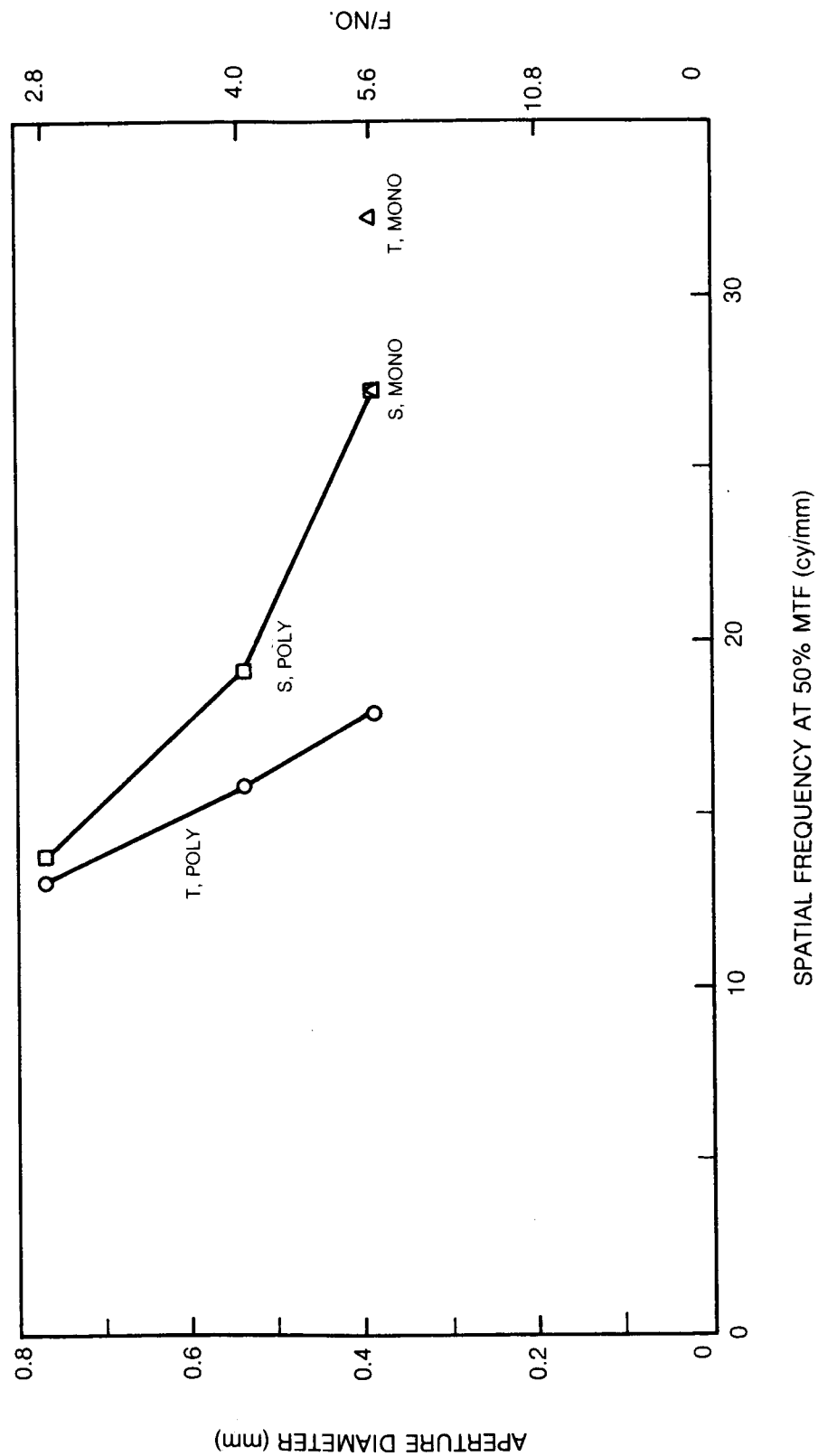

FIG. 7 90° LENS PERFORMANCE VS APERATURE DIAMETER AT FULL FIELD ANGLE

82-3-90-9

A viewing test was performed with each lens to actually measure the true lens resolution, depth-of-field, FOV, and position of focus in the image plane. A USAF resolution bar chart was observed with the lenses coupled through an image conduit. The output image from the conduit was examined with a low power microscope mounted on a micrometer positioning stage along with the conduit. Figure 8 shows the results of the test for the 90° FOV lens. The image plane distance or distance between the lens and image conduit is plotted in Fig. 8 for different distances between the lens and test pattern object. The vertical bars indicate the range between lens and conduit over which the image remained in focus. The number in the circle above the bars indicates the resolution in lines/mm that could easily be distinguished over the image range. For instance, with the resolution chart at 10 cm we could resolve one line/mm. The image conduit surface could be placed between 1.19 mm and 1.36 mm away from the last lens surface to maintain this resolution. One can see from the envelope of the vertical lines in the figure that we would have objects in focus from 5 cm to 30 cm and beyond. The resolution in the object plane decreases, of course, as the distance to the object increases.

A resolution of 1 line/mm in the object plane at 10 cm or 0.45 lines/mm at 20 cm corresponds to a resolution distance of 21 μm and 24 μm in the image plane of the conduit. This distance corresponds roughly to about twice the distance between fibers or the expected resolution limit of the fiber optic conduit. These data were taken near the on-axis view. Thus, on-axis the resolution is solely limited by the fiber optic. For the wide angle, 90° FOV lens, the resolution diminished significantly at the full field angle and was limited by lens aberrations.

The 90° FOV lens was also observed to exhibit a significant barrel distortion due to a decrease in the magnification towards the edge of the field. This kind of distortion is common with most wide angle lenses. The actual measured FOV was close to 90°, but the usable field, due to the distortion, was about 80°.

2.2.3 60° FOV Lens - A similar set of data and ray trace drawing are shown for the 60° FOV lens design in Fig. 9. The effective focal length of the doublet is 2.6 mm. Scale magnification in Fig. 9 is 10 times. The 1 mm aperture in this case was placed 1.25 mm in front of the lens on the left hand side. The separation allows for purging gas flow to keep the lens soot free. Note that the design was for sapphire. In actual practice, the sapphire lens was replaced with a glass plano-convex doublet of 3 mm focal length.

The results of the resolution tests, described previously for the 90° lens, are shown in Fig. 10. For a lens placed at 2.1 mm from the image conduit we also get a depth-of-field from about 5 cm to 30 cm and beyond. For object distances closer than 5 cm the field depth is considerably reduced.

FIG. 8 RESOLUTION AND FOCAL RANGE VS OBJECT DISTANCE FOR 90° FOV LENS

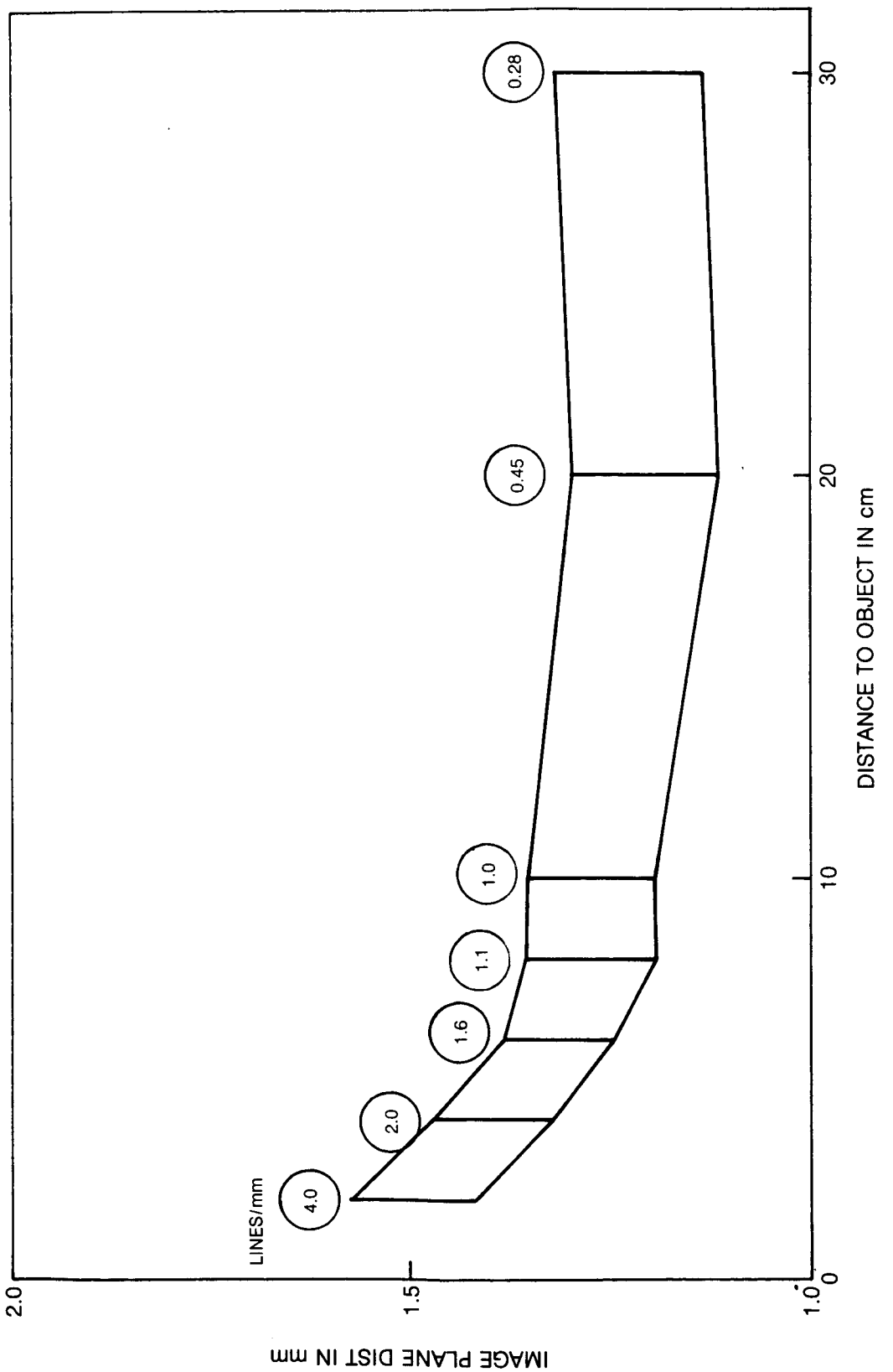

83-6-95-4

FIG. 9 60 DEGREE F-O-V LENS

SURF	RADIUS	THICKNESS	GLASS	APERTURE	REMARKS
		100.0000			OBJECT.
1	0.000	1.220	AIR	0.500	STOP. ENTRANCE PUPIL.
2	0.000	2.000	1.7682	2.200	
3	-4.000	0.000	AIR	2.200	
4	0.000	0.010	AIR	2.200	DUMMY SURF.
5	4.000	2.000	1.7682	2.200	
6	0.000	1.456	AIR	2.200	
7	0.000	0.100	AIR	2.200	DUMMY SURF.
8	0.000	0.000	AIR	1.513	DUMMY SURF.

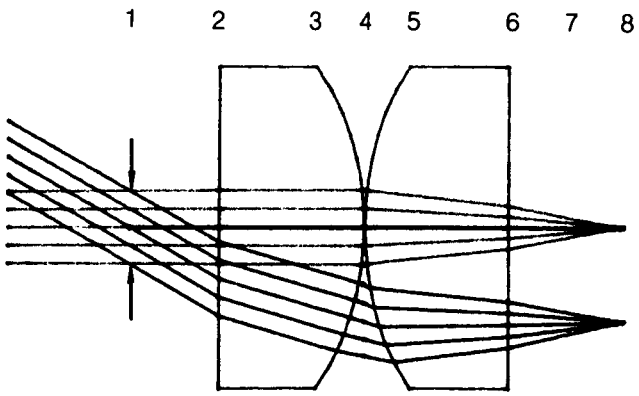

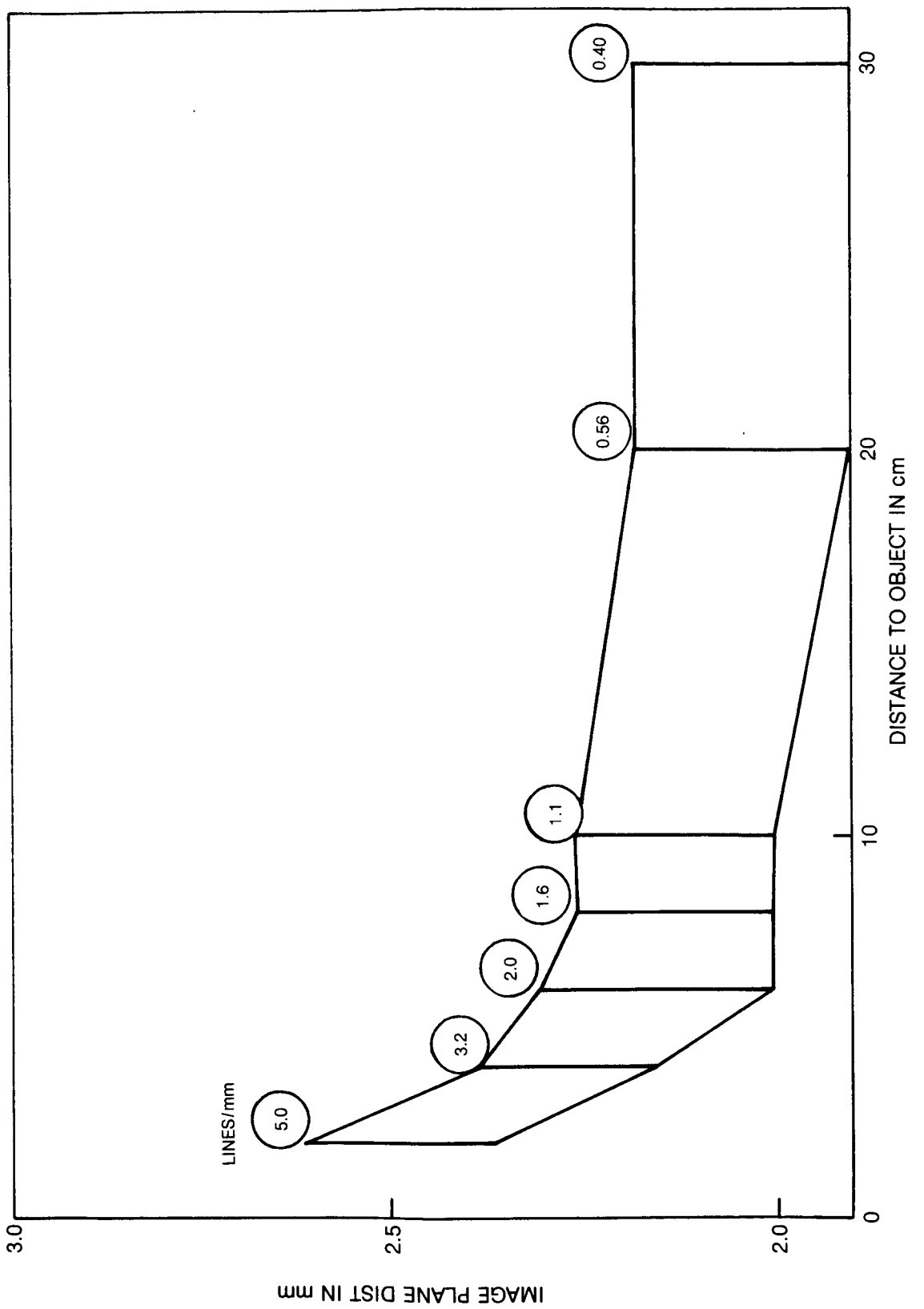

FIG. 10 RESOLUTION AND FOCAL RANGE VS OBJECT DISTANCE FOR 60° FOV LENS

Resolution in the object plane listed at the different object distances give a 26 μm resolution distance at the image conduit. This result indicates as before that the resolution is limited by the fiber optics. The 60° lens also had some barrel distortion, but not nearly as much as the 90° lens.

2.2.4 35° FOV Lens - Data and the ray trace drawing for the 30° FOV lens design is shown in Fig. 11. The effective focal length of the lens doublet was 5.2 mm. Magnification for the ray trace drawing was 10 times. In this case the designed sapphire lens was replaced with a glass lens doublet of focal length 5 mm, and the actual FOV was measured to be 35°. The standard glass microlenses had to be reduced to the proper 4.4 mm diameter. The measured resolutions and focal range versus object distances for the 35° FOV lens and image conduit system is shown in Fig. 12. We can see that the depth-of-field is more restrictive for object distances less than about 10 cm as compared with the 90° and 60° lenses. The image plane resolution distances average 28 μm which is slightly larger than the previously discussed lenses. This is not far from the ideal 20 μm or twice the distance between fiber elements.

2.2.5 13° FOV Lens - In this case the 15° FOV designed lens gave a 13° measured FOV using the glass lens substitute for the sapphire lens. Figure 13 shows the data and ray trace for the sapphire 15° FOV design. The ray trace magnification is 5 times and the effective focal length 10.37 mm. The design aperture is 3.6 mm and placed 3.8 mm in front of the lens. The resolution and focal range versus object distance plot made from the test measurements with the lens and image conduit is shown in Fig. 14. In this case, the depth-of-field is much more restricted than with the other lens systems. For example, if the lens to image conduit distance is set at 7.8 mm then the object will be in good focus at distances between 7 and 8 cm. This would be a typical viewing distance in the combustor liner. When we use the 13° FOV lens, then, the viewing distance has to be determined and the lens to image conduit distance preset. It would be desirable, especially for on-line video viewing, to have the viewing lens focus remotely controlled in this case. A small actuator driven device could be redesigned into the probe, but this was beyond the scope and scheduling of the program. The resolution of the 13° lens was better than 0.25 mm for an object at 10 cm. In the image plane the resolution distances averaged 22 μm for the different object distances. This is very close to the 20 μm ideal resolution distance.

The 35° and 13° FOV lens used a mirror to turn the view (cf., Fig. 4) so that the view could be scanned when the probe was rotated. The mirror was made of polished copper, coated with nickel and repolished, aluminized, and then overcoated with silicon monoxide for scratch and oxidation resistance.

2.3 Illumination Optics - As mentioned previously, one of the objectives of the illumination system was to be able to record video and film camera images when the combustor was off. One could examine liner surface details that may not be as clearly visible when the combustor is in operation due to obstruction from

FIG. 11 30 DEGREE F-O-V LENS

SURF	RADIUS	THICKNESS	GLASS	APERTURE	REMARKS
		100.0000			OBJECT.
1	0.000	3.530	AIR	0.650	STOP. ENTRANCE PUPIL.
2	0.000	2.000	1.7682	2.200	
3	-8.000	0.000	AIR	2.200	
4	0.000	0.010	AIR	2.200	DUMMY SURF.
5	8.000	2.000	1.7682	2.200	
6	0.000	4.214	AIR	2.200	
7	0.000	0.100	AIR	2.200	DUMMY SURF.
8	0.000	0.000	AIR	1.407	DUMMY SURF.

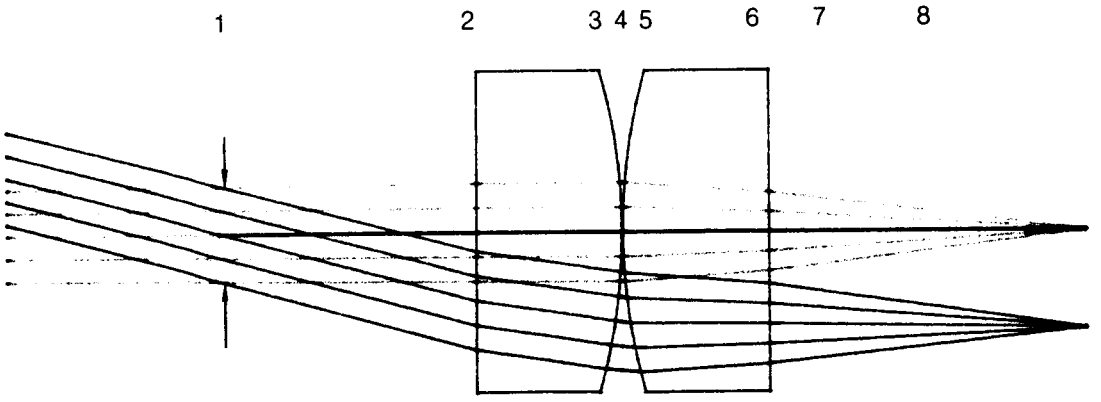

FIG. 12 RESOLUTION AND FOCAL RANGE VS OBJECT DISTANCE FOR 35° FOV LENS

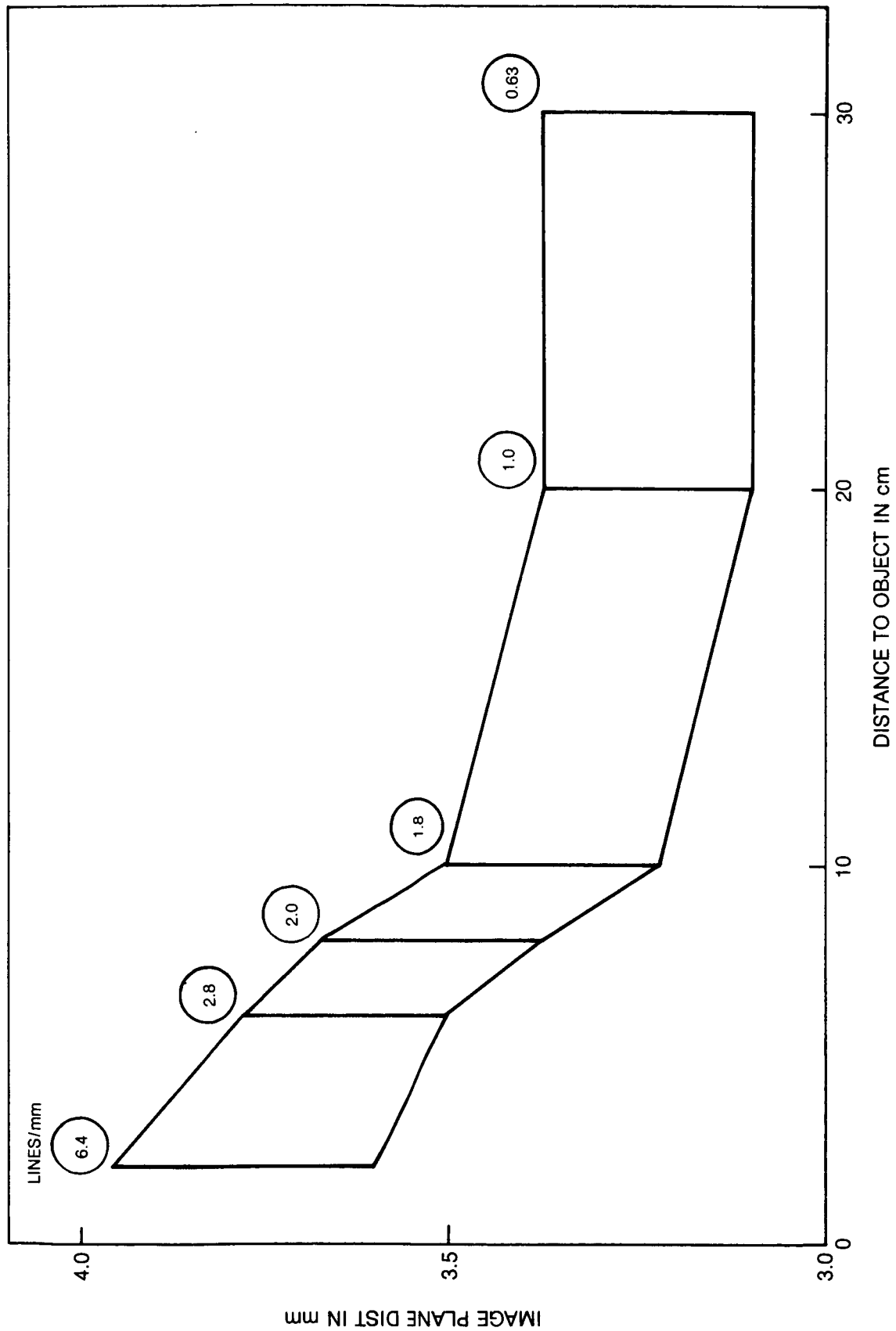

83-6-95-2

FIG. 13 15 DEGREE F-O-V LENS

SURF	RADIUS	THICKNESS	GLASS	APERTURE	REMARKS
		100.0000			OBJECT.
1	0.000	2.842	AIR	1.300	STOP. ENTRANCE PUPIL.
2	0.000	2.000	1.7682	2.200	
3	-10.202	9.500	AIR	2.200	
4	0.000	0.010	AIR	2.200	DUMMY SURF.
5	10.202	2.000	1.7682	2.200	
6	0.000	2.703	AIR	2.200	
7	0.000	0.000	AIR	1.370	DUMMY SURF.

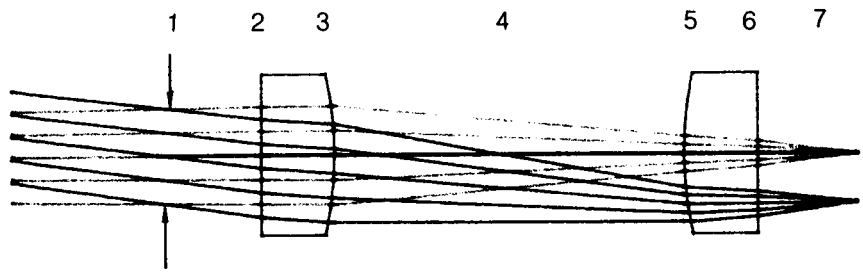

84-7-78-7

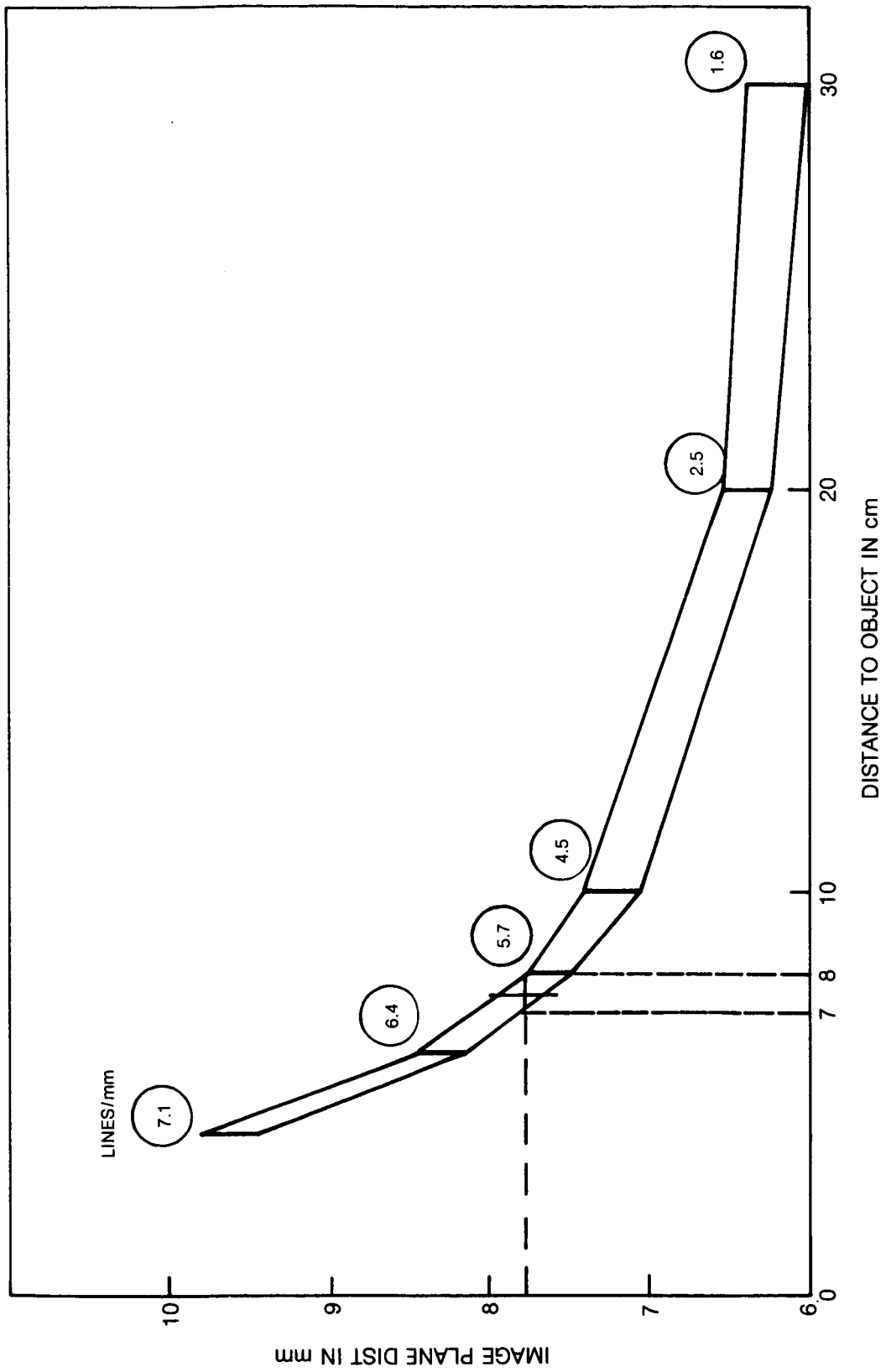

FIG. 14 RESOLUTION AND FOCAL RANGE VS OBJECT DISTANCE FOR 13° FOV LENS

the flame. A second objective of the illumination was to assist in viewing liner surfaces in the presence of the flame. An analysis, to be discussed in Section 4.0, showed that a pulsed laser would provide the best illumination source for viewing in the presence of the flame.

The illumination light was transmitted to the distal end of the viewing probe by way of two 5 meter long, plastic clad silica fibers that had 1 mm core diameters. The two illumination fibers were bound together in a special mount at the optics interface board where the focusing optics for the arc lamp and laser illuminators are located. At the other end the 5 m long fibers were coupled to corresponding fibers at the probe housing with a special connector. Two shorter sections of fibers (60 cm long) transmitted the illumination light from the connector to the distal end of the probe.

A 200 watt mercury arc lamp was used as a continuous light source for viewing when the combustor was off. The arc lamp emission was collimated with a low F number lens that came with the lamp unit. The nearly collimated beam was focused into the two fibers, placed side by side, with a 50 mm focal length, F1.25 lens. Use of two fibers rather than one made more efficient use of the oblong arc lamp image for transmitting the greatest amount of light efficiently. We were able to transmit 0.6 watt from the arc lamp to the distal end of the probe. Due to space limitation at the end of the probe, no lens was provided at output of the illuminating fibers. We felt that the lens was not needed in this case, since the numerical aperture of the fiber (NA = .3) gives a cone of light 35° wide. Expanding the light to greater cone angles with a lens would only reduce the illumination intensity on the liner walls, and making the beam smaller, which may be desirable for increased intensity would not fill the FOV of three of the lenses. The 35° emission is a reasonable trade-off.

The continuous part of the mercury arc lamp spectrum is similar to a 6000°K blackbody emitter. This is considerably brighter than the flame emission which is probably closer to a 2400°K emitter. The illumination from the fibers, however, comes from only a couple square millimeters and consequently is much less than the illumination from the less intense but much larger flame as indicated by film exposures. The arc lamp also has extra intense line spectra emission at 400, 440, 545, and 580 nm. There is also an intense emission at 360 nm and further into the uv where the optics do not transmit. Color photographs taken with the arc lamp illumination came out green from the 545 emission line. The illumination appears white to the eye, however.

The illumination fibers are shown in the probe cross section schematics of Figs. 3 and 4. In order to illuminate in the direction of view, the fibers had to be bent at the viewing angle with radii of curvature from 3.5 mm to 5 mm. Bending losses in a fiber are proportional to the fiber radius divided by the

bend radius. In our case the large core fiber and small bend radii produced losses on the order of 10 percent. That is, about 10 percent of the illumination light would leak out at the fiber bend. This leakage caused two problems. First, there was a crescent shadow near the center of the illumination pattern, and then a fraction of the light leaking from the bend could reflect from the first surface of the viewing lens or from the mirror back into the image conduit. The reflected light interferred with the image from the combustor view. The illumination light pattern can be seen in Fig. 15b. For comparison, Fig. 15a shows a photo taken with a floodlamp illuminating a white screen with 2X2 cm squares. The screen is viewed through the fiberscope with the 60° FOV lens and is placed 10 cm in front of the probe. Figure 15b shows the same picture except the arc lamp illumination through the fiberscope is used. The probe orientation for the photo was horizontal and on the left hand side. One can easily see the dark crescent shadow in the center of the pattern of Fig. 15b and also a bright spot to the right. These are produced by the required fiber bend. Figure 15b required an exposure time 4.5 longer than Fig. 15a.

The plastic cladding material had to be removed from the illumination fibers before the bend was made with a torch. After the bend was made and the fiber cleaved to the proper length, it was reclad with a special epoxy compound and then painted with a high temperature silver paint. A dark paint would burn off from the high intensity light leaking from the bend. The silver paint could remain without burning up to a level of 1 watt of optical power being transmitted. This was measured with an argon ion laser signal transmitted through the illumination fiber.

An incoherent bundle of small diameter fibers could be used in place of the large core fibers to provide the illumination light. With the small diameter fibers the bending loss could be made very small, however, there would be a 40 percent to 50 percent coupling loss at the input to the fiber bundle and the interstitial light would have to be absorbed before reaching the distal end of the probe. There would also be a construction problem with the incoherent illumination fiber bundle. The fibers would have to be bound together at their ends with epoxy and a protective buffer coating could not be used on the fibers, subjecting them to breakage. A protective shield would have to be used. A 1 mm fiber conduit made for the illumination may be a better solution if the interstitial light could be absorbed.

An important reason to use the large core illuminating fibers was for the high intensity, pulsed laser illuminating source. In order to transmit a sufficient pulse energy for photographic exposure (10 mJ to 100 mJ from the fibers) in 1 μsec, we have to use a large core fiber with a cleaved end. While the maximum bulk transmission energy flux for fused silica, the fiber material, is 500 J/cm^2, we are limited to about 50 J/cm^2 (ref. 7) from the surface breakdown at the input

FIG. 15 ILLUMINATION PATTERNS

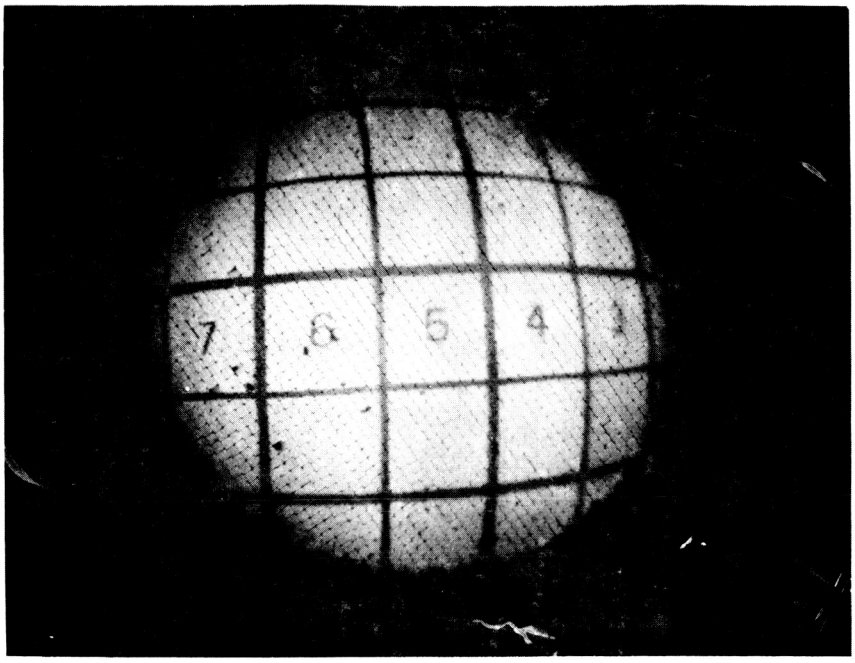

a) WITH FLOOD LAMP

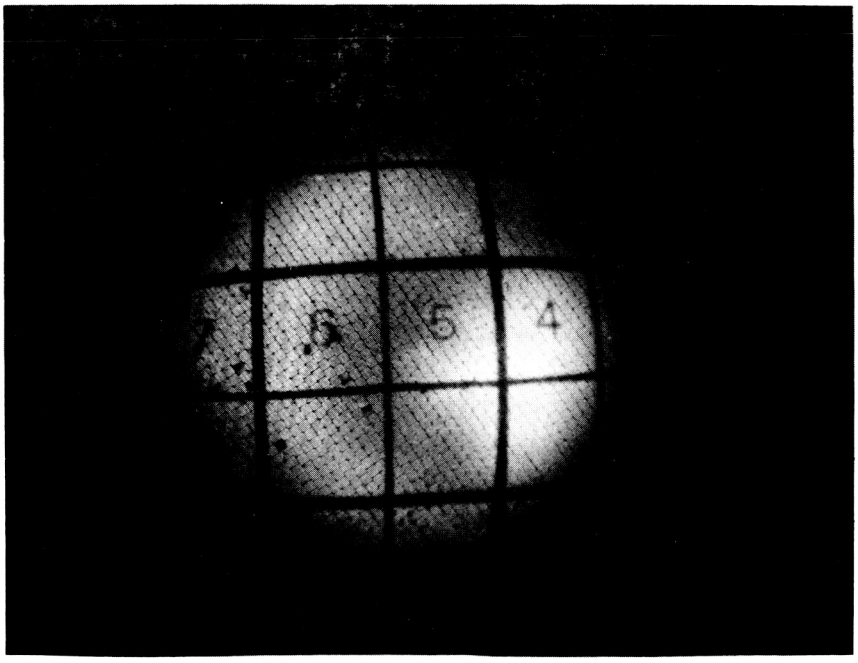

b) WITH ARC LAMP AND FIBER OPTICS

to the fiber. The breakdown threshold depends on the surface conditions. Small pits and scratches or dirt particles can act as local focusing centers that enhance the optical E-field to the point where ionization can take place. At this point a gas breakdown occurs at the surface, a spark is produced, and the end of the fiber shatters. We found that with a cleaved fiber end we could transmit 37.6 J/cm^2 or 295 mJ through the large core fiber without a breakdown. With a ground and polished fiber or fiber bundle end the maximum pulse energy transmission was invariably much smaller.

2.4 Optics Interface Unit - At the optics interface board we transfer the image at the output end of the fiber bundle to a video or film camera. An intervening filter on a selectable 8 position filter wheel is placed between the output of the fiber bundle and the cameras. The interface board also contains the mercury arc lamp with power supply and focusing optics for the two illumination fibers. An additional lens is also provided for focusing an external laser illumination source into one of the two fibers.

A photograph of the optics interface board is shown in Fig. 16. The image recording cameras and filter wheel are on the left hand side of the mounting board and the arc lamp, power supply, and illumination fiber holder and lenses are in the right hand side. There is also a plastic dust cover, not shown in the photograph, that protects the components on the board. The video and film cameras and filter wheel optics were elevated on adjustable mounts to permit the use of a range of optical instruments including a high speed motion picture camera. A pneumatically operated mirror reflects the image to a video camera for on line monitoring or retracts to let the image be in direct view of the film cameras.

A schematic of the interface board with the various components enumerated is shown in Fig. 17. The components are:

1) 61 cm by 122 cm optical breadboard with mounting holes,
2) universal mounting platforms on vibrationally damped rods,
3) translation slides,
4) 50 mm, F2.8 camera lenses (enlarging lenses reversed),
5) cable harness connectors,
6) relays for 24 volt ac remote actuation,
7) video camera remote focus motor,
8) arc lamp power supply,
9) optical slide rail,
10) 150 mm focal length, 42 mm dia lens and holder for coupling laser beam into fiber
11) mirror on pneumatically operated vertical slide,
12) fiber mount and positioner,
13) two 1 mm core dia plastic Clad fused silica fibers,

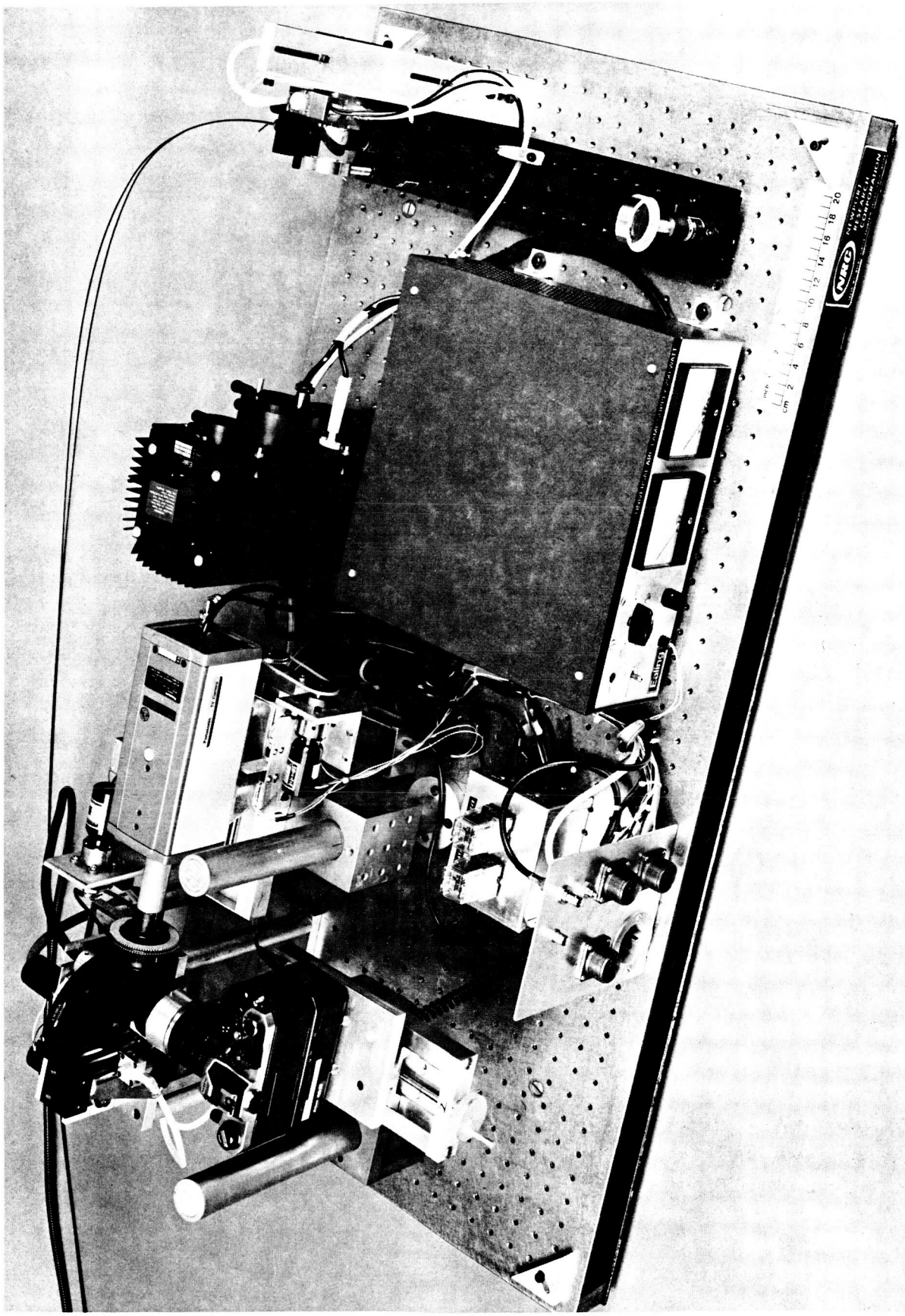

FIG. 16 OPTICS INTERFACE BOARD

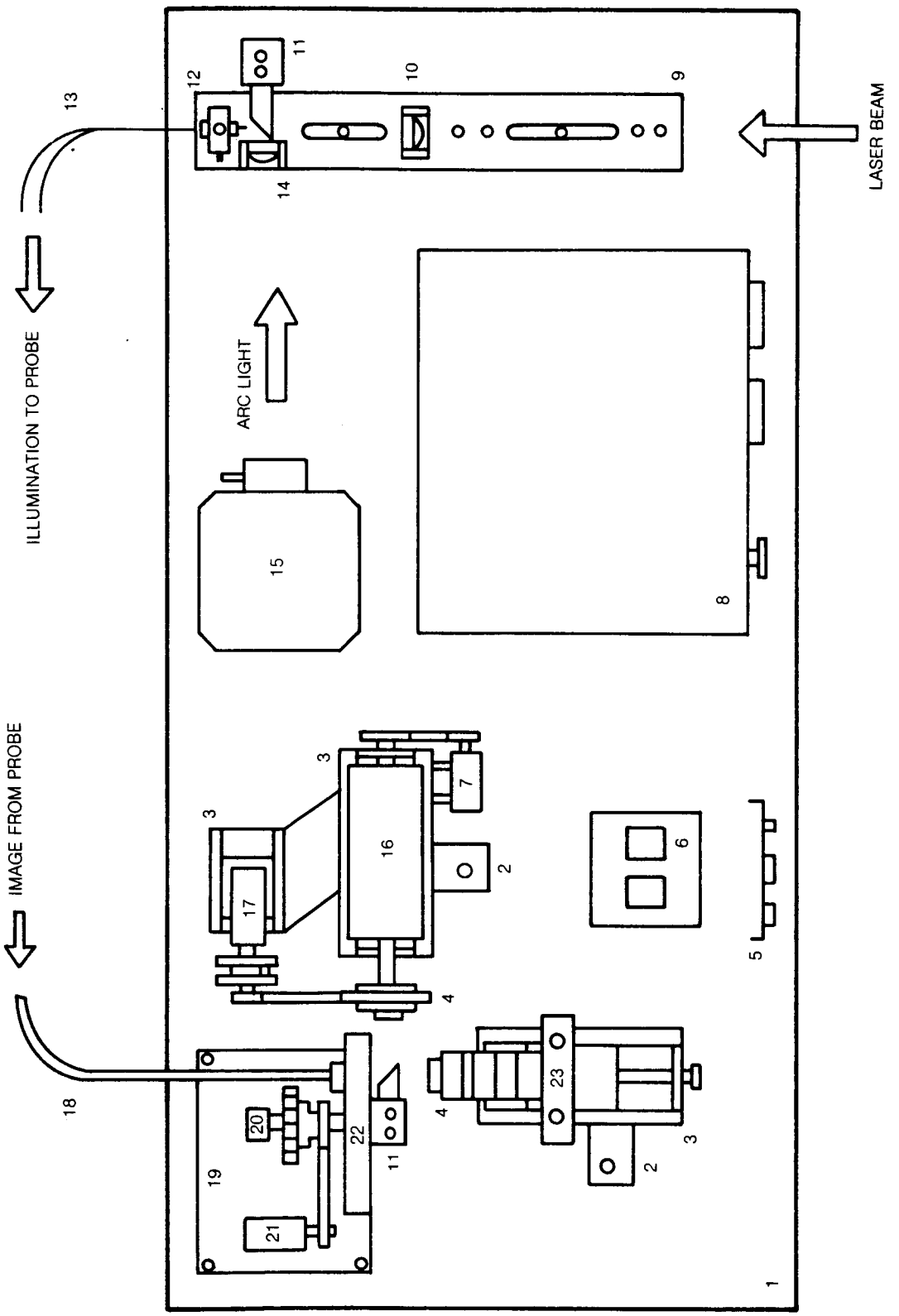

FIG. 17 OPTICS INTERFACE BOARD SCHEMATICS

84-7-78-9

14) 50 mm focal length, 40 mm dia lens and holder for coupling arc illuminator into the two fibers,
15) 200 watt mercury arc lamp and housing,
16) black and white, high sensitivity video camera,
17) video camera aperture control motor,
18) 3 meter flexible fiber image bundle,
19) stand for filter wheel and actuator motor,
20) filter wheel position switch indicator,
21) filter wheel drive motor,
22) 8 position filter wheel for 2.54 cm dia filters, and
23) 35 mm film camera with automatic film advance and remote shutter actuation.

The remote control unit for optics interface board is shown in Fig. 18. Thirty meter lengths of cable harnesses connect the two units; the control unit is placed in the test stand control room and the interface board is near the probe on the combustor rig. The control panel shown in Fig. 18 has the camera select and control on the right hand side, the filter select and indicator in the center, and the illumination select and triggers on the right hand side. Note that the video camera has a remote aperture and focus control while the film camera has only a frame advance. The aperture and shutter speed on the film camera have to be preset. The exposure for the film camera or the video camera can be step adjusted by using the series of neutral density filters on the filter wheel.

One of the eight filters on the filter wheel is a clear glass piece of nearly the same thickness as the 4 neutral density filters. There is also a blue, red, and an interference filter centered at 580 nm for the dye laser illuminations. The last 3 filters have different thicknesses and require a slight readjustment of the camera focus. The filters in the wheel can be readily removed and replaced if other wavelengths or neutral densities are desired.

We can also select the desired illumination source and trigger the illumination source on. In the case of the arc lamp the trigger initiates a high voltage spark to start the continuous arc operation, which takes a couple of minutes to warm up to full brightness. For the laser, the trigger initiates a pulse of laser light just after actuation of the film camera shutter. The film camera shutter and advance will operate with the laser trigger button provided the camera select is in the film camera position. The film camera shutter should be set at a speed for synchronization. For our film camera the fastest sync speed was 1/200 sec.

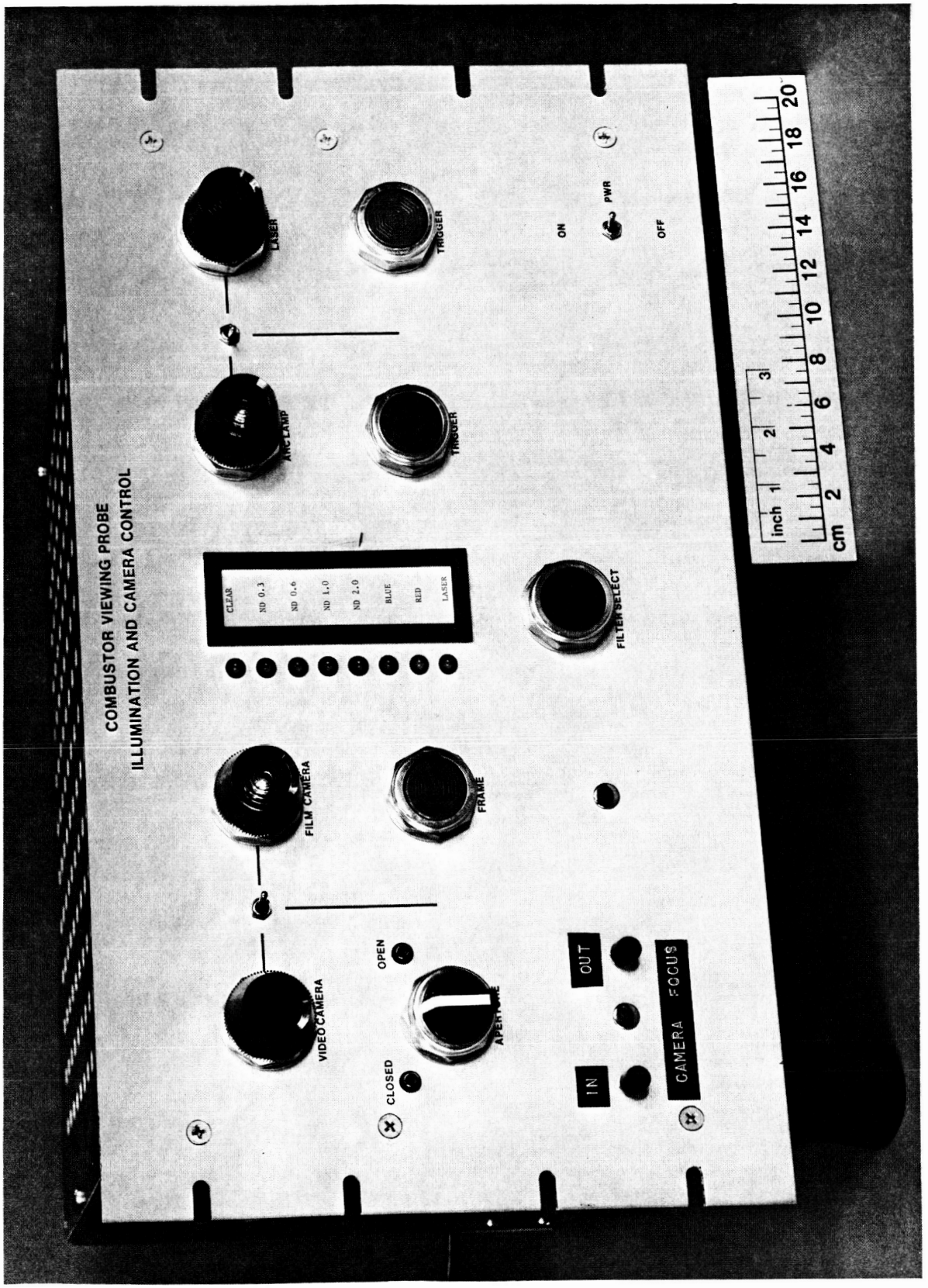

FIG. 18 REMOTE CONTROL UNIT FOR OPTICS BOARD

3.0 MECHANICAL DESIGN

3.1 Objectives - There were two basic objectives in the mechanical design of the viewing system. One was to design a probe that could be placed into the primary combustion zone or into the combustion exit zone of a gas turbine engine. The probe had to protect the optics and withstand the high temperature, high speed-hot gas flow, and the highly oxidizing and high pressure environment of the combustor. High pressure gas seals had to be made with the probe and optics to the combustor environment. A second basic objective was to be able to traverse the probe in and out of the combustor and to rotate the probe a full 360° to scan the view inside and outside the combustor liner. The probe actuation was to be controlled remotely with indicators to show the position of the probe in depth and rotation.

In order to accomplish the first objective we would have to design a water cooled probe. The first problem in the design was to determine the thermal loading on the probe at different locations in the combustor. A second problem was to determine the best material for the probe that could handle the high heat loads. A probe with water cooled walls and a gas purging system to protect the optical components could then be designed. As mentioned before in Section 2.0, two probes were designed with different viewing end sections to accommodate the full range of viewing fields desired. A finite element analysis was performed to estimate the temperature field at the viewing end of the probe which is immersed in the combustor. Problems with the gas purge and cooling design were worked out with a preliminary test probe. These topics along with the actuator and remote control units will be described in the following subsections.

3.2 Thermal Loading - To keep the optical components cool inside the viewing probe we must carry away a sizable amount of heat per unit area per unit time. The heat flux into the probe comes from two principal sources: radiant heating from the flame and convective heating from the hot gas flow. Since the temperature and flame conditions in the combustor are not known accurately and they vary significantly in time and location, we can only approximate what the greatest heat loading might be. We will estimate the maximum heat loading at two locations: the primary combustion zone (pcz) and the combustor outlet (ce).

In the primary combustion zone, the temperature may be near the stoichiometric temperature of 2400 K. We will assume the flame is optically dense and therefore blackbody like. The emissivity of a copper probe would only be 0.1 or a stainless steel probe 0.35. Let us assume, however, that there is a thin deposit of carbon on the probe giving the surface an emissivity of 0.8. We will also assume that the probe surface temperature is approximately 400 K. The heat flux component into the probe from the flame radition is

$$F_{r,pcz} = \sigma \varepsilon_p (T_o^4 - T_p^4)$$
$$= 5.67 \times 10^{-12} \times 0.8 \times (2400^4 - 400^4)$$
$$= 150 \text{ W/cm}^2$$

At the combustor outlet the gas temperature will be taken as 1800 K which is probably on the high side for most commerical engines. We will again use 0.8 for the emissivity of the probe surface, but at this location the emissivity of the gas will be approximately 0.3 from a calculation in ref. 8. The heat flux at the combustor exit is thus

$$F_{r,ce} = 5.67 \times 10^{-12} \times 0.3 \times 0.8 \times (1800^4 - 400^4)$$
$$= 14.3 \text{ watts/cm}^2$$

There is also radiation heating of the probe at the combustor exit from the upstream flame at 2400 K. The visible and near infrared wavelengths, which contain about one half of the total radiation are the principal contributors. Using an estimate of the fraction of the hemisphere that the view of the flame to the probe presents, the component of heat flux from the flame is roughly 8 watts/cm. The total heat flux from radiation at the combustor exit would then be about 22 watts/cm^2.

To determine the convective heat loading from the hot gas flow we must first calculate the average heat transfer coefficient $\bar{h}$. This coefficient can be determined for a cylinder in a gas flow from the empirical relation between the average Nusselt number and the Reynolds number of the flow, namely:

$$\frac{\bar{h} D}{k} = 1.5 C \left(\frac{v_o D \rho}{\mu} \right)^n$$

(ref. 9). The empirical constants vary with Reynolds number. For the high velocity flows with which we are dealing, c equals .024 and n equals .805. For a turbulent stream we should increase the heat transfer coefficient by 50 percent. This is given by the 1.5 factor in the above equation. The quantities in the above equation are taken as:

cylinder diameter, D = 1.27 cm

Thermal conductivity if air @ 30 atm

$$k = \begin{cases} 3.59 \times 10^{-4} \text{ cal/cm/sec/K @ 2400 K} \\ 2.66 \times 10^{-4} \text{ cal/cm/sec/K @ 1800 K} \end{cases}$$

Air density @ 30 atm

$$\rho = \begin{cases} 4.41 \times 10^{-3} \text{ g/cm}^3 \text{ @ 2400 K} \\ 5.88 \times 10^{-3} \text{ g/cm}^3 \text{ @ 1800 K} \end{cases}$$

viscosity @ 30 atm

$$\mu = \begin{cases} 7.36 \times 10^{-4} \text{ g/(cm-sec) @ 2400 K} \\ 6.07 \times 10^{-4} \text{ g/(cm-sec) @ 1800 K} \end{cases}$$

freestream velocity

$$v_o = \begin{cases} 8590 \text{ cm/sec @ Mach .25} \\ 1720 \text{ cm/sec @ Mach .05} \end{cases}$$

A mach number of .05 is taken for the primary combustion zone and a mach number of .25 is taken for the combustion exit. The film coefficient in the primary combustion zone calculates to be .021 cal/(cm^2.sec). The heat flux from convection in the primary combustion zone is then

$$F_{c,pcz} = .021 \times 4.18 \ (2400 - 400)$$
$$= 176 \text{ watts/cm}^2$$

Likewise at the combustor exit

$$F_{c,c} = .083 \times 4.18 \ (1800 - 400)$$
$$= 486 \text{ watts/cm}^2$$

The total heat flux is the sum of the radiative and convective components. At the primary combustion zone we have a total heat flux of 326 watts/cm^2 and at the combustion exit 508 watts/cm^2. The calculations for the thermal stress and probe tip temperature analysis are based on the removal of heat at 490 watts/cm^2 (3 Btu/(sec in.^{2})).

3.3 Stress Analysis - In order to safely remove the large heat flux to cool the optics a careful choice of material from which to construct the probe had to be made. The heat flux transferred through an infinite slab wall of thickness t is proportional to the temperature differential across the wall and to the thermal conductivity, k. That is,

$$F = k\Delta T/t$$

A maximum hoop stress develops in a thin wall circular cylinder and is given by

$$\sigma = \alpha E \Delta T/2(1-\nu),$$

where E is Young's modulus, α is the temperature expansion coefficient, and ν Poisson's ratio. Thus, for a given heat flux and wall thickness the hoop stress is

$$\sigma = \alpha EFt/2k(1-\nu).$$

Since we are limited to a maximum stress, there will also be a maximum allowable thickness for a given material. That is we are limited to how thick we can make the probe walls and carry the given heat load.

On the other hand, the probe must also support itself in the high speed gas flow and support the full cooling water pressure when the combustor is off; that is, when there is no external pressure. These requirements place a lower limit on the probe wall thickness. Since the maximum hoop stress varies as the inverse of the wall thickness for the cooling water pressure and directly as the wall thickness for the thermal stress, we see that there will be an optimum thickness. Given a maximum allowable stress there will be a range of allowable wall thicknesses to carry the heat load and internal water pressure. The relationship between the stress, σ, and wall thickness, t, is given by

$$\sigma = \alpha EFt/2k(1-\nu) + pr/t,$$

where p is the cooling water pressure and r the cylinder radius. Figures 19 and 20 show plots of σ verses t for stainless steel and copper. The optimum thickness for stainless is 0.158 mm with a safe range of 0.09 mm to about 0.23 mm. For copper the optimum thickness was 0.91 mm with a safe range of 0.3 to 2.8 mm. Even though stainless steel has a higher stress limit, the much greater thermal conductivity of copper makes it the best choice of material for the probe. With copper we have a wider latitude of allowable thickness to copper thickness sections that may be designed into the end of the probe. For Figs. 19 and 20 the heat flux was taken to be 490 W/cm^2, the water pressure 2 MPa, and the tube radius 7.94 mm.

There are alloys of copper with trace amounts of silver or zirconium (ref. 10) that have much higher yield strengths (~400 MPa) than that listed for the oxygen free-high conductivity (OFHC) copper used for Fig. 20. The copper alloys retain about 95% of the conductivity of the OFHC copper. To get the higher yield strengths, however, the copper alloys must be cold worked and heat treated. If the heat treating temperatures are approached (350-400 C) at any later time, the alloy will loose its high tensile strength. Since high temperature brazes or e-beam welds were to be used at the probe tip that might destroy the high tensile strength, we decided against using the alloy coppers and used OFHC copper for the probe material.

3.4 Probe Design - In this section we will discuss some of the basic ideas that went into the mechanical design of the probe. The probe was to have water cooled walls that contain and protect the imaging and illuminating optics from the combustor environment. Most water cooled probe designs we studied were constructed with three walls. Cooling water flows down the inside wall, turns at the end of the probe and flows up the outside walls or vice versa. While this cooling design lends itself to easy construction, our desire was to keep the probe size to 12.7 mm O.D. and still leave enough room inside for the optics. This led us to a two wall design with flow guides. Four flow guides were placed in the annular cross section between the two tubes and run parallel to the probe axis. The guides were equidistant and divided the annulus into four quadrants. Cooling water would flow down two opposing quadrants, split and return back up the other two quadrants. The flow guides were machined into the outside surface of the inner tube. An interference fit was formed between the O.D. of the inner tube with the guide ribs and the I.D. of the outer tube to make the seal. The overlap between the outer and inner diameters of the two tubes was about 0.013 mm. Assembly of the probe cooling wall was accomplished by cooling the inner tube with dry ice and heating the outer tube to 260°C. E-beam welding and brazing were also considered for the wall assembly, but these procedures may lead to problems with distortion and non-sealing or constriction that may not be easily detected. The interference fit proved successful in the preliminary probe to be described and was the method choosen for construction. Copper was used for the probe material. This choice was discussed in the previous section, 3.3.

FIG. 19 STRESS VS THICKNESS FOR STAINLESS TUBE

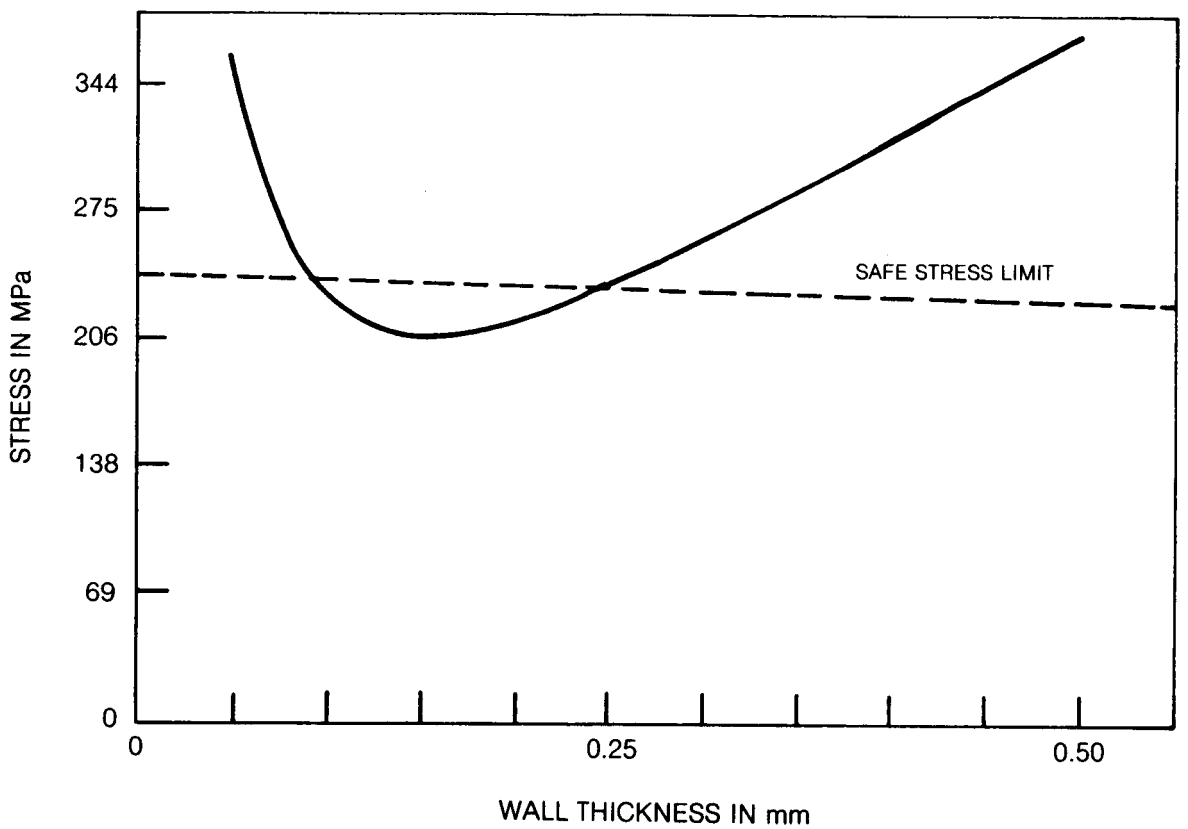

84–7–78–10

FIG. 20 STRESS VS THICKNESS FOR COPPER TUBE

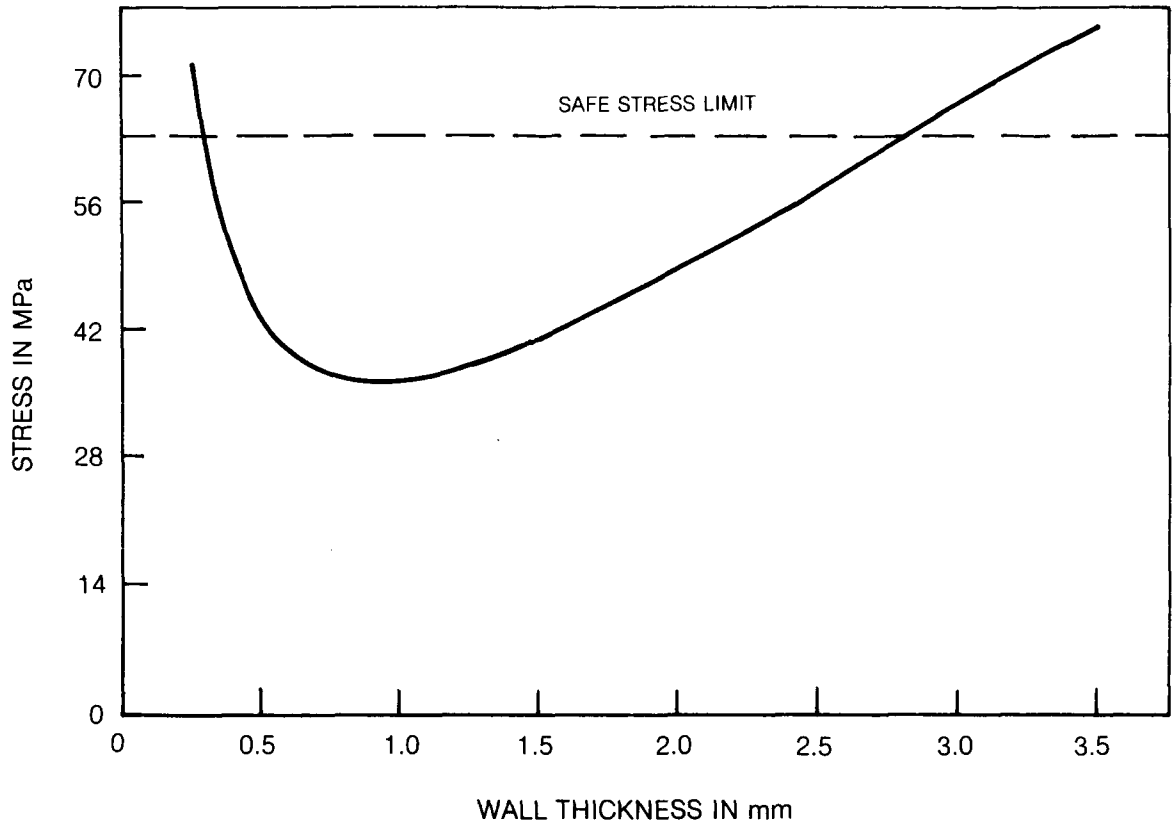

84–7–78–11

The design of the end of the probe was governed by consideration for the optical design as discussed in Section 2.0. In order to cover the wide range of viewing fields, two probes were constructed with different viewing ends as shown in Figs. 3 and 4. Since the probe was to be rotated 360°, the view was taken at an angle to the probe axis in each case so that we could scan the view. For the wide field probe the lenses were mounted into the end tip section at 45° to the probe axis as shown in Fig. 3. Small ribs on the i.d. of the lens barrel allow purge gas to flow around the lenses and out the lens aperture. Focusing is accomplished by turning the lens barrel and adjusting the lens to image conduit spacing. The illuminating fibers were prebent with a torch and inserted into holes that run parallel to the lens barrel axis. The end of the narrow angle probe was constructed differently. In this case a large opening was made at the end of the probe and a mirror attached to turn the direction of view 60° to the lens axis that is aligned parallel to the probe axis. This detail is shown in Fig. 4.

A preliminary probe was built for testing the water cooling design and gas purging design for keeping the exposed optical viewing surfaces clear of soot deposits. The preliminary probe was tested in a small laboratory rig that burned fuel oil. A photo of the preliminary test probe is shown in Fig. 21. Four connector fittings for each quadrant water cooling channel are visible in the figure. This probe was 15.9 mm in diameter while the actual viewing probe was made 12.7 mm in diameter. The probe came from the machine shop with a several degree bend and some small impact marks. The bend was carefully straightened in a lathe. Cooling water flow tests revealed that 70 percent of the flow traveled in the proper channels, while the remaining 30 percent crossed over the channel guides. The cross flow reduces the cooling effectiveness at the probe viewing end, and may have been caused by the interference fit separating at some points when the tube was bent. Another problem was encountered when the probe was connected to a laboratory hood water line that had not been used for some time. Particles that had accumulated in the line were driven into the probe at full flow, clogged the 1.1 mm channels, and restricted the flow to 10% of the initial value. The blockage was released with a reverse flow in an ultrasonic cleaning tank.

These two problems stress the importance of being careful when handling the probe. Copper is a soft material and small impacts can affect the cooling channels which are only 0.9 mm wide in the probes built for the high pressure combustor tests. The cooling water should be filtered with a filter that has sufficient capacity and pore size to prevent choking the critical water flow to the end of the probe from particulate matter in the water lines.

FIG. 21 PRELIMINARY TEST PROBE

The preliminary probe required 2 MPa of pressure drop to provide a flow rate of 24 ℓ/min. The prototype probes, however, required only 0.52 MPa pressure drop to give the same flow rate. Figure 22 gives the cooling water flow rate versus the pressure drop across the probe inlet and outlet for the prototype probes run on the high pressure combustor rig. In actual operation the water inlet pressure was increased to 0.84 MPa with a pump and the outlet plumbing was constricted a small amount to provide a 0.34 MPa back pressure. This back pressure increased the boiling temperature of the water to 150°C which helps prevent a serious problem of overheating the copper walls that could occur if the cooling water boils at any point. When operated in the lab combustor rig the preliminary probe carried away heat at the rate of 2270 watts. With about 90 cm^2 of probe surface area exposed this rate corresponds to an average heat flux of 25 watts/cm^2. For the prototype probes operating in the high pressure rig we carried away 4682 watts with an average heat flux of 112 watts/cm^2 with 42 cm^2 exposed. The cooling of the probes was sufficient that epoxy compounds could be used inside the probe surface at the tip end. Internal temperatures in the prototype probes only rose to 37°C at the probe end demonstrating the effectiveness of the water cooled copper probes. The preliminary probe was used for a series of gas purging tests to be described in Section 3.7.

3.5 Probe Assembly and Seals - A photo of the wide field probe with the internal components and attachments removed is shown in Fig. 23. The copper probe body is the component on the upper left in the figure. Next to the viewing end of the probe on the left hand side is the copper lens barrel that screws into the probe tip at 45°. At the other end of the probe we have four tubes with fittings for the cooling water attachment (one for each quadrant in the probe walls channel). The length of the probe not including the tubes is 31.4 cm.

Just below the probe are the two large core fibers used for illumination. The connectors that couple to 5 meter lengths of fiber running to the optics board where the arc lamp source is located are shown at the right hand side of the fibers. In the next row below the illuminating fibers we have from left to right, the image conduit with support spaces, an aluminum transfer block, and a stainless steel flange. The Buna N O-ring seal for the transfer block to the probe body is shown between the image conduit and the transfer block. A special tightening nut and Buna N O-ring, shown just after the transfer block, seal the image conduit at the transfer block. The O-ring seals for the flange to transfer block connection and small O-rings for the two thermocouple seals to the flange are shown next to the flange. The flange itself supports the purge gas tube and the fiber optic image bundle connection. Below the flange piece is a connecting "T" for the purge gas. The illuminating fibers run through the purge tube and are sealed at the end cap on the "T" fitting with the small O-rings and special plate shown on the right hand side of the fitting.

FIG. 22 COOLING WATER FLOW RATE FOR COMBUSTOR VIEWING PROBES

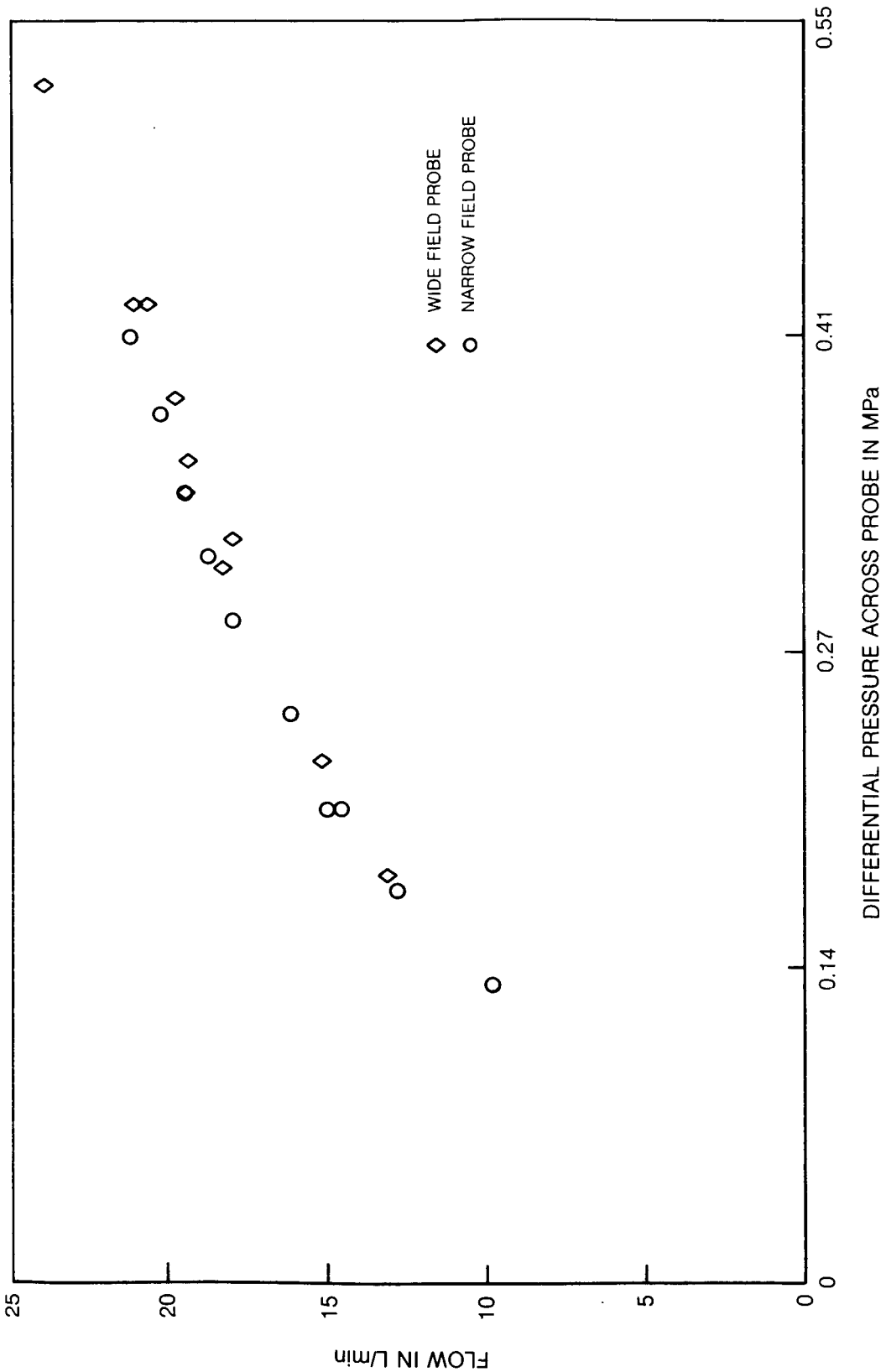

84–7–78–12

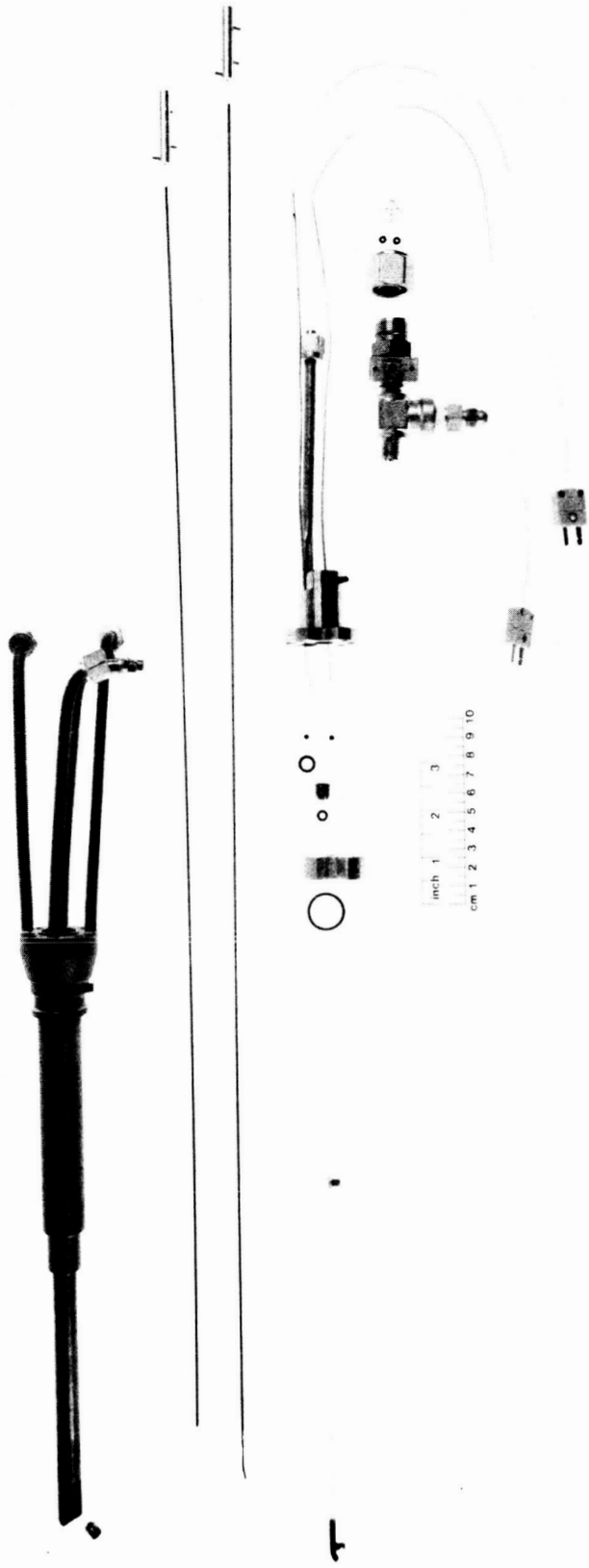

FIG. 23 WIDE FIELD PROBE ASSEMBLY

A component assembly photo of the narrow field probe is shown in Fig. 24. The narrow field probe is similar to the wide field probe just discussed except for a few details. The viewing end of the probe has a large opening on the side and a copper mirror mounted into the end as shown in Fig. 24. The viewing lenses, which are now directed along the probe axis, are mounted at the end of a long brass sleeve that slides into the probe. The sleeve also supports the image conduit and is shown just below the illuminating fibers on the left hand side of the figure. A special tie bar holds the end of the illuminating fibers apart at the viewing end' and a groove on each side of the brass sleeve supports the fibers inside the probe.

The probe pressure seal to the combustor test rig or an engine is made with two viton, quad seal O-rings in the adapter plate that mounts to the probe actuator unit. The probe slides through a sleeve on the adapter plate forming a dynamic seal with the O-ring. The O-rings, called quad seals, are four lobed to prevent potential rolling of the seal from the sliding motion of the unlubricated probe. Figure 25 shows a photo of the probe and actuator assembly. The adapter plate is shown on the left hand side in the figure. To the right of the adapter plate are the two quad seal O-rings and the actuator unit with covers removed. Below the actuator unit is the assembled probe, and below the probe are the thrust bearings and probe turning gear. The probe inserts into the center of the actuator and through the adapter plate. A small amount of water cooling is provided by a loop of copper tubing on the adapter plate. This cooling is to prevent overheating and subsequent damage to the O-ring seals.

Initially, only one O-ring was used to seal the probe. During bench testing of the probe unit for high pressure sealing (3 MPa) we found that the single O-ring was not sufficient to form a good seal with the probe at all rotation angles and insertion depths. A second O-ring was placed 2.5 cm below the original O-ring in the adapter plate for rig testing. With the second O-ring a good seal was produced for all probe positions in rotation and depth.

A deterioration problem was experienced with the second O-ring during the high pressure combustor rig testing. We found that the inside surface of the second O-ring was torn and had small pieces removed after every test run and had to be replaced. The first O-ring showed no signs of deterioration, however. We initially assumed that the hot combustor inlet gases (430°C) were eroding the exposed O-ring. A third groove was placed just below the exposed O-ring and a small hole was drilled in the adapter plate to allow a second source of purge gas to enter the groove. The groove acted as a mainfold to distribute the purge gas around the probe and out from the gap between the probe and adapter plate and into the rig. The new purge, then, would keep the hot combustor gases from contacting the O-ring. It turned out, however, that the O-ring purge had no effect on the deterioration problem. The second O-ring is removed further away from the adapter plate water cooling loop and would see temperatures closer to

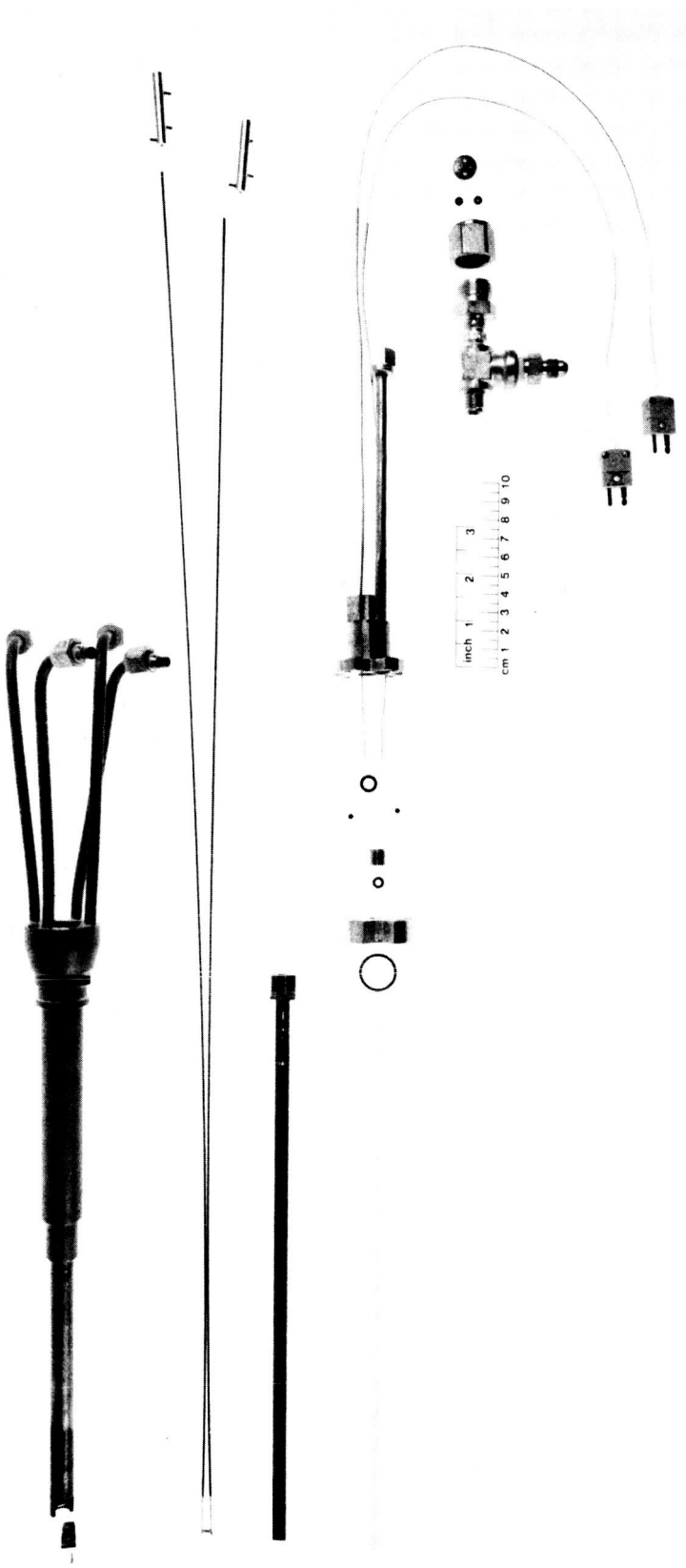

FIG. 24 NARROW FIELD PROBE ASSEMBLY

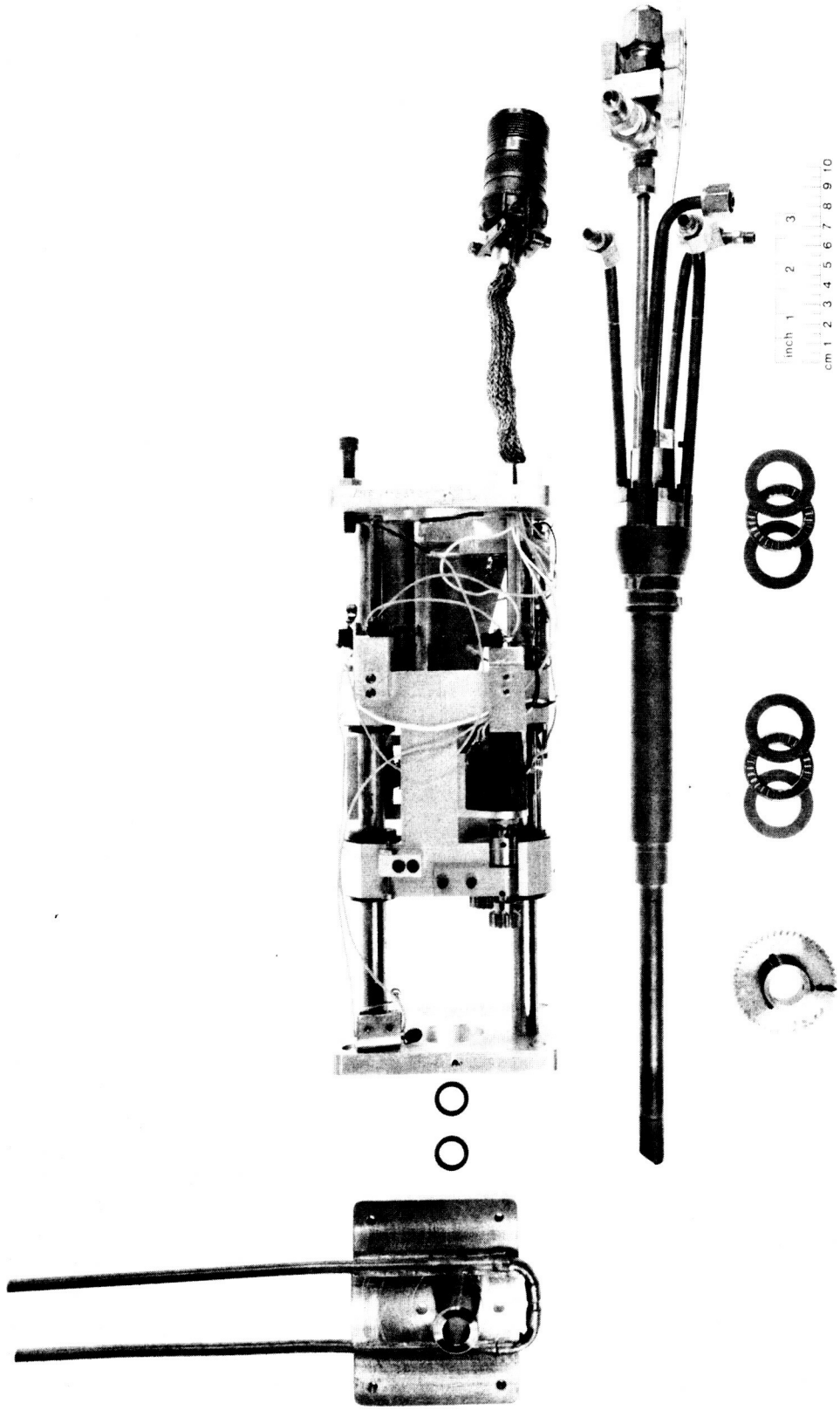

FIG. 25 PROBE ACTUATOR ASSEMBLY

the rig boss temperature, measured to reach peak temperatures of 305°C.* The high ambient temperatures and light abrasive action on the second O-ring from the sliding probe probably contributed to the deterioration. This problem was solved for the engine tests by placing the second O-ring closer to the original O-ring which is also closer to the water cooling loop on the adapter plate. This modification, has also been made on the NASA adapter plate.

When the probe was tested on the engine for over 3 hours of operation, which probably had higher base temperatures than the rig, no deterioration of the viton seals was observed.

3.6 Thermal Analysis - A finite element analysis program was run to determine the temperatures on the viewing probe ends that are exposed to the combustor flame and hot flow stream. Heat transfer rates on the exposed surfaces were taken for the worst case of 490 watts/cm^2 (3 Btu/(sec/in^2)) as discussed in Section 3.2. The film coefficients for water cooling were computed from the flow channel thickness of 0.89 mm and a water flow rate of 20 ℓ/min. A purge gas flow of 9.1 kg/hr gave the film coefficients for the gas cooled surfaces.

Figure 26 shows the element and surface temperatures for the wide angle probe tip. The computation was based on an axially symmetric approximation to the actual probe tip design. Only half of the probe tip is shown in the figure and the probe elements and surfaces are rings generated by rotation of the figure about the axis indicated. The six rectangular elements next to the rotation axis are the sapphire lens elements. The remaining elements are made of high conductivity copper. For the case shown in Fig. 26, three of the element surfaces are water cooled, as indicated in the figure. Temperatures on the cooled surfaces remain below the boiling point of the water coolant and a maximum temperature of 263°C occurs on the lens aperture surface. A program was also run for the case where only one surface element was water cooled. In this case, the water cooled surface temperature went above the boiling temperature, and maximum surface temperatures went up to 419°C.

The finite element temperatures for the narrow angle view probe tip are shown in Fig. 27. In this case, the problem was solved in three dimensions by dividing the probe tip into six slices. There is a mirror symmetry and the temperatures are only indicated for one side of the probe, the other side being the same. On the last, one sixth slice, we have an exposed end surface. The end surface temperatures are indicated on half of the probe cross section with the numbers in parenthesis. The element and side surface temperatures are given on the opposite half of the cross section. Water cooled surfaces are indicated by

*Viton, the material used for the O-ring, has a specified work temperature to 204°C, and for periods of a couple hours it can withstand 260°C.

FIG. 26 TEMPERATURES FOR WIDE FIELD PROBE TIP

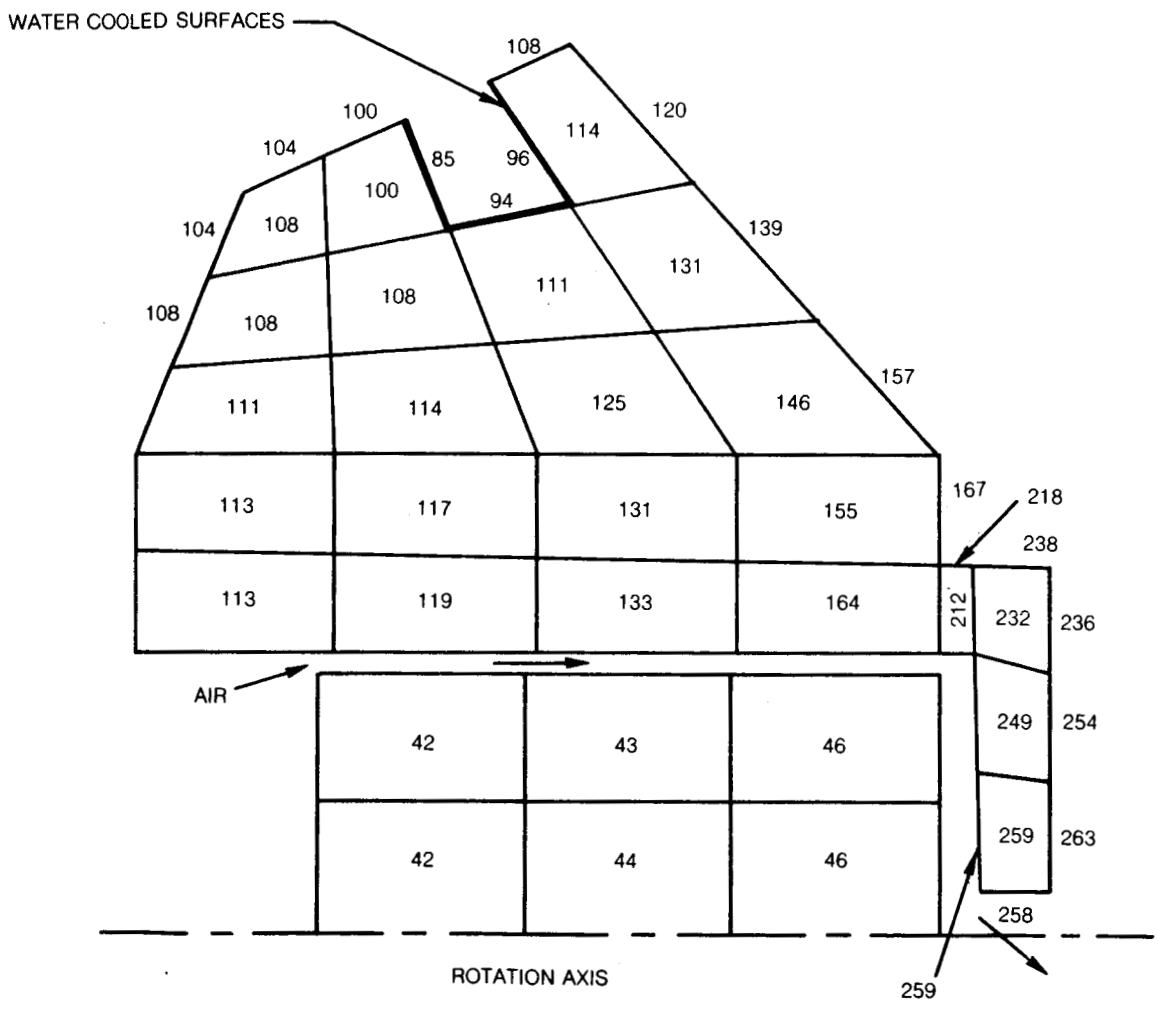

84-7-78-30

FIG. 27 TEMPERATURES FOR NARROW FIELD PROBE TIP

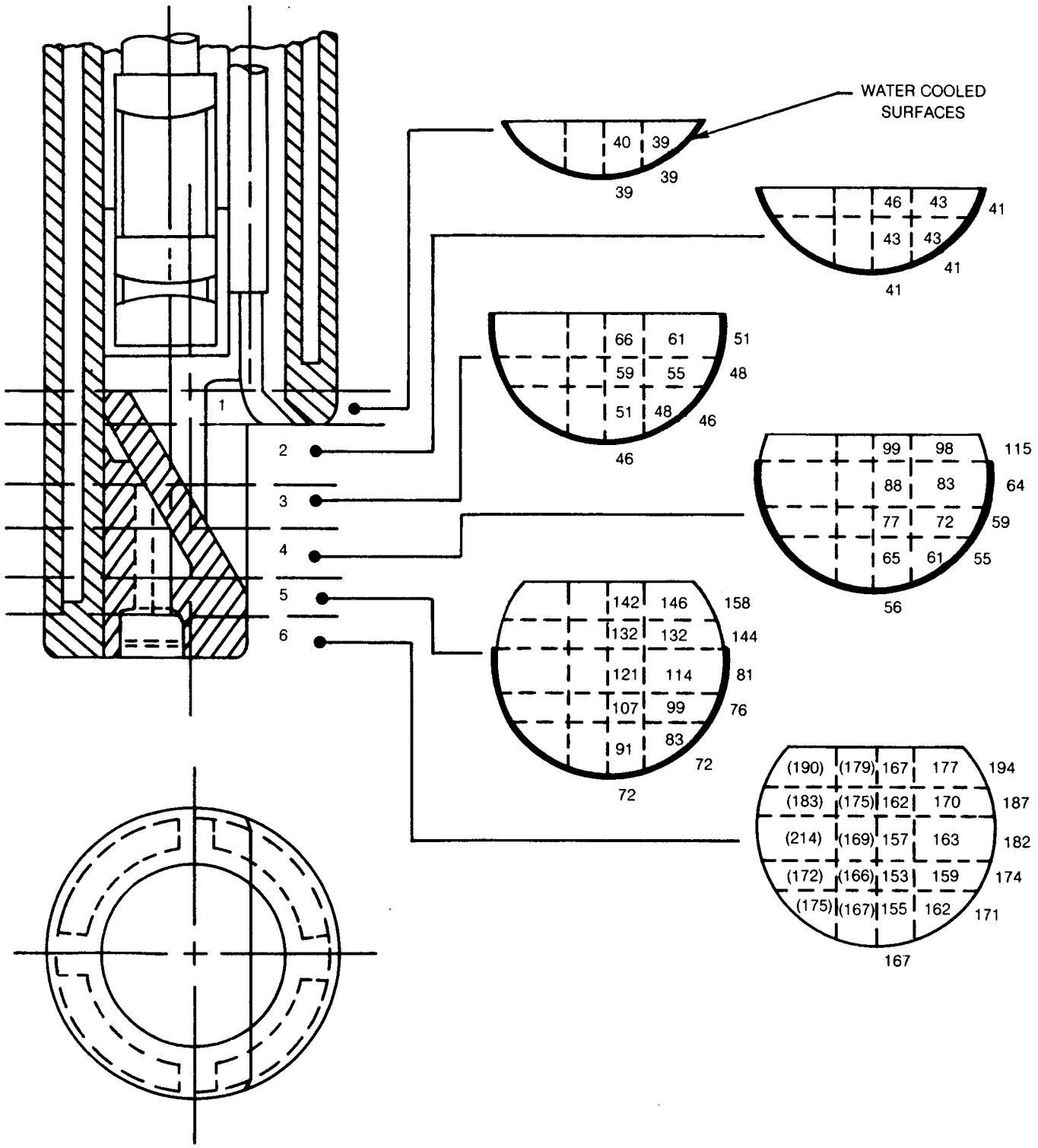

84–7–78–16

the heavy lines as in Fig. 26. Temperatures on the narrow angle probe are sufficiently low that no problems should occur. This assumes, of course, that the purge gas flow keeps the hot combustor gases from contacting the viewing mirror. Small holes could be added to the probe tips to direct additional purge gas over the end surfaces for transpirational cooling.

Maximum temperatures of 204°C were observed in both probes from thermocouples mounted in the probe tips driving combustor rig testing. For the wide field probe the thermocouple was mounted at about the positions of the 146°C element in Fig. 26. The measured temperature, then, was 58°C greater than the analysis indicated. The analysis is only approximate, however, and in actual practice the thermocouples were placed inside small steel set screws (1-72) that are screwed into the end of the probe. Since steel has a thermal conductivity 7.7 times smaller than copper, one could expect a higher temperature in the set screw.

For the narrow field probe the thermocouples were placed in the small holes in the copper mirror near the probe end at the location of the 163°C element in Fig. 27. In this case we also observed a maximum temperature of 204°C or a difference of 41°C from the analysis value. The thermocouples were located near the steel screw (2-56) that holds the mirror to the end of the probe. The presence of the steel screw could have raised the surrounding temperatures over the values indicated from the analysis where only copper parts were considered.

3.7 Gas Purge - A clean gas purge on optical surfaces exposed to the combustor gases is required in order to prevent the inevitable deposit and accumulation of soot from obstructing the view. In general, we want to prevent the mixing of clean purge gas in front of the viewing surface with the heavily soot ladened gases in the combustor. This can be accomplished by recessing the optical surface behind a small aperture and keeping the intervening chamber replenished with clean purge gas. A long recess from a small aperture may not provide the best optical design in some instances, especially if high speed optics are desired. In some cases it may be desirable to keep a sizeable window surface clean. Experiments have been done (ref. 11) that spray jets of purge gas across the exposed window surface. This method can actually make the soot deposit rate worse. The gas jets create a low pressure zone and pull the soot ladened gases into their stream to mix and deposit on the cooler window.

A purge test experiment was set-up using the preliminary test probe and laboratory combustor rig discussed previously. Purge gas was injected into the center of the probe at a port in a window mount at the proximal end of the probe. The window at the distal end of the probe, which we attempt to keep free of soot, had an exposed diameter of 5.8 mm when placed in its holder. The window and holder, which slide into the i.d. of the probe, had a series of eight passages around the diameter of the holder to pass purge gas. The purge gas was then directed onto the exposed window surface with the lip of the window holder.

Figure 21 shows the probe with the window mounted in the end. The probe was inserted into the laboratory combustor through a viewing port in the rig. The end of the probe was in the center of the combustor flame where the highest soot densities occurred. An amplitude stabilized He-Ne laser beam was sent through the opposite combustor viewing port, through the flame zone and along the axis of the probe through the two probe windows. The change in window transmission was measured before and after a combustion run of a specified length of time.

Seven different configurations to direct the purge gas flow onto the window were tested. Two of these configurations are illustrated in Fig. 28. The illustrations show a cross section of the end of the probe above the center line axis. In the first configuration tested (not shown) the gas flow was directed onto the window surface with a right angle lip. Gas flow rates were 5.7 kg/hr (12.6 #/hr). After 10 minutes of operation in the combustor the window transmission decreased by 9% or at a rate of -0.9% per min. We observed that a slower gas flow rate would increase the rate of soot deposit and vice versa.

To try and reduce the window soot deposition rate, eight channels were placed in the probe wall to pass a second flow of gas around the window holder and directly into the combustor. This configuration made matters considerably worse by increasing the soot deposition rate and reducing the window transmission by 60% in 2 min. of operation or -30% per min. The total gas flow was the same as before. In this case, contrary to before, increasing the gas flow gave a greater soot deposition rate. This was probably caused by the low pressure created by the streaming gas jets at the end of the probe. The channels in the probe wall were then filled with a high temperature epoxy to block the second air flow around the window and holder for further testing.

Figure 28 shows two typical purge flow configurations. In Fig. 28a the flow is turned gradually and leaves the window aperture through a tapered ring. On the other hand, in Fig. 28b the purge flow is turned more abruptly with a sharp edge and no taper on the outlet. In general, configurations like Fig. 28a produced significant sooting of the viewing window while those like Fig. 28b produce little or no sooting.

To investigate this effect, a small pitot tube and water monometer were used to measure the impact or total pressure across the end of the probe with purge air flowing. We found that in the configurations where the flow was turned slowly at the aperture there was a large region approaching the aperture that was below atmospheric pressure. When the flow was turned more strongly at a sharp boundary or edge the size of the region of low pressure was reduced significantly.

FIG. 28 WINDOW PURGE TESTS

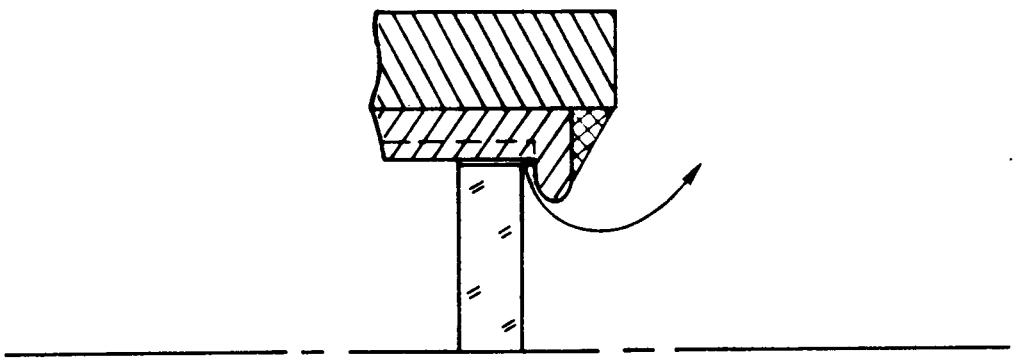

a) 23% DECREASE IN WINDOW TRANSMISSION

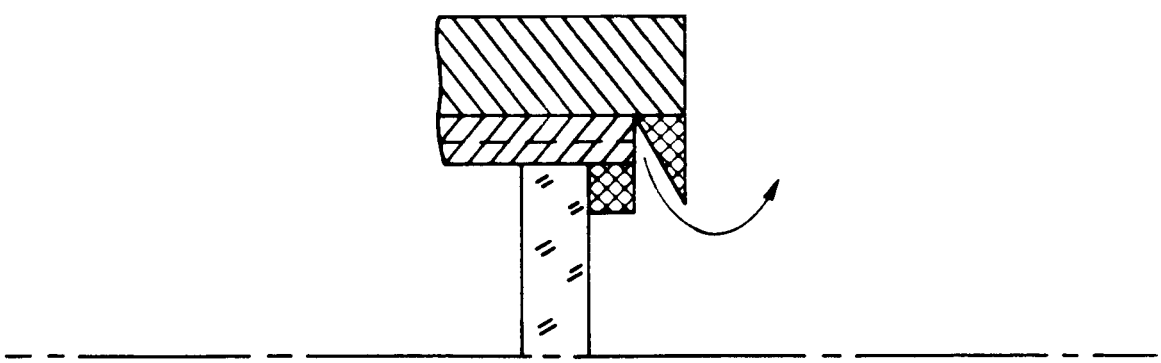

b) 0% CHANGE IN WINDOW TRANSMISSION

84–7–78–17

We also attempted to keep the window clean by removing the purge gas flow and letting the window temperature rise. This idea could work if the temperature of the window rises high enough. The walls of the viewing probe were strongly cooled, however, and prevent the window from reaching a high enough temperature to keep clean. Rapid sooting of the window was observed in all cases when the purge flow was removed.

In the wide field probe the lenses are recessed slighty behind a small viewing aperture. The aperture is constructed with a sharp boundary rather than fluted to the outside. In the case with the narrow field probe, the view turning mirror is exposed to the combustor. A large aperture or opening is required to pass the viewing angle of the lens placed upstream in the probe body. The viewing field of this probe is limited by the mirror and opening size. The purge gas in this case impacts the mirror and is directed into the combustor at the viewing angle. If excessive turbulence is not generated the purge may keep the useful part of the mirror clean, however, one could not expect the mirror purging to work as well as the purge on the wide field lenses.

The illuminating fibers are recessed to some extent in their mounting holes in the wide field probe (cf. Fig. 3), and placed near the edge and just inside the view opening in the narrow field probe (cf. Fig. 4). Purge gas flows around the fibers and into the combustor. Nitrogen is the gas used for purging the probes and is supplied from a high pressure line through a sonic flow constrictor that limits the mass flow to about 7 kg/hr provided the upstream pressure is sufficiently greater than the rig pressure. With the sonic flow constrictor we can always keep a positive nearly fixed mass flow of purge gas through the probe as the rig or engine pressure varies upwards from one atmosphere.

During the high pressure combustor tests no sooting was observed on the viewing optics used in the wide field probe, as expected. The exposed mirror in the narrow field probe, to our suprise, did not accumulate soot to the extent we expected even though the probe was placed directly into the flame and pointed upstream into the flow. In no instance was the view obstructed by soot deposits. There was usually some soot deposits around the mirror edge which can be carefully cleaned after the test run.

The illumination fibers, to the contrary, became darkened with soot soon after operation in the combustor. There were a couple instances, however, where no sooting was observed. In one case, after the last test run, one of the illumination fibers had been extended accidentally about 1 mm from its mounting hole and was exposed to the flow stream. The quartz fiber end had probably become hot enough to keep the soot from depositing.

3.8 Actuator Unit - The actuator unit supports the viewing probe, provides mounting to a rig or engine, traverses the probe in and out, and rotates the probe through angles up to 360°. The unit is remotely controlled and feedback signals are provided to indicate the probe position in depth and rotation. Figure 29 shows a photo of the probe and actuator unit assembly with the covers removed. In this figure one can see the viewing end of the wide field probe extending through the adapter plate on the right hand side. The probe is attached to a carriage that rides on two shafts with 4 ball bearing slides. A rack and pinon gear driver with a small motor attached to the frame, shown on the upper side of the photo, traverses the probe back and forth over a range of 7.6 cm. A linear potentiometer, visible in the front of the unit, indicates the probe position. Probe rotation is produced with the small motor, located in front and just behind the potentiometer, that rides along with the carriage. The potentiometer just visible underneath the carriage in the front indicates the angular position. Limit switches (not visible in the photo) prevent overranging and possible damage to the probe.

A 30 meter long cable harness connects the actuator to a remote control unit for operation of the probe from a control room. Figure 30 shows a photo of the actuator-probe assembly and the probe control unit. Water cooled covers have been placed on the actuator as shown in the photo. The water cooling tubes for the covers and adapter plate are connected in series as shown.

The angular position controls and readout for the probe rotation are shown in the right hand side of the probe control panel in Fig. 30. Two push-to-actuate button switches are used to actuate the probe rotation clockwise and counterclockwise. Angular positions from +180° to -180° are indicated with the digital meter above the switches. The rotation rate can be adjusted with the speed control. Probe insertion is actuated with the two push button switches mounted one above the other in the center of the panel. The upper button actuates the probe in, the lower button actuates the probe out. No speed control was used for the probe insertion which runs from about 0.3 cm/sec to 0.16 cm/sec depending on the rig pressure. An LED bar graph meter mounted above the switches indicates the probe position in depth to an accuracy of 0.8 mm.

On the left hand side of the probe control panel is the probe tip temperature indicator with a limit set switch, a sonic alarm, reset button switch, and three red warning lights. The warning lights indicate over temperature, insufficient purge gas flow, and insufficient probe cooling water flow. If any of the three indicators (temperature, gas, or water) are tripped on, the sonic alarm will sound and the probe will automatically withdraw. The reset button overrides the alarm system and any of the three limit switches.

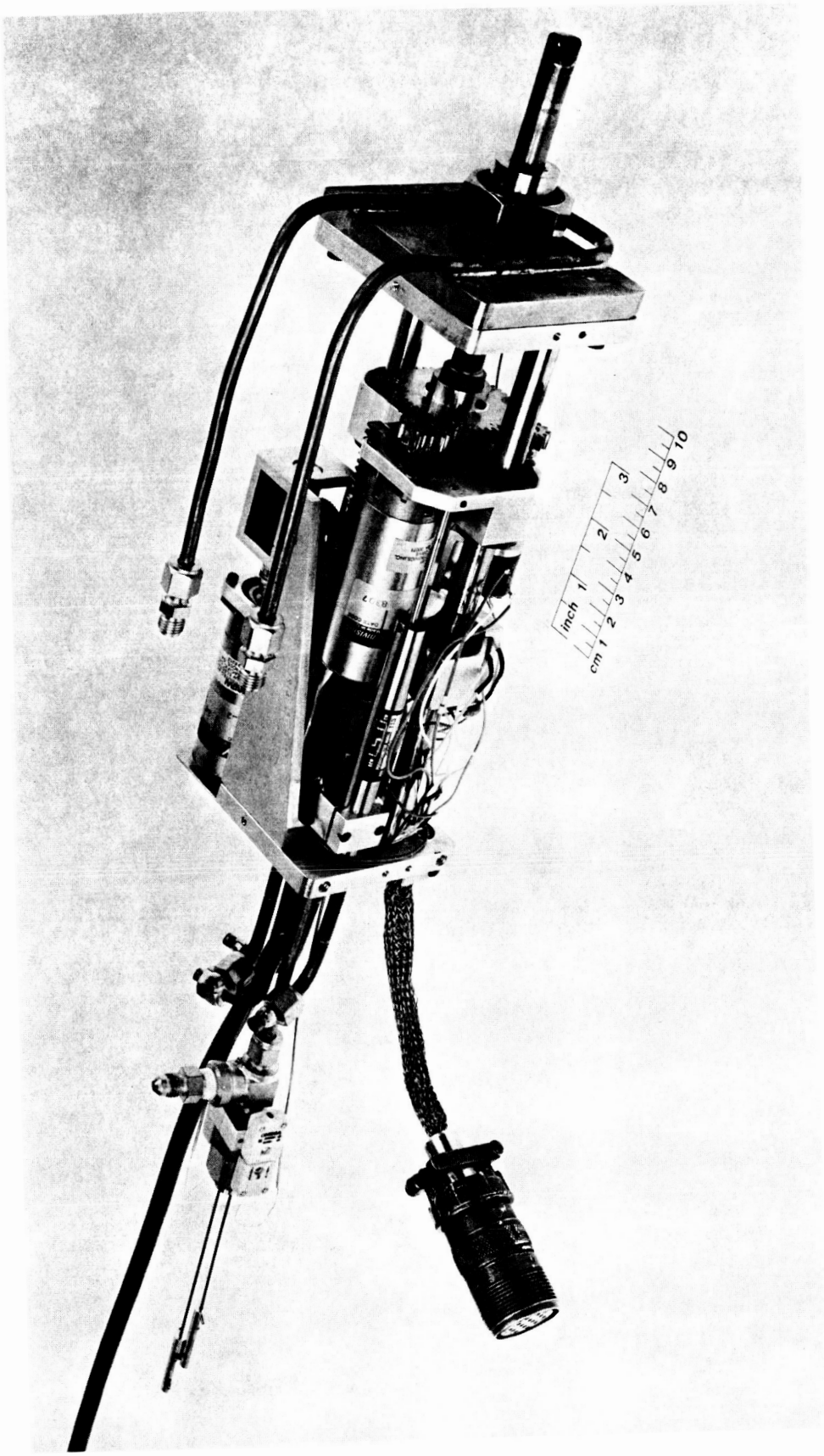

FIG. 29 COMBUSTOR VIEWING PROBE WITH COVERS REMOVED

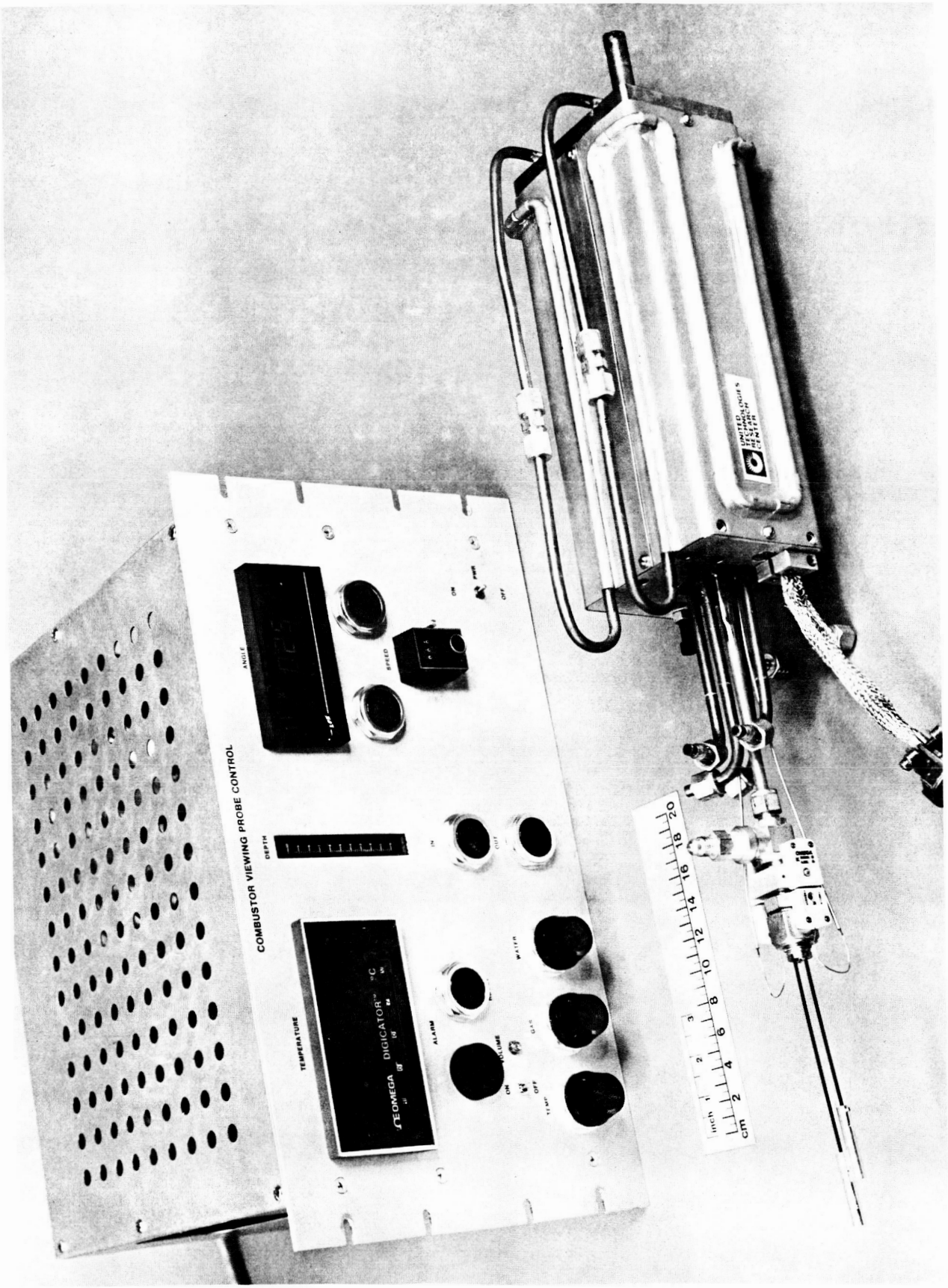

FIG. 30 COMBUSTOR VIEWING PROBE AND REMOTE CONTROL UNIT

The wires that run inside the actuator box to the motor, potentiometer, and limit switches are mounted on the moving carriage and must flex back and forth during the probe traversal. Care had to be taken in placement of the wires to prevent them from catching on moving components during actuation. We also found that the wire at some of the solder connections could fatigue and break loose after many operations. This problem was eliminated by placing heat shrink tubing supports around the wire and solder joints and using small clips for strain and bending relief at the connections where needed.

4.0 COMBUSTOR VIEWING

4.1 Introduction - One of the objectives of this program is to observe combustor liner surfaces during operation of the combustor. Being able to observe the liner would allow one to see the formation of cracking and buckling, for example. There are two principal problems in accomplishing this task - one is distortion of the view from the hot turbulent gases, and the other is the presence of the luminous flame. The distortion problem may be very difficult to solve. In a combustor the degree of distortion is not well known and it will undoubtedly vary considerably from place to place in the combustor. There are digital image analysis techniques, although somewhat elaborate, that can help restore an image from a known or estimated quantity of distortion.

The luminous flame, which is partially transparent to varying degrees, creates a problem in viewing a surface through the flame that is darker than the flame itself; namely, the contrast of the surface features can be greatly reduced. We may, for instance, be looking through a luminous, but optically thin flame at surface features. An exposure or recording set for the flame intensity will place the surface details at a much lower exposure or recording sensitivity. This effect reduces the contrast of the surface features. On the other hand, an exposure made for the reflected light levels from the surface would be overexposed or saturated by the flame. What we need is a detector with a large dynamic range so that the flame exposure can be subtracted and still leave surface details with a sizeable signal-to-noise ratio. For contrast enhancement, we experimented with wide latitude photography and digital image processing. These topics are discussed in Sections 4.5 and 4.6.

Another approach to viewing surfaces in the combustor is to discriminate against the flame signal. This can be accomplished using pulsed or modulated monochromatic illumination. Discrimination can be achieved in both the time and wavelength regimes. Successful discrimination of the flame was demonstrated in laboratory tests using pulsed laser illumination. This result is discussed in Section 4.4. There is also a discriminating technique that uses a modulated illumination light source. This technique has a scanning image detector whose sensitivity can be set to the modulation frequency. In this case each of the 80,000 picture elements are detected synchronously at the same time. Barrett et al. in ref. 12 discusses the use of an image orthicon camera in such an application. Since this was a unique device we felt that considerably more development effort would be required to implement it with combustor viewing system.

A small laboratory combustor and viewing probe were used in the preliminary test program to examine various problems that might be encountered with visualization inside a combustor. The laboratory rig and optical transmission measurements of the flame are discussed in the next Section 4.2. A discussion of optical distortion measured in the laboratory rig and observed in the high pressure combustor rig will follow in Section 4.3. We then discuss the use of illumination in Section 4.4 to enhance the view through the flame and calculate the expected ratios of optical signals from the liner surfaces to the signals from the flame for different types of illumination sources. We also show that backscattering from soot particulates is not a problem with illumination. In the last section we discuss steroscopic viewing and the results of laboratory measurements. Steroscopic viewing was not chosen for the prototype probe mainly because of the large size probes required.

4.2 Laboratory Combustor Rig - Preliminary viewing tests were carried out in a small laboratory combustor rig shown in Fig. 31. The tests were made to help resolve viewing problems that would occur with the prototype probe in a high pressure combustor. Number 2 fuel oil was used in the laboratory rig at the rate of 3.0 ℓ/hr. Air was supplied for combustion by a small fan, and the air flow rate was adjusted by a rotating vent on the inlet side of the fan. A retention head surrounded the fuel nozzle to create turbulence in the incoming air that helps retain the zone of combustion at a distance not too far downstream of the nozzle. A more complete combustion of the fuel is obtained in this way. There are six viewing ports on each side of the burner box axis. Each port is aligned with its opposite on the other side of the burner. The viewing ports have removable fused quartz windows.

The visible flame in an oil burning combustor consists mainly of a cloud of luminous soot particles generated copiously during the process of the combustion of small atomized fuel oil droplets. The particles are principally composed of carbon atoms with some hydrogen and impurities. The mean diameters of the soot particles is less than the wavelength of light, making them much better absorbers than scatters of visible radiation. Since the mixing of the incoming combustion air with the fuel spray is very turbulent, the flame is inhomogeneous and rapidly changing. In general, there is no well defined edge to the flame and the large quantities of soot particles generated in the primary combustion zone are practically all consumed by the time they leave the combustor.

The large variability in the flame density can be observed from transmission measurements made in the laboratory rig using a stabilized helium-neon laser. The laser beam was sent through two opposite viewing ports and care was taken to detect the entire beam which would spread with the turbulent distortion in the combustor. Separation of the detector from the combustor and a narrow wavelength filter eliminated flame radiation at the detector. Figure 32 shows the transmission of the laser beam through the burner as a function of time. Traces are

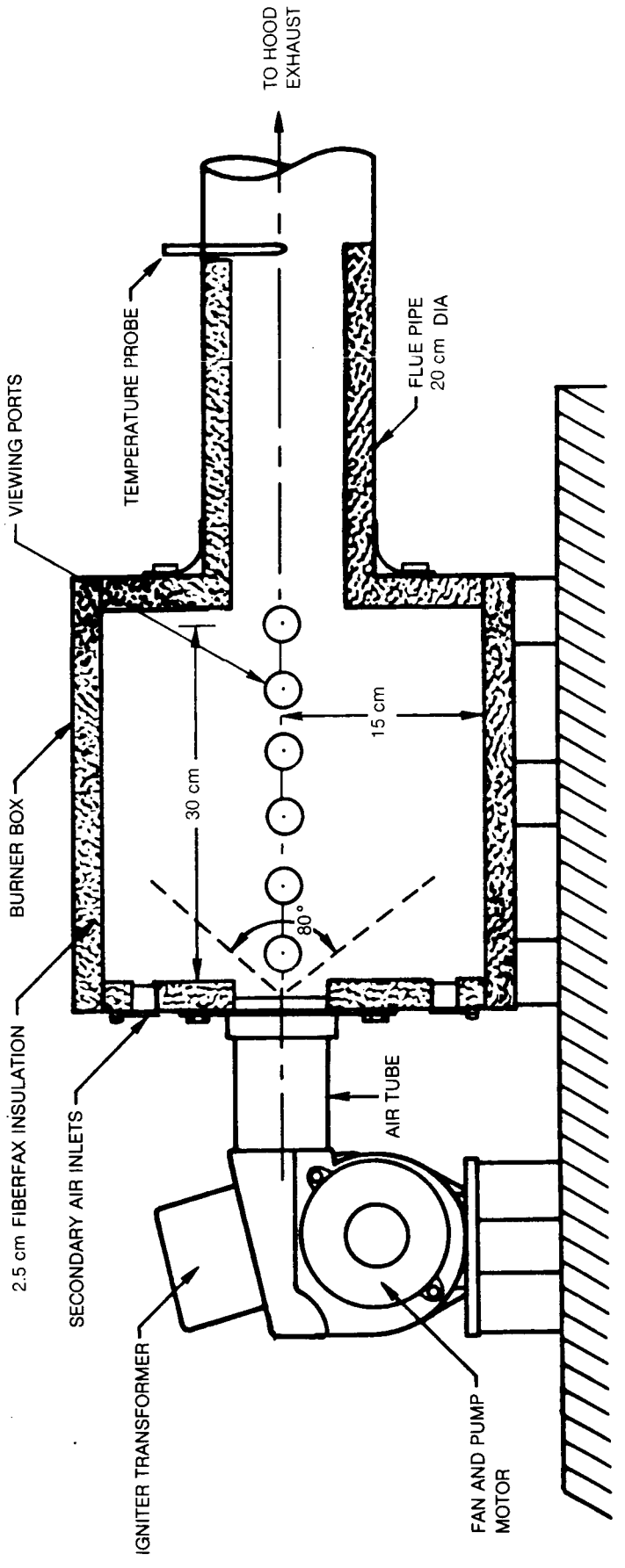

FIG. 31 OIL BURNER RIG FOR FLAME MEASUREMENTS

FIG. 32 OPTICAL TRANSMISSION THROUGH OIL BURNING FLAME

a) LEAN FUEL/AIR SETTING

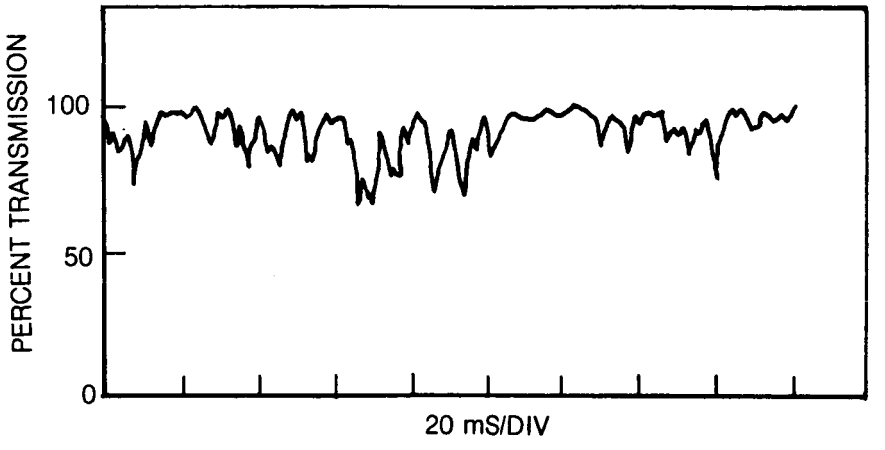

b) RICH FUEL/AIR SETTING

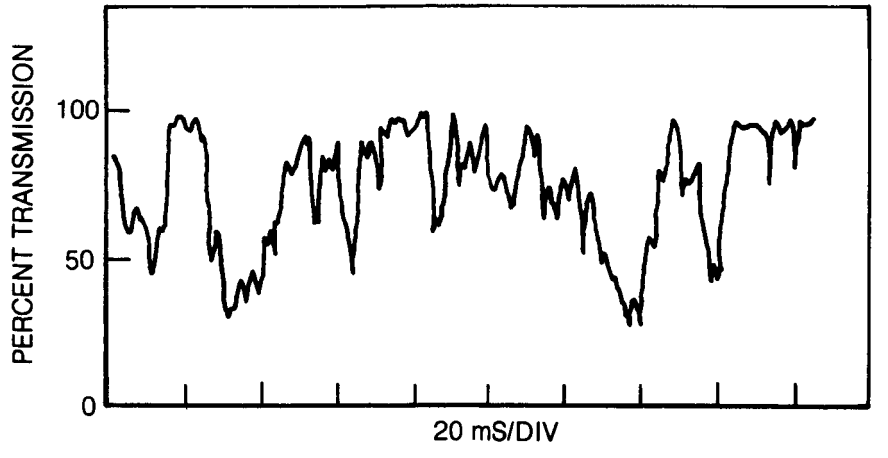

82-5-7-1

shown for two air flow settings; one slightly lean and the other rich in fuel/air. At the low air settings instantaneous transmissions can go as low as 25% and as high as 100% for brief moments. This is indicative of the very turbulent combustion process. Changes in the transmission occur on the order of a few msec. In a high pressure combustor or an engine, where the gas flow rates are much greater, the time scales would have to be reduced about 50 times. Changes in this case would take place in tenths and hundredths of a msec. Therefore, there may be favorable time intervals for viewing sections of the combustor liner when the flame density is reduced.

A small viewing probe was constructed for tests viewing through the flame at combustor liner sections. A schematic of the probe is shown in Fig. 33. Different focal length lenses and apertures were used for different fields-of-view. A short piece of image conduit carried the image away from the inside edge of the burner viewing port to a microscopic objective and view camera for magnifying and recording the image from the end of the conduit.

4.3 Optical Distortion - Turbulent mixing of combustor inlet air with the fuel spray to provide complete combustion produces cells of hot combustor gases with strong thermal gradients. The cells of hot gas move rapidly through the combustor and are mixed with cooler dilution air through holes in the side of the liner. This latter process probably enhances the fast moving thermal gradients. An optical ray traversing through such a medium is deflected by index of refraction gradients which are produced by the thermal gradients. The amount of deflection of an optical ray traversing an index gradient perpendicular to the ray is given by

$$\Delta\theta \approx -\frac{\ell}{n}\frac{dn}{dz}, \qquad (1)$$

where ℓ is the path length of the ray through the gradient. The gradient is in the direction z, perpendicular to ℓ. The displacement of the ray in the image plane of a viewing lens is then

$$\Delta z \approx f\,\Delta\theta, \qquad (2)$$

where f is the focal length of the lens. We can relate an index gradient to a thermal gradient through the ideal gas equation and the fact that the index of refraction is related to gas density by

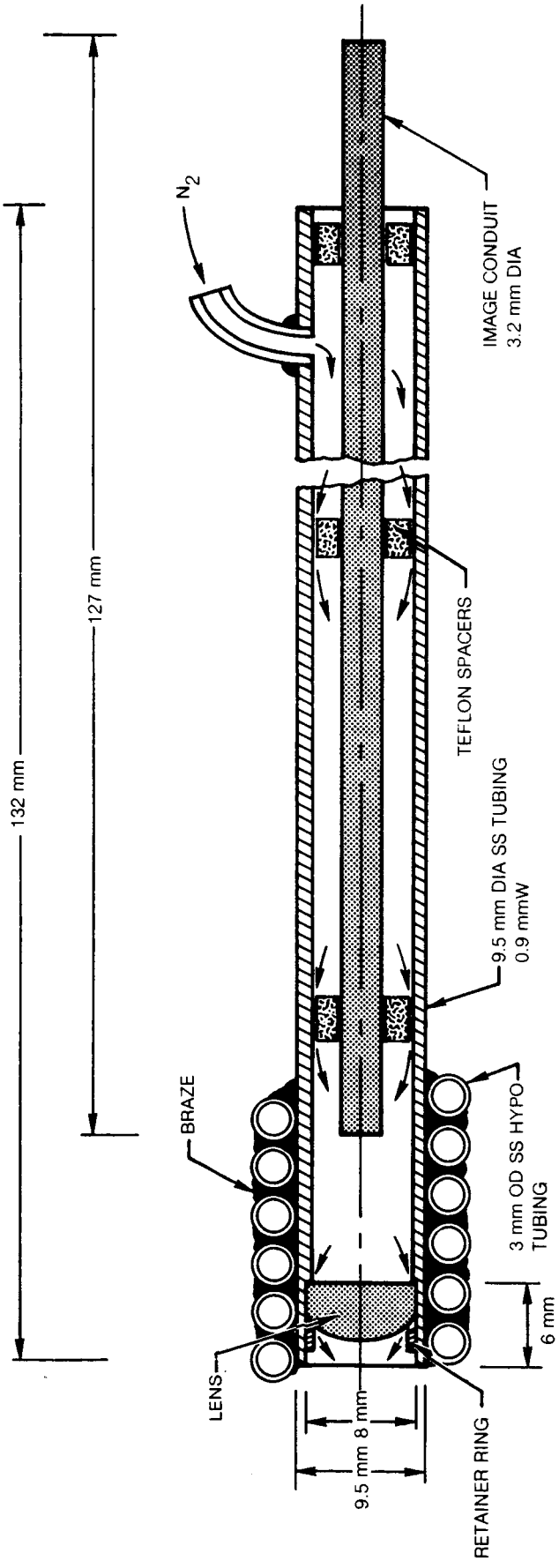

FIG. 33 VIEWING PROBE FOR LAB BURNER RIG

82-3-90-15

FIG. 34 OPTICAL DISTORTION IN COMBUSTOR

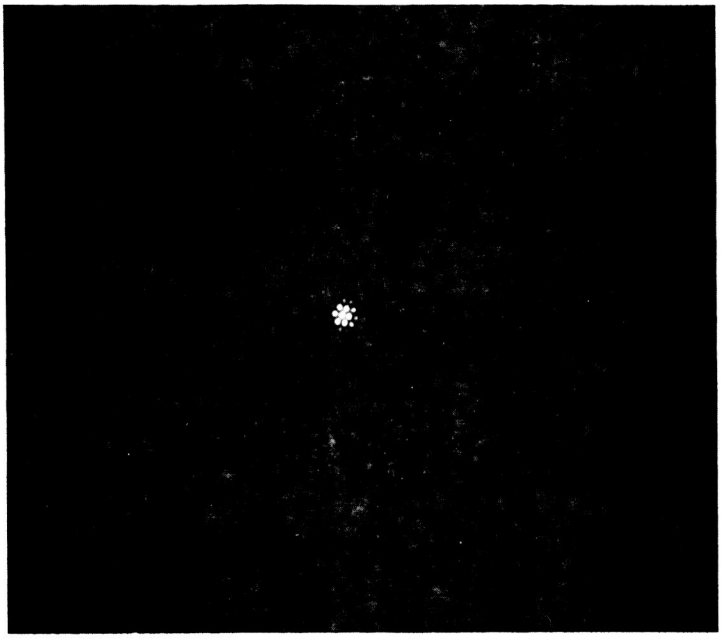

a) COMBUSTOR OFF

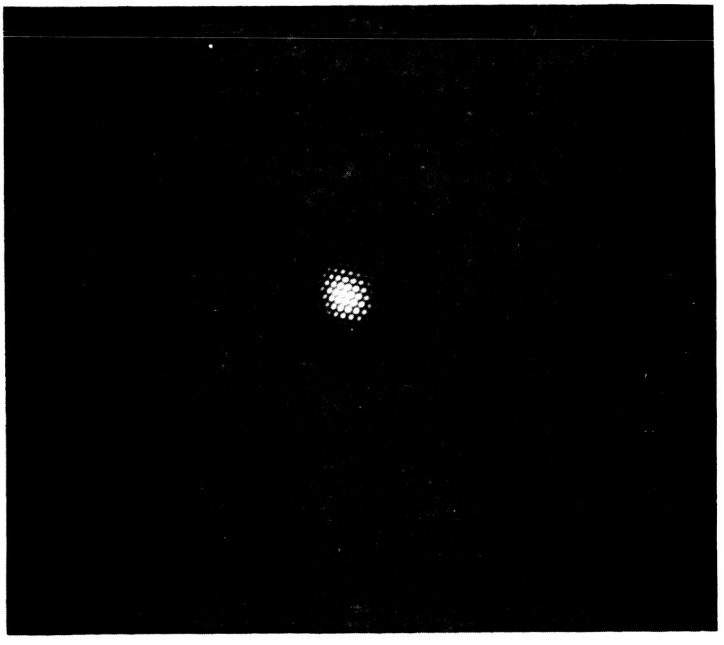

b) COMBUSTOR ON

$$(n-1) \sim \rho.$$

Using the ideal gas relation.

$$\rho = pm/RT,$$

where p is the pressure, m the molecular weight, R the universal gas constant, and T the absolute temperture, we can relate the index at some pressure P and temperature T to normal conditions of pressure and temperature, $(n-1)_o, P_o, T_o$. Standard handbooks list,

$(n-1)_o = 2.78 \times 10^{-4}$ at λ 500 nm

$P_o = 1$ atm

$T_o = 288$ K.

The index at some P and T is then given by

$$n-1 = 8.01 \times 10^{-2} P/T. \qquad (3)$$

where the pressure is in atmospheres and the temperature in Kelvin.

A test was performed with the laboratory combustor to measure the optical distortion of a ray traversing through the burner box, perpindicular to the flow. A 250 μm pinhole, placed in one of the viewing ports, was illuminated from behind by a high intensity lamp. The aperture was imaged at the opposite viewing port, 35 cm away, with the small viewing probe (cf. Fig. 33) and a 27 mm focal length lens. At the output end of the probe the pinhole image was magnified with a microscope objective and recorded with a 4x5 view camera. A picture of the pinhole image is shown in Fig. 34a. Note that the magnification is sufficient to see the individual fibers in the image conduit which are 10 μm in diameter. The pinhole image is 30 μm in diameter. Figure 34b shows how the image is distorted when the combustor is in operation. Since the flame was not nearly as bright as the lamp, no exposure of the flame was recorded. The exposure times for Figs. 34a and 34b were 1/60 sec and 1/30 sec respectively. The average beam deflection from the moving thermal gradients or hot cells can be estimated from Fig. 34b. If we assume that the deflections add up in a random fashion as the sum of squares, then the distortion which spreads the image diameter from 30 μm to 70 μm is about 63 μm. Since the rays are deflected in both directions the ray deflections are 31.5 μm. This corresponds to deflection angles of 1.2 mrad when we divide by focal length of the lens (26 mm).

If we assume that the temperatures ranged from ambient (300 K) to the maximum combustor temperature (2000 K), we can estimate the index gradient from Eq. (3) as

$$\left(\frac{\Delta n}{\Delta Z}\right)_{\text{lab comb.}} \approx \frac{(n-1)_1 - (n-1)_2}{\Delta z} = \frac{2.3 \times 10^{-4}}{\Delta z} ,$$

where Δz would represent the length of the thermal gradient or cell size.

In the high pressure combustor rig with 15 atmospheres of pressure, inlet temperatures of 673 K, and maximum combustor temperatures of 2400 K

$$\left(\frac{\Delta n}{\Delta Z}\right)_{\text{HP comb.}} \approx \frac{1.3 \times 10^{-3}}{\Delta z}$$

Therefore, if the cell sizes (Δz) are the same one could expect the optical distortions to be about 5.6 times greater in the high pressure (HP) combustor rig as compared to the laboratory combustor results. Thus, we may expect deflections in the range of 6.8 mrad in the HP combustor. For a 30 atmosphere engine combustor one may expect optical distortions about 11 times greater (13.7 mrad) than we observed in the laboratory rig.

Figure 35 shows two photos of an air mixing hole in the liner used in the high pressure (HP) combustor tests. The view of the hole is from the inside about 6 cm away. The 60° FOV lens was in the probe. Using a digital image analysis routine, an intensity profile was taken across the air hole in each of the two photos. The contour profile position is indicated with the vertical bar shown in the photos. Note that with the lamp illumination the hole edges are more clearly defined than with the flame illumination from the combustor. The edges are distorted from the temperature gradients that pass by the hole during the video exposure (1/30 sec). Using the fact that the hole is 12.7 mm in diameter and 60 mm away from the viewing lens, we can estimate the distortion in Fig. 35b to be about 8.4 mrad. This distortion is larger than we estimated above, but is in the range of variability that one may expect at different locations and time intervals inside a combustor. Also, the turbulent cell size could be smaller in the HP rig.

FIG. 35 CROSS SECTION PROFILES OF AIR MIXING HOLE

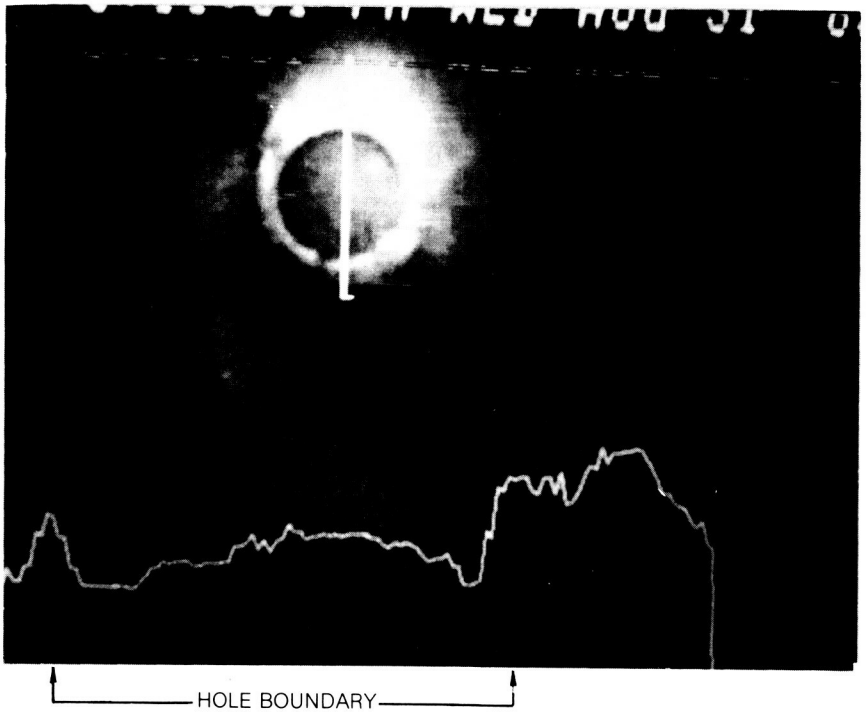

a) LAMP ILLUMINATION: COMBUSTOR OFF

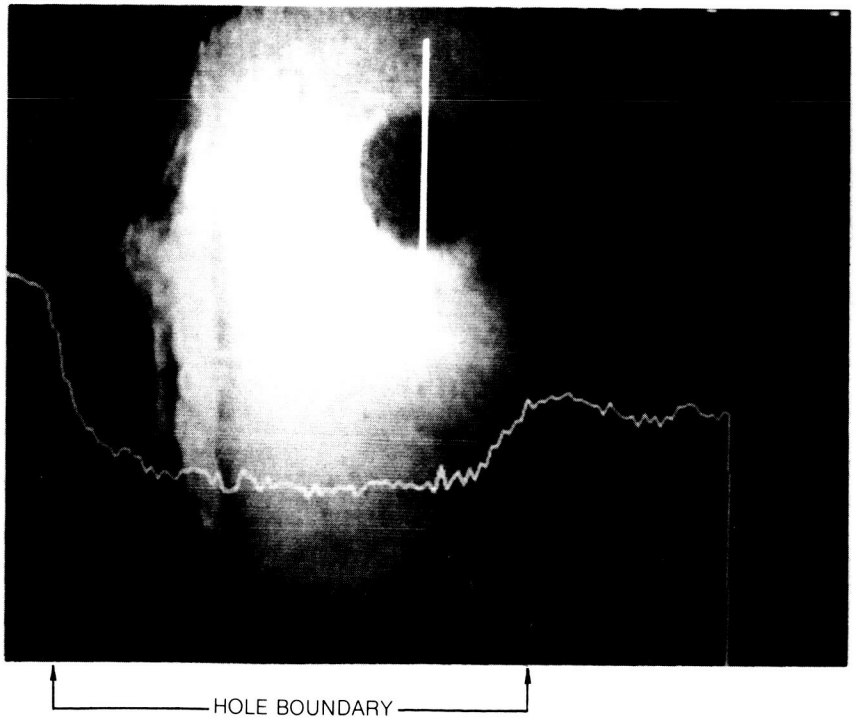

b) FLAME ILLUMINATION: COMBUSTOR ON

84–7–78–18

The amount of optical distortion one sees at the image plane of the viewing lens depends on the lens focal length (cf. Eq. (2)). And of course, the lens focal length is related to the field-of-view. With the high resolution 13° FOV lens (focal length 10 mm) the distortion would be 84 μm in the image plane for 8.4 mrad angular distortion. This amount of distortion is greater than the observed 20 μm resolution distance transmitted by the image guide and an image would appear significantly distorted. For a 90° FOV lens (focal length 2.17 mm) the distortion would be 18.2 μm in the image plane of the lens. In this case the image would appear only slightly distorted for the on axis views and would hardly affect the already highly lens distorted views at the full field angles.

4.4 Illumination

4.4.1 Background - Illumination light was provided with the viewing probe for two reasons: to illuminate the dark interior of the combustor liner when the combustor is off and to aid the view in the presence of a luminous flame when the combustor is on. There are several different kinds of sources for illumination. The choices range from coherent to incoherent sources with operating conditions of high power pulsed, modulated, or continuous duty. Each type of illumination source is different mechanically, spectrally, and in its coupling to optical fiber elements. The question of which source was best to use for the viewing system was answered with two sources: a continuous broadband source for inspection when the combustor is off and a pulsed laser source for viewing in the presence of the flame.

One of the problems that we initially expected to encounter was the possibility of backscatter glare from particulates in the flame. We demonstrate in the next section that backscatter glare is not a problem. In the sections following we will compare, by way of model calculations, the radiation received by the viewing lens from the illumination light reflecting from the liner surface to the direct flame radiation for different types of sources. This will give us a comparison of the different sources to determine the best source and wavelength to use for the illumination. Experimental results will be presented for the illuminating sources.

4.4.2 Backscatter Glare - When we try to view the liner surface through the flame with an illuminating light source, a small fraction of the light will be backscattered towards the viewing receiver by the soot particles in the flame. The backscattered light may give a glare to be reflected light signal from the liner surface that we want to record. The intensity of the backscattered light into the receiver aperture is given by the expression

$$I_{scat} = I_o(\Omega_i/8\pi)(Q_{scat}/Q_{ext})(1-\tau^2),$$

where I_o is the emitted intensity at the illuminating fiber, Ω_i is the solid angle of emission from the illuminating fiber, Q_{scat} the scattering efficiency, Q_{ext} the extinction efficiency, and τ the transmission through the soot cloud. For the derivation see Appendix 1.

The diffusely reflected illumination intensity from the liner surface into the receiver aperture can be shown to be

$$I_{refl} = I_o(\Omega_i/\pi)r\ \tau^2$$

where r is the reflectivity of the liner surface. This result is also derived in Appendix 1. We can then compare the size of the two signals by taking the ratio

$$I_{refl}/I_{scat} = 8r(Q_{ext}/Q_{scat})[\tau^2/(1-\tau^2)]$$

The extinction and scattering efficiencies, Q_{ext} and Q_{scat}, can easily be calculated in the limit where the particle diameters are much less than the wavelength of light. Using the complex index of refraction m=n(1-ik) for the soot particles, it can be shown (ref. 13) that

$$Q_{ext}/Q_{scat} = \frac{9n^2k}{x^3\{[n^2(1-k^2)-1]^2+4n^4k^2\}}$$

where $x=\pi D/\lambda$ and D is the particle diameter. Typical soot has m=1.57(1-0.34i) at λ550 nm (ref. 14). Using this value for the index of refraction and a reflectivity of 0.7, the reflected to scattered signal ratio becomes

$$I_{refl}/I_{scat} = 0.32(\lambda/D)^3[\tau^2/(1-\tau^2)].$$

For a wavelength of 0.58 μm and a mean particle diameter of 0.04 μm, a typical mean value for soot particles in the primary combustion zone (ref. 15) and flame transmissivities of 30%, the reflected intensity is 96 times greater than the scattered intensity. At greater transmissions and for smaller particles the ratio becomes even larger. Only for very dense clouds of soot in the flame or

with larger soot particles ($\lambda/D \leq 2$) will the scattered intensity become equal to the reflected intensity. In the typical case, then, we do not expect backscatter glare from the flame to be a problem.

If backscatter glare does become a problem, it can be eliminated or reduced with the use of polarized illuminating light and a crossed polarizer at the receiving aperture (ref. 16). The soot scattered light is polarized in the same manner as the incident light and will be removed at the receiver by the crossed polarizer. The surface reflected light, however, consists of multiple reflections and will have a certain fraction of the crossed polarization present. Optical multimode fibers used in the viewing probe depolarize light signals. In order to implement polarization into the illumination, we would have to place the polarizing elements at the distal end of the viewing probe.

In tests made with pulsed laser illumination, to be discussed in Section 4.4.4, we viewed liner surfaces through flame regions of different soot particle densities. The laser illumination is considerably brighter than the flame luminosity so that film exposure can be set to record the reflected laser illumination, but not the flame. Figure 41 shows a good example of an exposure taken with some dense regions of soot. Even where regions of soot density are great, we do not see any backscatter of laser light. Instead we see only a dark cloud. This result is probably due to the fact that the absorption of light by the soot is much greater than the scattering and verifies the fact that the mean soot particle diameter is smaller than the wavelength of the illuminating light.

4.4.3 Incoherent Illumination - Several incoherent sources were considered for use with the viewing system. Tungsten-halogen incandescent lamps have color temperatures up to 3200 K. The spectral distribution of xenon and mercury arc lamps consists of resonant lines superimposed on a thermal radiation continuum. The xenon lamp operates at a 6000 K color temperature and is used for solar simulators. The mercury arc lamp has very bright spectral line emissions in the blue-green and uv part of the spectrum. As a consequence, the mercury lamp was chosen for the viewing system, since we wanted as much visible light as possible for photographic recordings.

Color temperatures of flames in combustors can range up to 2400 K. It may be possible to see through thin regions of flame if the illuminating source has a higher color temperature than the flame; especially, if we can take advantage of the large difference in brightness in the blue region of the spectrum. We can calculate the intensity of the flame light at the viewing lens aperture for a model system. The intensity of light per unit wavelength from the luminous flame at the viewing lens aperture is given by

$$I_f = \Omega_r(1-\tau)N(T_f),$$

where Ω_r is the solid angle of the viewing lens ($\Omega_r \approx \pi\ (FOV/2)^2$), τ the wavelength dependent transmissivity through the flame ($1-\tau$) is the absorption or emissivity of the flame), and $N(T_f)$ is the blackbody spectral radiance at temperature T_f in watts/cm^2/μm/steradian (cf. Appendix 2).

The transmission through the flame is given by

$$\tau = \exp\ (-k_\lambda L)$$

where L is the pathlength through the flame and k_λ a wavelength dependent factor given by Dalzell and Sarofim (ref. 14). The wavelength dependence of k_λ has a factor of $1/\lambda$ taken from Mie theory and another factor whose λ dependence depends on the composition (H/C ratio) of the soot particles. Empirically $k_\lambda \sim 1/\lambda^\alpha$ where α can have values from 1 to 2. We measured α values of 1.2 in our laboratory rig under another program.

The spectral irradiance in watts/cm^2/μm on the liner wall from an illuminating source at temperature T_i and emitting area A_i would be

$$H = \Omega_i\ \tau_i\ N\ (T_i)$$

where

$$\Omega_i = A_i/R^2$$

is the solid angle to the emitting area A_i at range R, and $N(T_i)$ is the spectral radiance at temperature T_i. We neglect the loss in the illuminating fibers which is very small in the wavelength region of interest. The illumination light is diffusely reflected to the receiver from the liner wall and again passes through the flame with transmission τ. The light intensity per unit wavelength at the viewing lens aperture from the illumination source would be

$$I_i = \Omega_r\ r\ \tau\ H/\pi$$

$$= \Omega_r\ \Omega_i\ r\ \tau^2\ N(T_i)/\pi,$$

where r is the reflectivity of the liner surface and Ω_r the solid angle of the receiver.

The ratio of reflected illumination intensity to the flame intensity at wavelength λ would then be

$$I_i/I_\delta = r(\Omega_i/\pi)\ [\tau^2/(1-\tau)]\ \exp[C_2/\lambda\ (1/T_f - 1/T_i)], \qquad (4)$$

where the exponential factor gives the ratio of the two blackbody radiance values. To get a clear view of the liner surface, we want the illuminating intensity at the viewing lens to be greater than the flame intensity. This result would be hard to achieve except for optically thin flames (i.e., τ close to unity), because of the small solid angle factor from the illuminating aperture (Ω_i). The exponential factor is greater than unity when the illuminating source temperature is greater than the flame temperature; and we can see that one would want to use short wavelengths to take advantage of the higher radiance of the illuminating source. The wavelength dependence of the transmission factor (τ) favors longer wavelengths, however, and the optimum wavelength, if there is one, would have to be calculated.

Consider a model of the viewing system where T_f = 2400K, T_i = 6000K $\Omega_i/\pi = 1.56 \times 10^{-4}$, and for simplicity we will take the illuminating angle to just fill the field-of-view ($\Omega_i = \Omega_r$). The reflectivity of the liner surface can actually vary with temperature and oxidation state; we will take a reflectivity of 0.7 which would be the highest expected. A more realistic value may be half this reflectivity. The wavelength dependence of the transmission is given by

$$\tau = \exp\ (-k/\lambda^{1.2}) \qquad (5)$$

In equation 5 we redefined the k parameter from the previous expression for τ in order to explicitly represent the wavelength dependence. The k parameter now includes the dependence on length. We can choose the transmission value as a parameter and plot the ratio, equation 4, as a function of wavelength. Figure 36 shows a plot of the intensity ratio in dB for a 6000K arc lamp illuminating source at flame transmissions of .1, .3, .5, .7 and .9. From this figure we see that only for very thin flames and deep blue wavelengths will the illumination intensity approach that of the flame. Unfortunately, the image transmission bundle of fibers have high losses for the blue wavelengths and we cannot take advantage of this portion of the spectrum. In any event, the light from the flame itself on the liner wall will be more intense than the illumination light in this case because the flame, even though it is not as bright as the illumination from the end of the fibers, has a much larger emitting area and can produce a larger irradiance on the liner surface. As a consequence, the arc lamp illumination is not useful for combustor viewing when the flame is on, and is used exclusively for viewing inside the dark combustor when it is not in operation. With the arc lamp illuminator we can get a comparison liner view before and after a run.

FIG. 36 RATIO OF REFLECTED ILLUMINATION TO FLAME INTENSITY WITH A SOURCE TEMPERATURE OF 6000 K. CURVES WITH DIFFERENT FLAME TRANSMISSIVITIES ARE INDICATED

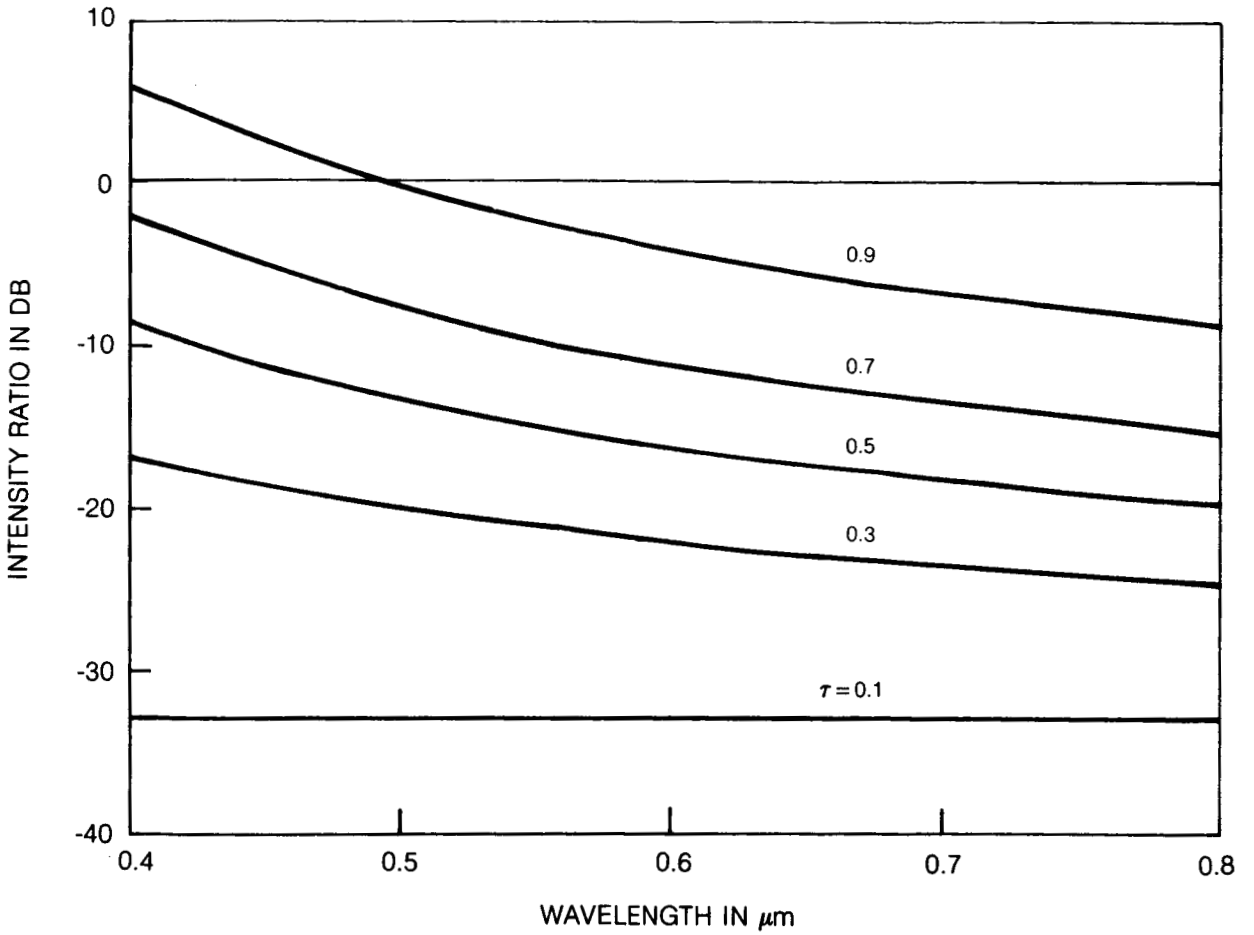

84-7-78-19

Pulsed illumination from a xenon flashlamp can have color temperatures up to 12,000K for times on the order of a msec. A plot of the illumination and direct flame intensity ratios for the 12,000K radiator is shown in Fig. 37. This lamp source provides an improvement over the arc lamp but is still not intense enough in the green to red portion of the spectrum for moderate flame densities. The best answer to viewing through or in the presence of a flame is to use a pulsed laser source, and this will be discussed in the next section.

It was interesting to note that color photographs taken with the viewing system and a mercury arc lamp came out green. This came about from the poor transmission by the image bundle of the strong blue emission from the lamp; only the intense green lines were recorded. For a video camera, whose response is peaked in the near infrared, a xenon arc lamp may be a better illumination source. We compared a 75 watt xenon lamp with the 200 watt mercury lamp in the viewing system, and got about equivalent results with the video camera.

Exposures made with the mercury arc lamp on liner surfaces at 10 cm distant from the viewing lens were typically 1/8 to 1/15 sec with 400 ASA film. The viewing lens F numbers were 3 and 3.8 for the tests; and we had about 1/2 watt of optical power from the end of the illuminating fibers.

4.4.4 Laser Illumination - Coherent laser illumination has a few advantages over incoherent illumination. First the optical power can be easily coupled into fibers without a large sacrifice of the source emission power; then, the light source is very monochromatic so that wavelength filtering can be used to discriminate against the wide spectral distribution of the flame, and most importantly, we can send a great deal more optical power through the fiber delivery system with a laser source. One of the problems with a laser source for illumination is the speckle pattern produced by the coherent light in the illuminated surface. Moreover, coherent light from a multimode fiber will also produce a modal interference pattern that may make viewing more difficult especially if the interfering modes produce large cells with dark boundaries. The speckle and modal patterns can be shifted about by variation of the beam angles at the input to the fiber. By scanning the input angles we can average out the speckle patterns. This technique would work for a continuous laser source, but would be hard to apply to a short pulse laser system due to the fast scanning speeds required.

To determine how well the illumination systems work in the presence of a flame, we can calculate the intensity ratio of the illumination light at the viewing lens aperture after it has traveled through the flame and diffusely reflected from the liner surface to the direct flame intensity in the field-of-view of the illumination. The spectral irradiance in watts/cm^2/μm on the liner surface at distance R from a laser source of power P_L emitting from a fiber and into solid angle Ω_i is given by

FIG. 37 RATIO OF REFLECTED ILLUMINATION TO FLAME INTENSITY WITH A SOURCE TEMPERATURE OF 12000 K. CURVES WITH DIFFERENT FLAME TRANSMISSIVITIES ARE INDICATED

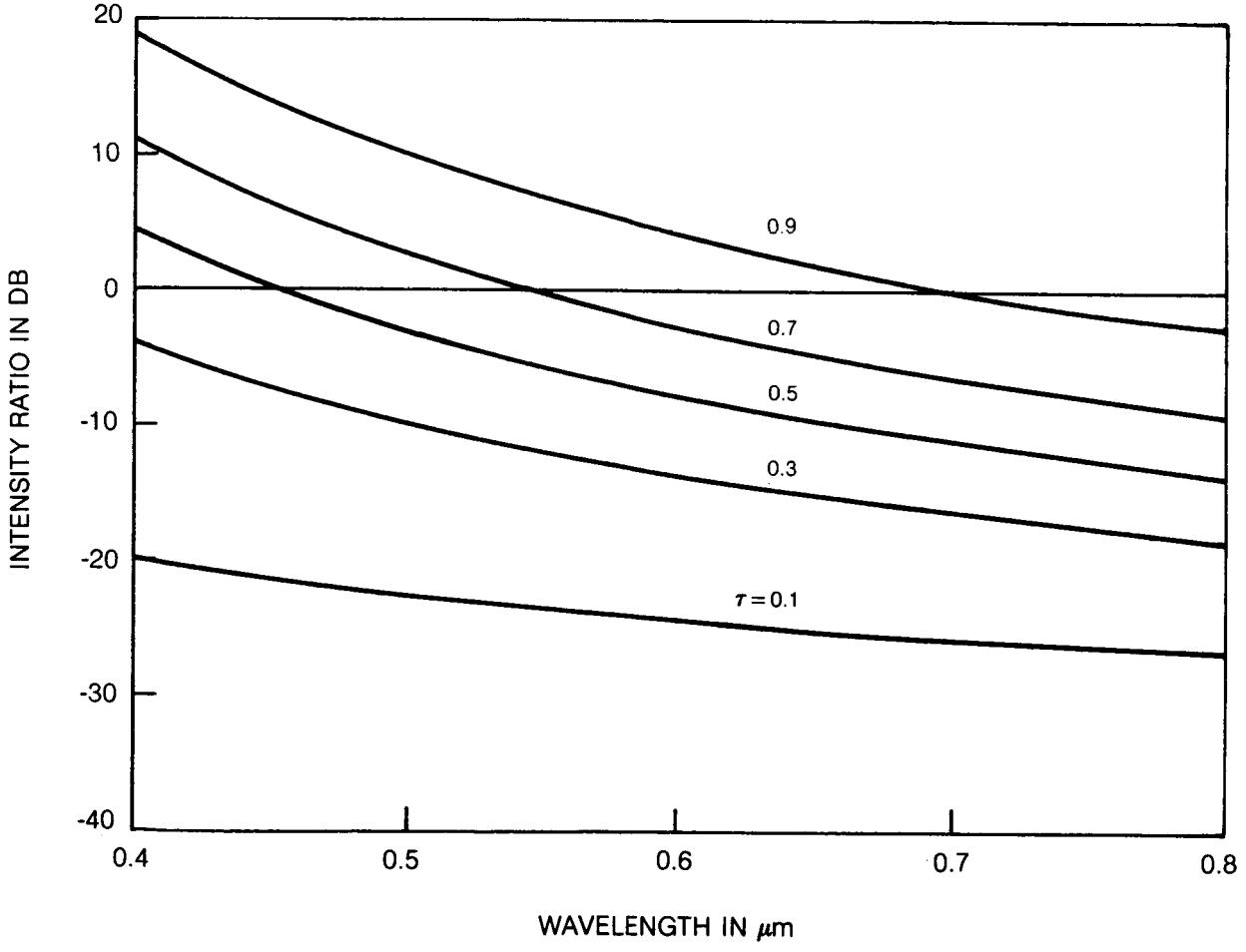

84-7-78-20

$$H = P_L \tau/\Omega_i R^2,$$

where τ is the wavelength dependent transmission through the flame (cf. Eq. 5). After a diffuse reflection from the surface and a retransmission through the flame, the intensity of the illumination at the viewing aperture is then,

$$I_i = H r \tau \Omega_i/\pi = P_L \tau^2 r/\pi R^2.$$

The illumination intensity at the viewing aperture in the wavelength passband $\Delta\lambda$ from the flame is given by

$$I_f = \Omega_r (1-\tau) N (T_f) \Delta\lambda.$$

We take $\Omega_r = \Omega_i$ as before and

$$N (T_f) = (C_1/\lambda^5) \exp(-C_2/\lambda T_f)$$

The ratio of the laser illumination intensity to the flame intensity at the viewing aperture is given by

$$I_i/I_f = (P_L \lambda^5 r/\pi A \Delta\lambda C_1) \left[\tau^2/(1-\tau)\right] \exp (C_2/\lambda T_f)$$

where A is the area illuminated by the core of laser light emitted by the fiber ($A = \Omega_i R^2$), and C_1 and C_2 are the first and second radiation constants.

If we consider typical values for a continuous wave laser with a 5 watt emission, a reflectivity of 70%, an illumination area of 28 cm^2 (fiber NA = .3, R = 10 cm), a wavelength bandpass of 10 nm, and a flame temperature of 2400 K, we obtain the curves shown in Fig. 38 for the intensity ratio versus wavelength for different values of flame transmissivities indicated on the curves. For this case we have more illumination intensity than flame intensity for transmissions greater than 70% at the blue-green wavelengths. Since the reflectivity chosen was probably the highest to be expected, the use of this type of illumination for viewing through flames would be marginal and helpful only for optically thin flames.

FIG. 38 RATIO OF REFLECTED 5W LASER ILLUMINATION TO FLAME INTENSITY AT DIFFERENT FLAME TRANSMISSIVITIES

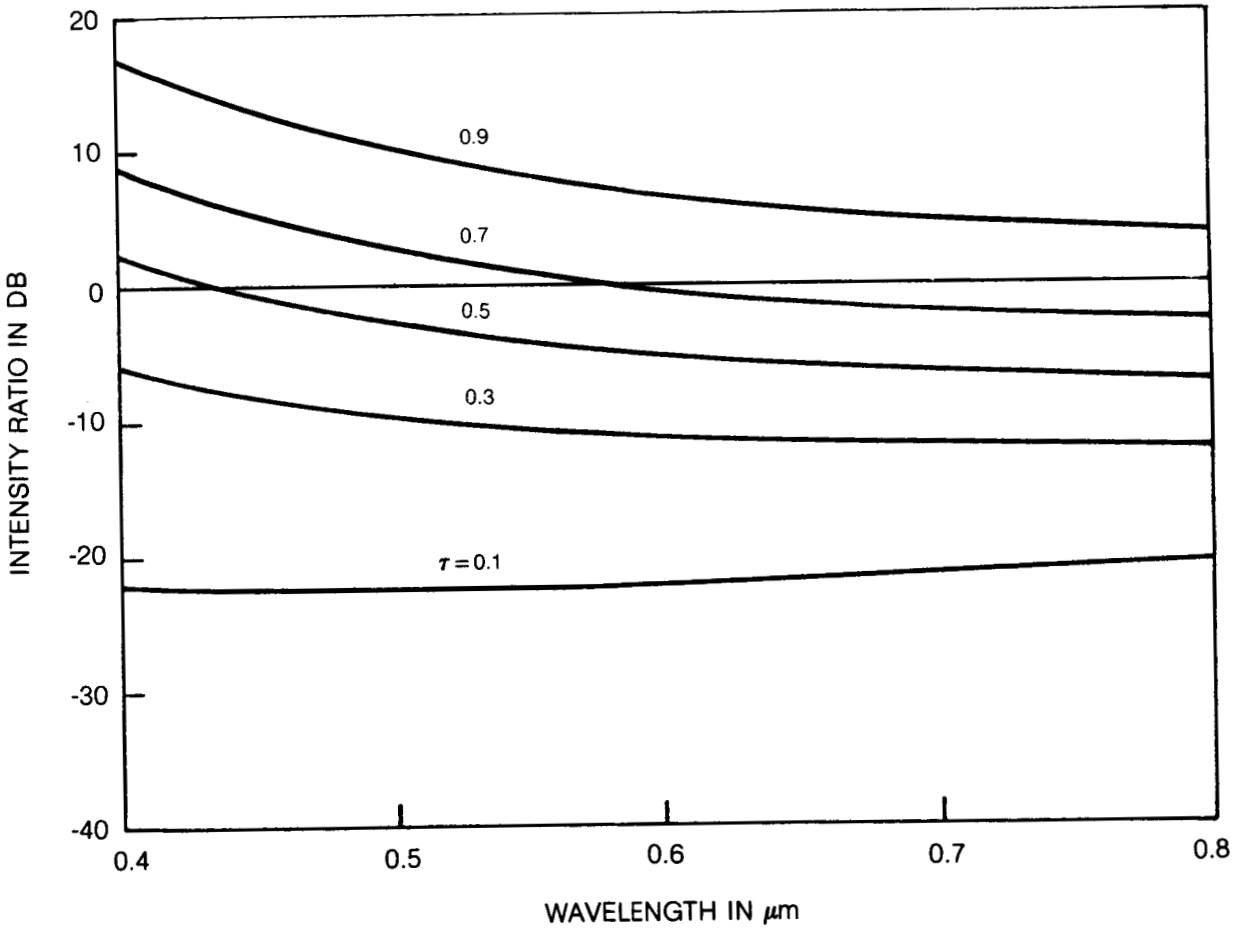

84-7-78-21

With pulse laser illumination we can transmit power levels of 10^5 watts through large core diameter fibers with sufficient energy for camera exposures. To make full use of the pulse laser illumination, however, we have to make the exposures only during the time the laser is emitting. In this case the laser illumination intensity will far exceed the flame intensity and we can view surfaces through fairly dense flames. Figure 39 shows the intensity ratio curves for the laser illumination at 10^5 watts and a bandpass of 100 nm. Typical laser pulse widths can be as short as 1 μsec. To make full use of the laser intensity we would also need an exposure time of 1 μsec. Exposures times this short are not practically possible through mechanical means. Special electronic image converter cameras, however, can be gated on for these short exposure times. With special mechanical shutters 1 msec is a realizable exposure time. With a 1 msec shutter we would have 1000 times the exposure to the flame as compared to the laser. This effect would reduce the intensity ratios in Fig. 39 by 30 db. In this case we would still have sufficient laser intensity for flames with transmissivities greater than 50%.

Since the calculations show that pulse laser illumination is far superior for viewing in the presence of the flame, a test was performed with the laboratory rig (Fig. 31), viewing probe (Fig. 33), and a flashlamp pumped dye laser system to record images made through the flame and illuminated with the dye laser. A schematic of the laser illumination test experiment is shown in Fig. 40. A portion of the dye laser beam was focused into an optical fiber whose output illuminated a liner piece through the flame zone as shown in the figure. An electromechanical shutter with an aperture of 6 mm and a speed of 1 msec was placed at the output of the fiber optic viewing probe. The image at the output end of the viewing probe was magnified and recorded with a microscope objective and view camera. A trigger delay was set so the 1 μsec laser signal occurred during the time the shutter was open. The 1 msec shutter is fast enough in this instance so that no flame signal is recorded.

Photographs of the liner taken with the dye laser illuminator (λ .58 μm) are shown in Fig. 41a, b, c, and d. The photographs show a picture of a cracked liner louver piece. In Fig. 41a the combustor is off. When the combustor is in operation the intervening flame will normally reduce the contrast and wash out the surface details. Using laser illumination as in Fig. 41b, we can see the liner surface as if no flame were present. The exposure was reduced slightly by the attenuation of the flame. The 1 μsec laser pulse energies were between 10 and 20 mJ for these exposures. Figure 41c and d show two more photos with the laser illumination in the presence of a more dense flame. In these photos and especially Fig. 41d the luminous flame appears as a non luminous dark cloud. There are also interference bands of unknown origin that can be seen in each photo, especially in the lower left hand corner. The flame in the photo of Fig. 41d was dense enough that the surface could not be seen with the self illumination by the flame or with an external incoherent illumination. The laser illumination, however, is intense enough to give an exposure of the surface.

FIG. 39 RATIO OF REFLECTED 10^5W LASER ILLUMINATION TO FLAME INTENSITY AT DIFFERENT FLAME TRANSMISSIVITIES

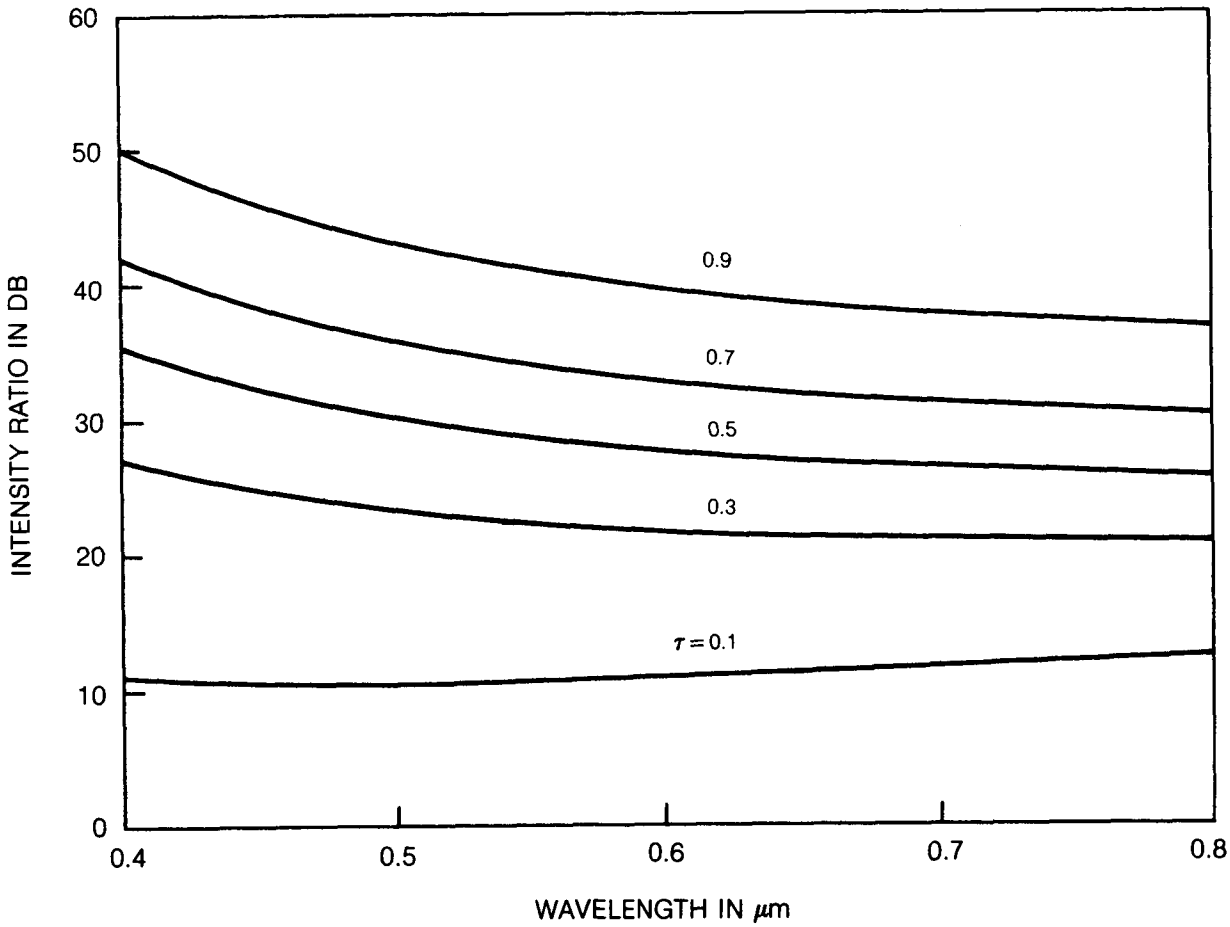

84—7—78—22

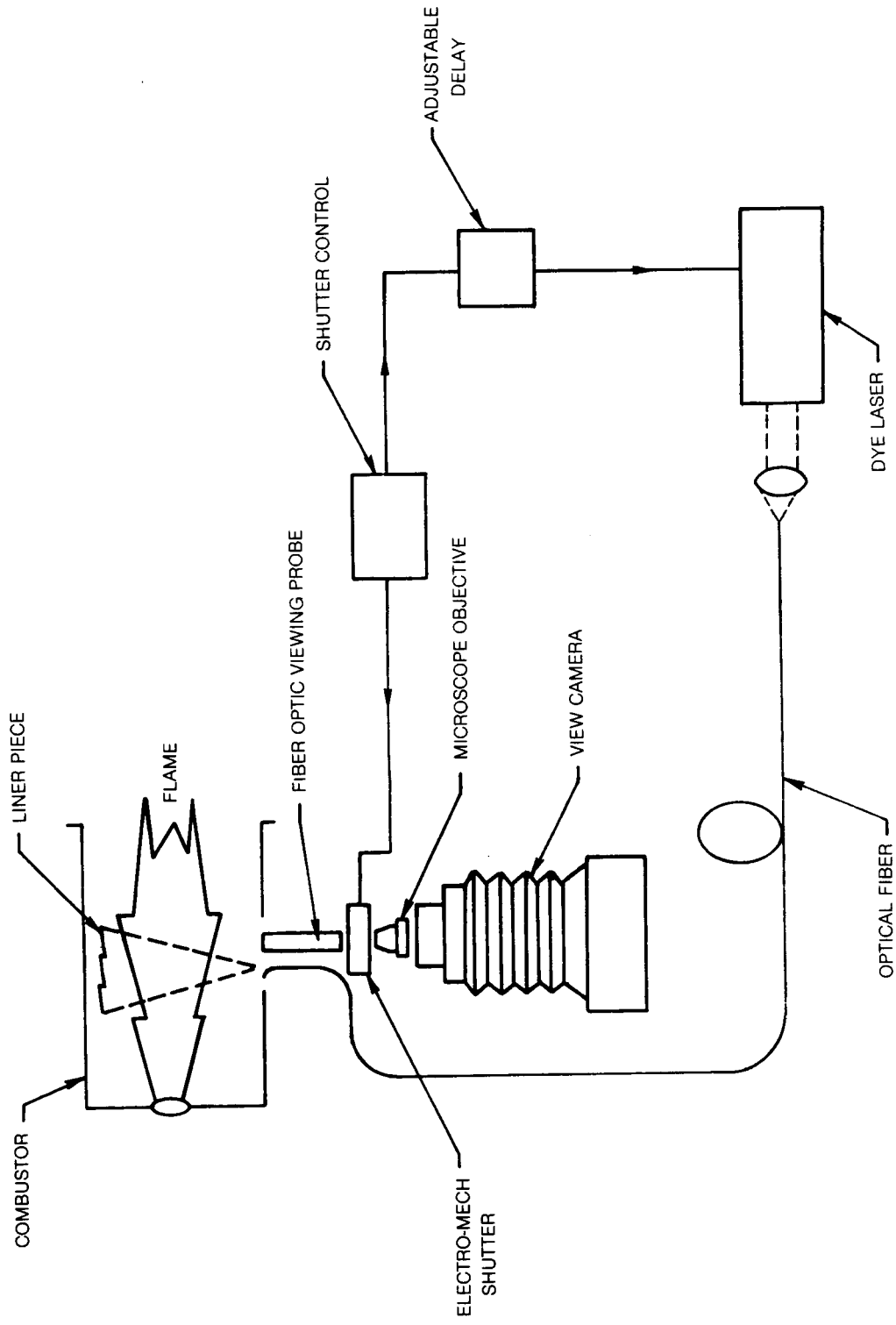

FIG. 40 PULSE LASER ILLUMINATION TEST

84-7-78-23

FIG. 41 VIEW OF COMBUSTOR LINER THROUGH FLAME

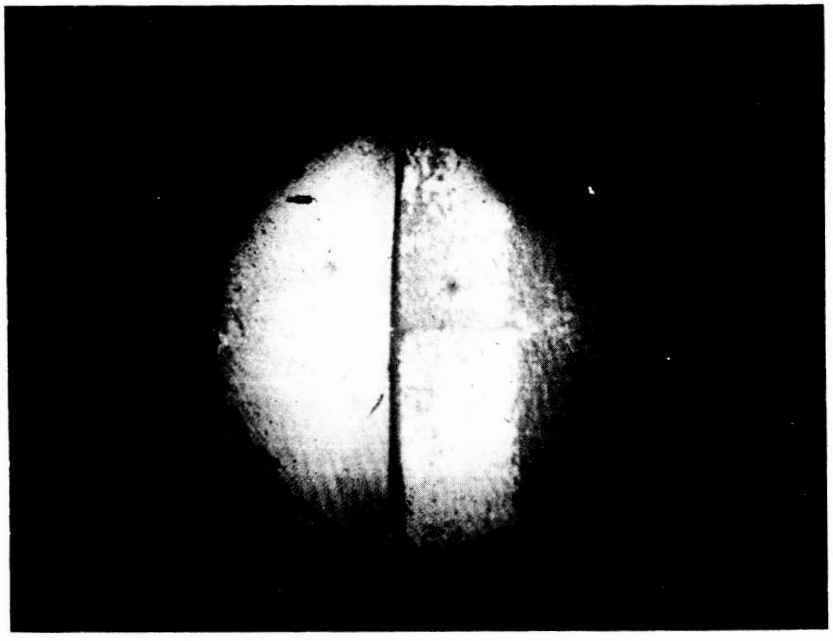

A) LASER ILLUMINATION, COMBUSTOR OFF

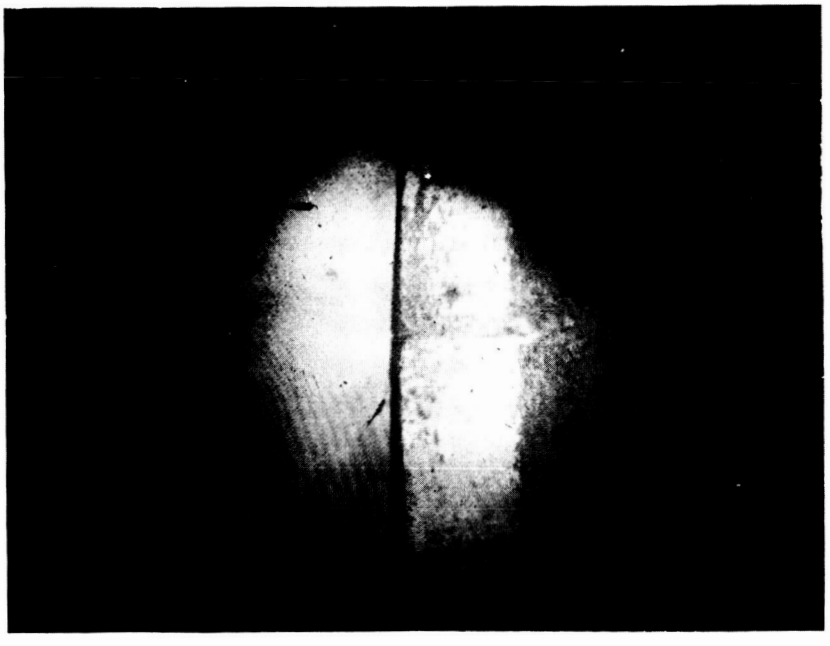

B) COMBUSTOR ON

82–6–109–2

FIG. 41(CONT'D) VIEW OF COMBUSTOR LINER THROUGH FLAME

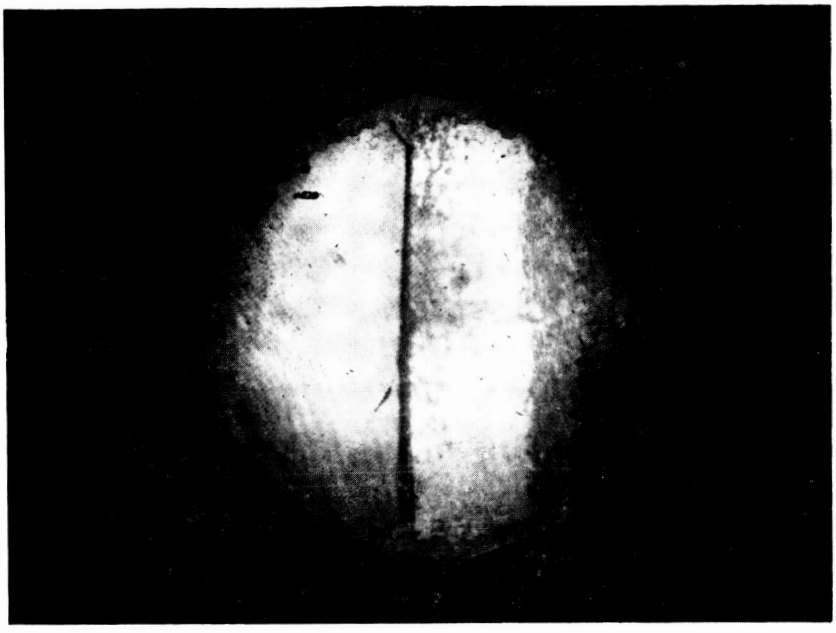

C) COMBUSTOR ON WITH INCREASED AIR FLOW

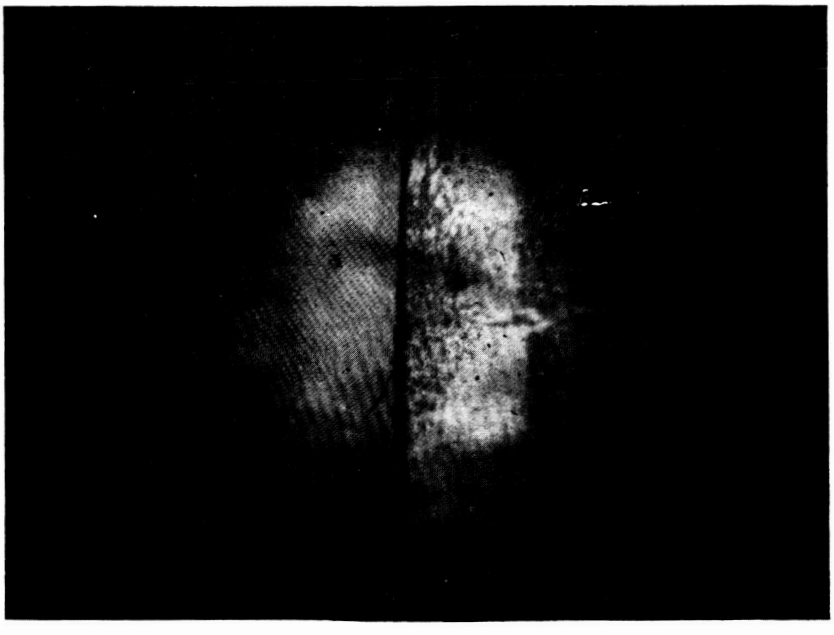

D) COMBUSTOR ON WITH DECREASED AIR FLOW

Pulsed laser illumination photos were also taken viewing a steel plate with 5 mm square grid lines. In this case the laser speckle pattern from the surface was clearly visible. When the flame was present the speckle pattern became distorted. The distortion cell sizes appeared to range from slightly under a mm to several mm. Since the dye laser pulse lasts for only 1 μsec, we essentially freeze the motion of the flame. We could also stop the motion of the fuel spray. Use of the short pulsed illumination may be an interesting method to study the flame combustion process in addition to liner damage.

Unfortunately, during the high pressure combustor rig tests, the distal end of the illuminating fiber would accumulate soot and prevent the use of external illumination during the combustor operation. After the last high pressure rig test we found on inspection that a slightly exposed fiber remained free of soot accumulation. This was probably due to the exposed fiber end reaching a sufficiently high temperature to prevent soot build-ups; or, possibly because it was exposed to the high speed flow stream. We also only had a minimum exposure time of 1/200 sec with the viewing system on the HP rig. An electronic or high speed disc shutter would be required to eliminate the flame exposure in this case.

We would also like to mention that 100 mJ of pulsed laser energy was usually more than sufficient to make an exposure on film (ASA 400) with the viewing system. We could also record a pulsed laser illumination with the video camera that frames in 33 msec (17 msec for half interlace frame). The video camera had to be stopped down to prevent saturation. The video exposure would remain for many frames especially if there was an over exposure.

4.5 Wide Latitude Photography - We mentioned previously that it is desirable to have a recording device with a wide dynamic range so that we can extend the contrast and enhance darker liner surface details in the presence of highly luminous flames. When we have brightness levels that vary over enormous limits conventional photographic film and processing cannot cover the range of exposures required to give a proper recording of the image. In 1965 EG&G, Inc. developed an extended range (XR) film that allowed luminance values ranging over a million levels to be recorded. This film used three color layers with different ASA's of 400, 25, and .004 to obtain the extended range. Two rolls of the XR film, supplied by NASA, were tested with the viewing probe. One roll was exposed during the Rig testing. Unfortunately, the film had a development date of June 1967 and was too old for development. The film was discontinued at about that date.

Another method of extending the latitude of conventional photography was developed by M. Levy (ref. 17). Using a special low contrast developer designated POTA, the exposure range of standard film can be extended several orders of magnitude. This method was also tried during the Rig testing. A roll of Tri-x film was exposed during one test run and developed with POTA. Two negatives of an upstream view into the flame with different exposures were printed and compared. The exposures were taken with camera settings of 1/200 sec and an F/4

aperture. One exposure had an additional neutral density (ND) 1.0 filter that reduced the light level to the camera by a factor of ten. Both pictures were printed for best detail. More liner surface detail could be observed from the picture taken with the ND 1.0 filter. The exposure from the luminous flame had been suppressed by the ND filter; but the wide latitude development allowed the much weaker surface detail to be printed. When using wide latitude photography, then, one can use shorter exposures to help suppress the overexposure and high contrast produced by the luminous flame background. Figures 42 and 43 show the two POTA developed photographs. In Fig. 42 we can see the flame around an air-mixing hole and one louver lip extending across the field-of-view. The hole and louver are being observed through the partially transparent flame. In Fig. 43 the flame exposure was suppressed relative to the background with the ND filter. The background was then brought out in the printing process. Two louver lips and the air mixing hole in the liner can be seen with much better detail. The 60° FOV lens was used for this test.

4.6 Digital Image Analysis

4.6.1 Photographic Images - The third approach to enhance the viewing of liner surfaces inside operating combustors utilizes digital image analysis. A given number of picture elements in a photographic or video image recording are digitized and stored in computer memory. Algorithms, written to perform specified modifications, operate on the image data to produce a new or modified set of image data that can be displayed on video monitor or reprinted as a photograph. With digital image enhancement techniques we can perform such operations as contrast modification (linear or nonlinear), background subtraction, pseudocoloring, image differencing, edge enhancement, profiling, image zoom, averaging, and spot removal.

Fourier domain processing, which operates on the spatial frequencies of the two dimensional image, can filter specified spatial frequencies or bands of frequencies to eliminate noise or sharpen edges. If information about a distortion is known, Fourier domain processing can also restore images. For instance, an out-of-focused image could be restored to a properly focused image if the optical transfer function of the defocused lens system is known. Similarly, if we know the optical transfer function of the combustor distortion, we could restore the combustor images. Fourier domain processing and the determination of distortion functions for image restoration is a fairly complicated analysis that requires a 2-D Fourier transform of the image data plus experimentation with distortion functions. This analysis, which would be interesting to apply to the combustor viewing data was beyond the scope of the program. We did, however, generate the distortion function for the point source distortion tests discussed in section 4.3 (cf. Fig. 34). The distortion function was generated by deconvolving the undistorted point source image (flame off) from the distorted image (flame on).

FIG. 42 WIDE LATITUDE PHOTOGRAPHY IN COMBUSTOR — FLAME EXPOSURE

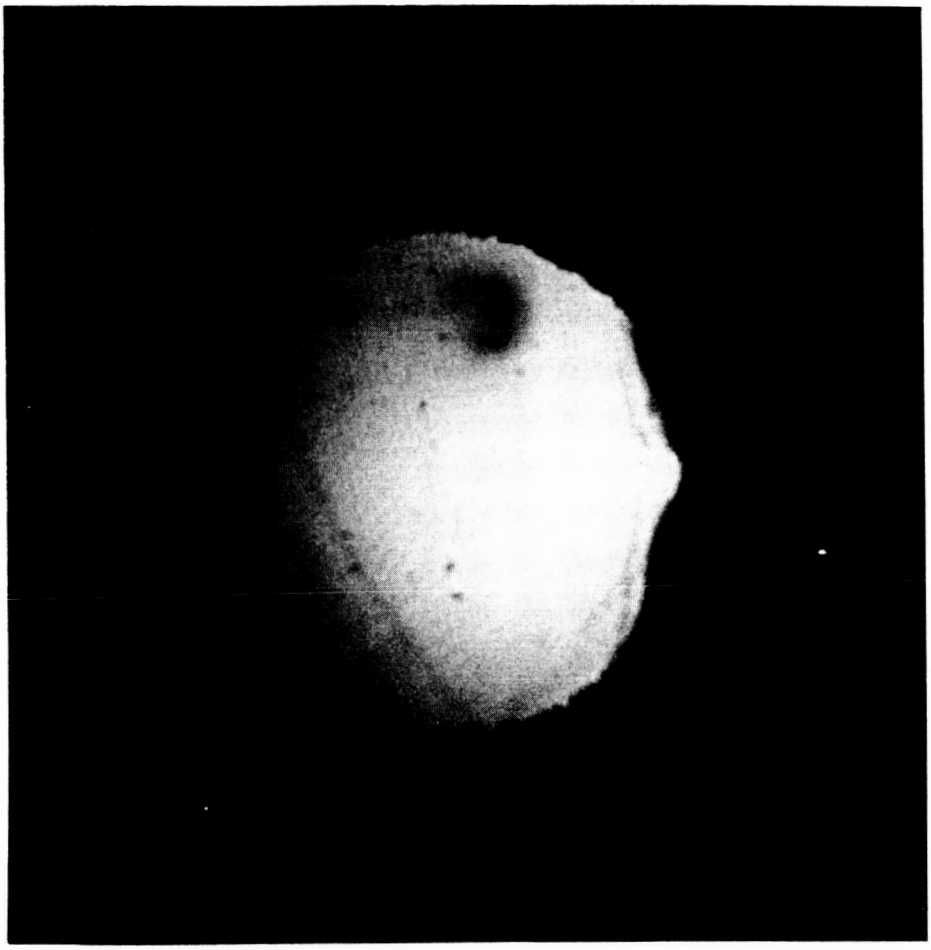

FIG. 43 WIDE LATITUDE PHOTOGRAPHY IN COMBUSTOR — LINER EXPOSURE

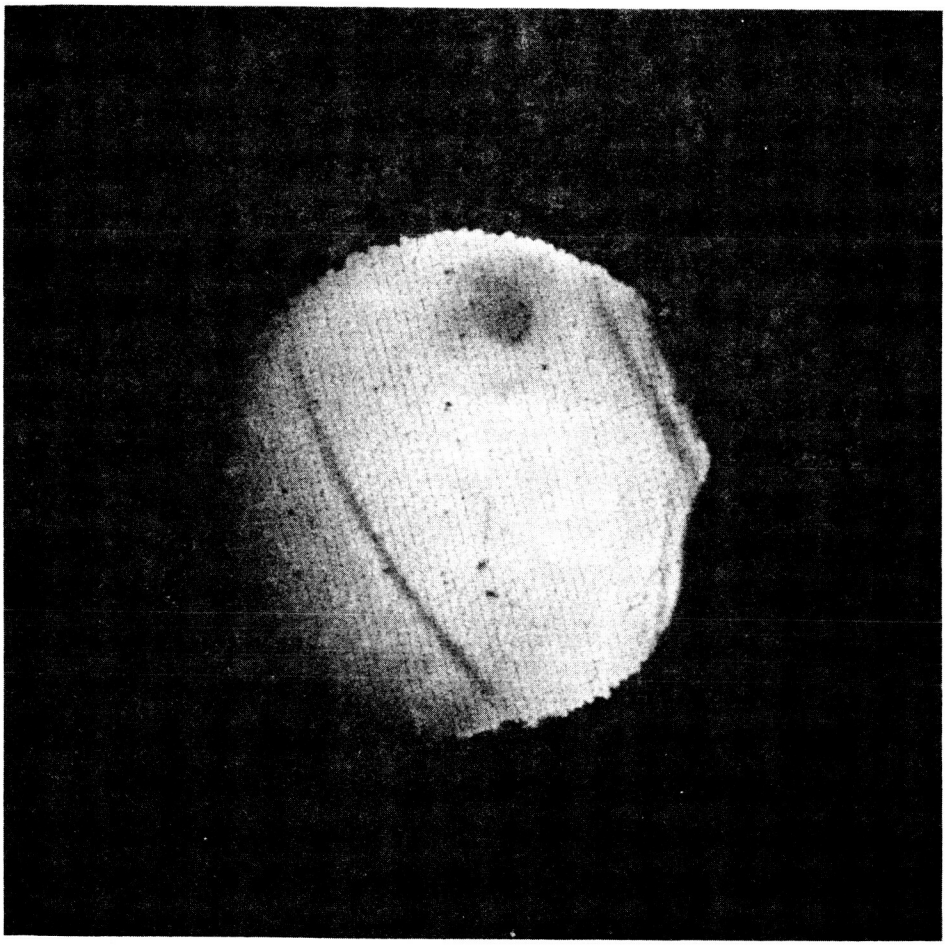

During the preliminary test program, photographs were taken of a cracked liner piece mounted on the opposite wall of the lab combustor rig. The photographs were taken through the fiber optic test probe (cf. Fig. 33) and recorded on 35 mm film. Images of the liner piece were taken with a small lamp for illumination when the combustor was off and with the flame for illumination when the combustor was on (the lamp being on or off does not make any difference in this case).

The negatives were digitized at Pratt & Whitney's image processing lab with a 25 micron sampling pixel to produce a 512 x 512 array of gray scale values. We experimented with a globally-referenced (i.e. entire image) histogram equalization subroutine. This computer program catalogs the pixels in the entire image with respect to their gray level. In the case of the flame-degraded picture, the data is clumped into a few gray levels, causing the bleached-out effect. The subroutine implements a statistical approach to reassign the gray level to pixels in such a way that the histogram becomes stretched out to encompass all 256 (8-bit) gray levels. The net result is an improvement in the dynamic range of the image, giving high visibility to details that were originally lost due to low contrast. Samples of the globally-referenced enhancement techniques are provided in Figs. 44 and 45.

Figure 44 gives a reproduction of the digitized image from the computer terminal with the original gray scale and with an enhanced gray scale for the best picture condition: namely, no background illumination and no distortion from a flame. The magnification of the liner piece in this case is about 5.2. For this no-flame case the computer enhancement subroutine gave marked improvements in feature visibility. Even more dramatic improvements resulted from operation on the flame degraded image of Fig. 45. In this latter case numerical enhancement techniques created an image with contrast as good as the unperturbed image. This data manipulation turns out to be very significant from the point of view that one can now observe the true amount of image smearing or geometrical distortion caused by the index of refraction perturbations generated by the flame. Prior to enhancement this side effect could not be detected in the picture. Quantitative measurement of the point spread function represented by this distortion was discussed previously.

Experimentation was also carried out with local histogram equalization to try and bring out finer details in local neighborhoods. Interference was observed from high spatial frequencies, apparent as graininess, when the algorithms stretched the image dynamic range. We also experimented with Fourier transform filtering to reduce the noise level. These techniques introduced prominent boundaries between individual neighborhoods. To alleviate this artifact a new type of contrast enhancement routine and Fourier transform process would have to be developed (see, for example, ref. 18).

FIG. 44 LINER CRACK IMAGE

FLAME OFF
DIGITIZED

ORIGINAL GRAY SCALE

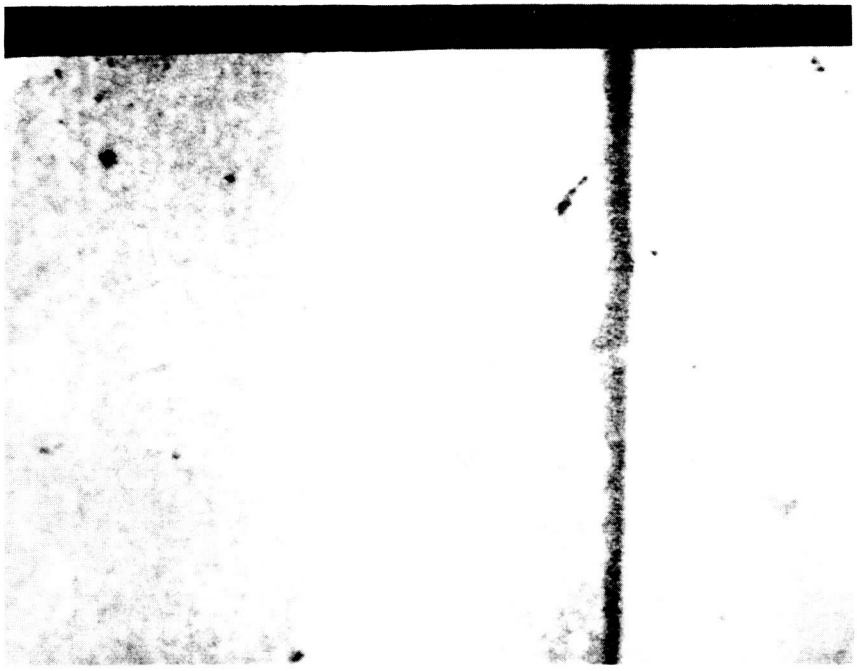

HISTOGRAM EQUALIZATION

FIG. 45 LINER CRACK IMAGE

FLAME ON
DIGITIZED

ORIGINAL GRAY SCALE

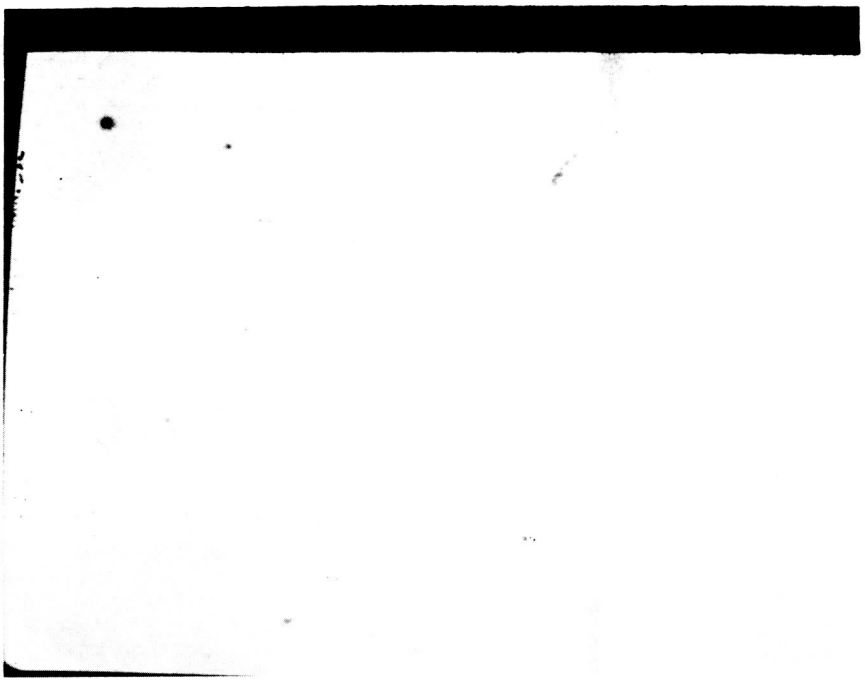

HISTOGRAM EQUALIZATION

82–8–6–7

4.6.2 Video Images - Video images were recorded on magnetic tape during the high pressure rig and engine tests. Selected images or frames from the recordings were digitized on UTRC's video image processing system. This system consists of a Perkin-Elmer model 7/32 32-bit processor with 256 K bytes of core memory; two disc drives that have a total storage capacity of ten Mbytes; an 800 BPI tape drive; a Versatec electrostatic line printer; and a Grinnell GMR-27 frame buffer. The Grinnell frame buffer can digitize at video rates so that television images can be acquired in real time. In conjunction with the Microtime time base corrector we can digitize television images from video tapes. Features of the frame buffer include: (1) a set of three independent video look-up transform matrices or synthetic color generation or other nonlinear gray scale transformations; (2) zoom and pan of the digitally stored image for magnified display on the color monitor; and (3) graphics and character generation capability. With the For-A color encoder it is possible to combine the separate red, green, and blue video output images of the Grinnell frame buffer into a National Television Standard Color (NTSC) image for recording on video tape and playback on a standard color television set.

Special software modifications were made to existing programs for processing the video images recorded during the high pressure combustor rig and engine tests. Table 1 lists the menu of image processing tasks available for the program. Single or a summation of multiple frame images can be taken from the

TABLE 1

Image Analysis Menu

1	Grab New Image
2	Get Image From Disk
3	Catalog Dark Spots
4	Change Gray Scale/Color-Enhance
5	Isometric Plot
6	Subtract Two Stored Images
7	Store Image For Later Processing
8	Image Zoom
9	List Names of Stored Images
10	Equalize Image (Average M By N Pixels)
11	Image Gradient (Edge Enhancement)
12	Test Image Generator (Sin (X)/X)
13	Graph Intensity Along Line
14	Fix Up Spots
15	Make Hard Copy on Line Printer
16	Compress Image to 64 By 64 Pixels
17	Compute Six Low Order Moments
18	Flatten Image Brightness
19	Insert Ruler In Image
99	Exit

video recordings with item 1 on the menu. This frame grabbing routine can also be written to average a specified number of frames. A frame grab is initiated with a key on the terminal. The images can be stored on disc for later processing or held in volitale memory for processing with other menu items. For example, with item 4 we can set upper and lower limits of the gray scale and expand this gray scale range either linearly or nonlinearly to the total gray scale range (0-255). A cursor, controlled from a pen and data tablet, is displayed along with the image on the monitor so that the results of the contrast manipulation can be observed almost instantaneously. We also have a choice of pseudocolor generation with item 4. In this case selected ranges of contrast values are assigned different colors. The pseudocolor operation, in effect, gives a contour plot of the image even when viewed in black and white.

Item 14, "fix up spots," is used to remove or "paint-out" broken fibers or other dark spots that distract from viewing the image. The points of maximum slope on each side of a cursor selected dark spot are determined for each video scan line through the spot. The values of the image intensity at 3 pixels away (+ 3 pixels on one side -3 pixels on the other side) from maximum slope points are read and a linear interpolation is applied to fill in the spot.

Several other menu items were used or tested with the combustor images including graph intensity along line (profile plot, Cf. Fig. 35), isometric plot, subtract images, image zoom, equalize image, edge enhancement, and flatten image brightness.

Figure 46 shows three fiberscope views inside the JT-12 liner used for the high pressure rig tests. The probe was inserted into the air hole nearest the fuel nozzle. The 35° FOV lens was used and the view was oriented upstream into the liner dome. For comparison, Fig. 46a shows the liner dome view when the liner was removed from the rig and illuminated with a flood lamp. The large hole in the lower right of Fig. 46a is where the fuel nozzle enters the liner. The 12.7 mm hole above the nozzle hole is for an igniter probe. Two rows of small 1 mm dia. air holes can be seen above the igniter hole. The distance from that probe to the small holes is about 7 cm.

Figure 46b and c shows the same view (except reversed with a mirror) with the liner in the combustor rig, which is operating under reduced air and fuel flow. In Fig. 46b there is no enhancement from the image processing system. Several broken fibers and a large dirt particle (at the image conduit and flexible image bundle interface) can be seen in this photo. The same image with contrast enhancement and dark spot removal is shown in Fig. 46c. Note that the two rows of 1 mm dia. holes are barely visible in the operating combustor. This reduction in resolution is probably due to distortion from the hot turbulent gases in the operating combustor. Most of the dark spots and broken fibers were also removed for Fig. 46a. The photos taken for Fig. 46 and the other video pictures in the report were taken directly from the video monitor with a 4x5 view camera and polaroid film.

FIG. 46 DOME IMAGES

a) VIEW IN DOME OF COMBUSTOR TAKEN WITH FLOOD LAMP

FIG. 46 DOME IMAGES

b) DOME VIEW WITH COMBUSTOR ON, NO ENHANCEMENT

c) SAME VIEW AS b) WITH ENHANCEMENT

An illustration of the use of the pseudocolor routine is shown in Fig. 47. In this figure we are viewing upstream at a 12.7 mm dia. liner hole. Dense flame obscures the liner surface. Airflow in the liner is from the upper right to the lower left. The air mixing hole appears cresent shaped due to heavy combustion taking place on the downstream side of the hole. The air streaming in the hole appears to act as a flame holder. The pseudocolor routine in Fig. 47b brings out the different intensity levels of the flame and clarifies the image.

Pseudocolor contour enhancement is also shown in Fig. 48. In this figure we are viewing an upstream air hole with the 35°FOV lens. The two successive video frames show the combustion around the air hole; namely, that the flame is being drawn into the downstream side of the hole. The process appeared to repeat itself in a somewhat periodic fashion.

4.7 Stereoscopic Viewing - One of the design options considered early in the program was a stereoscopic viewing probe. A stereoscopic probe would allow one to measure depth on liner surfaces using binocular parallax. In each stereo image pair an object point is displaced a different distance from the optical axis in accordance with its depth or distance from the two viewing lenses. The depth resolution, δz, can be shown to be given by

$$\delta z = z^2 \, \delta D' / [fS(M+1)] \qquad (6)$$

where z is the object distance; $\delta D'$ is the resolution in the image plane, which would be the fiber optic bundle face in our case; f is the viewing lens focal length; S is stereo pair lens separation (no tilt included); and M the magnification, which in our case for viewing across the burner would be about 0.1. The resolution of the image bundle is about 30 μm. Thus, for a 1 cm lens separation we can resolve about 1.1 mm at a distance of 6 cm when viewing the combustor liner. This resolution is not good enough to resolve crack depths in the liner, but may allow for a determination of flame positions relative to the liner surface, provided the surface can be observed relative to the flame. In order to resolve depths on the order of 250 μm we would have to move the probe to within about 3 cm of the liner surface.

During the preliminary test program, photographs were taken through the test probe (Cf. Fig. 33) with a view camera of a section of damaged combustor liner. The liner piece was placed inside the lab burner opposite the probe and at a distance of 23 cm from the probe. Figure 49 shows a stereo pair of photographs made with the probe at two different locations separated by 2.5 cm. A 2.6° rotation or tilt was included to keep the object view about the same in each case. The steoeoscopic view of the liner piece can be seen most easily from the photo pairs in Fig. 49 with a stereo lens viewer such as Air Photo Supply model PS-2. Otherwise, one can hold a card between the pictures so that each eye views

FIG. 47 COMBUSTION DOWNSTREAM OF AIR MIXING HOLE

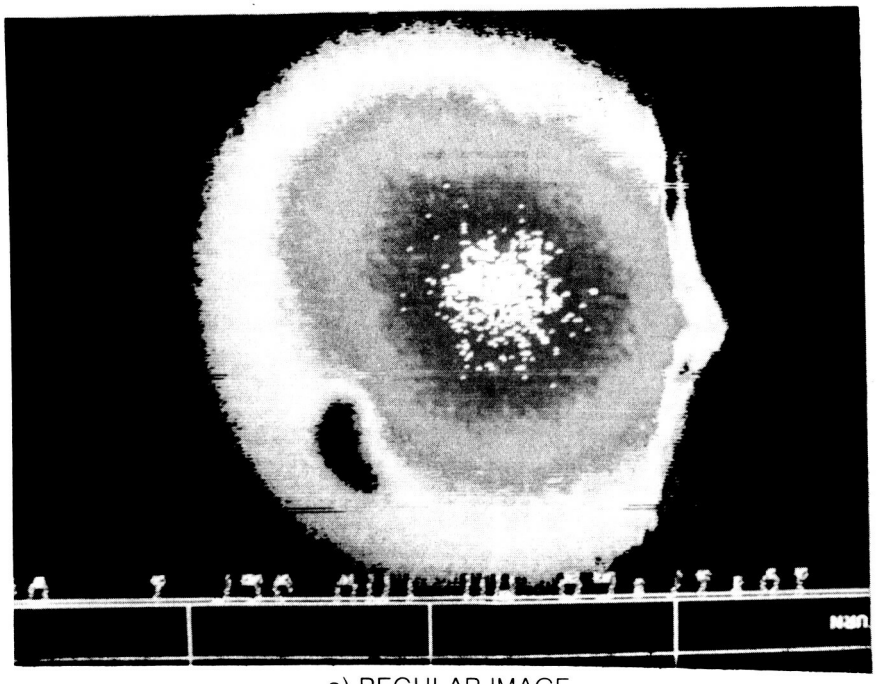

a) REGULAR IMAGE

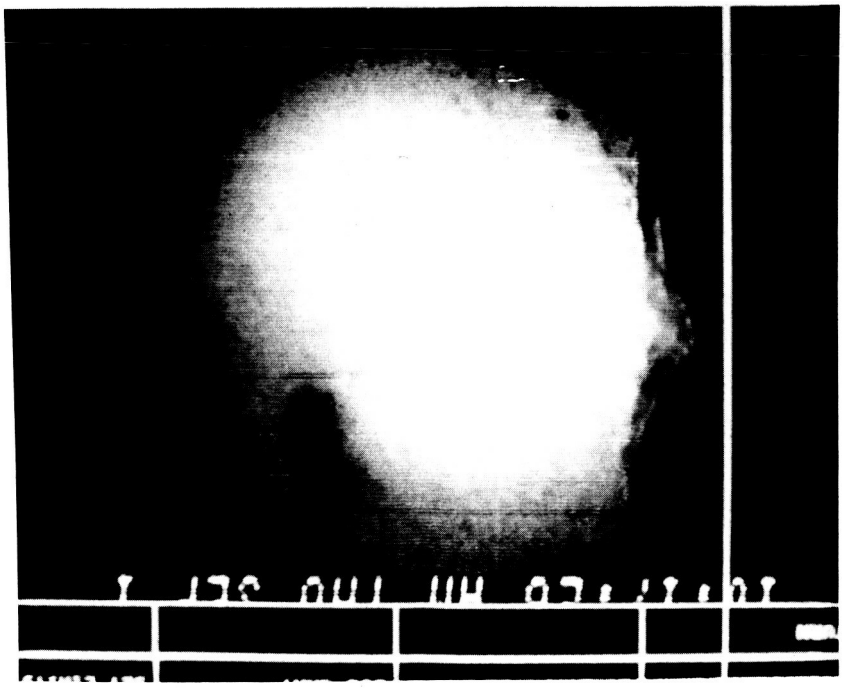

b) IMAGE WITH PSEUDOCOLORING

FIG. 48 TWO SUCCESSIVE VIDEO FRAMES OF COMBUSTION AROUND AIR MIXING HOLE

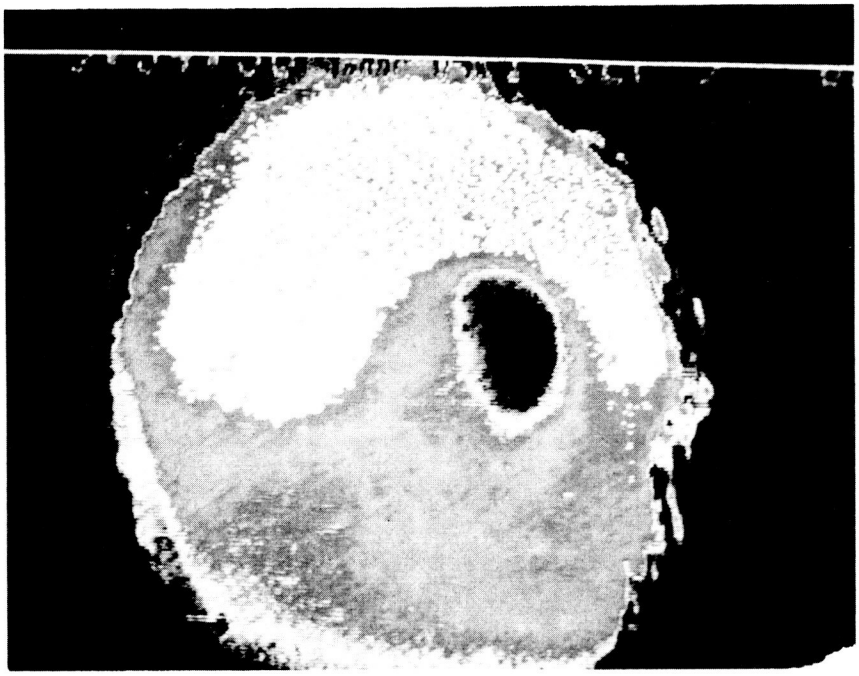

a) FIRST FRAME IMAGE

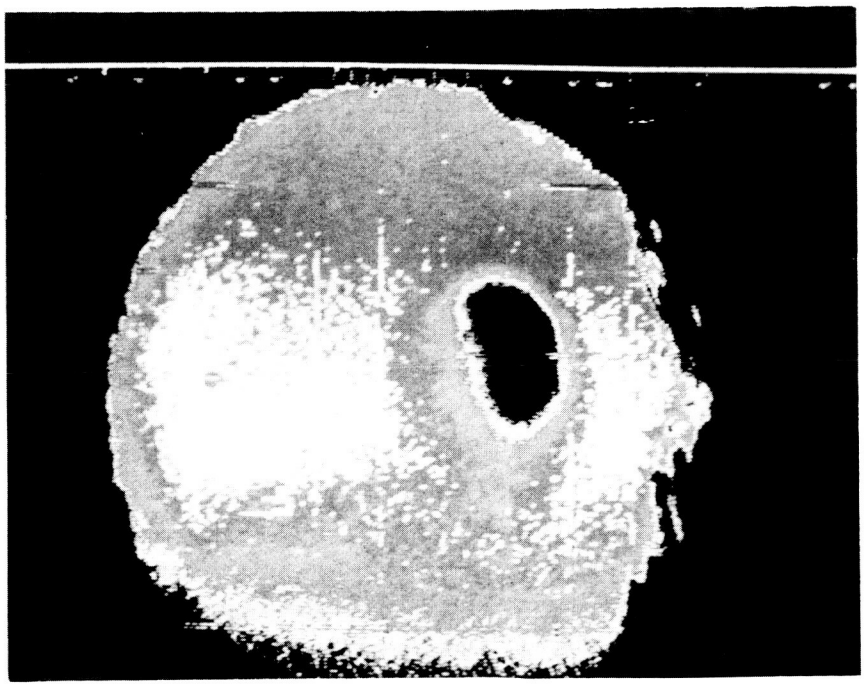

b) SUCCEEDING FRAME IMAGE

FIG. 49 STEREO PHOTO PAIR OF BURNER LINER

a) COMBUSTOR OFF

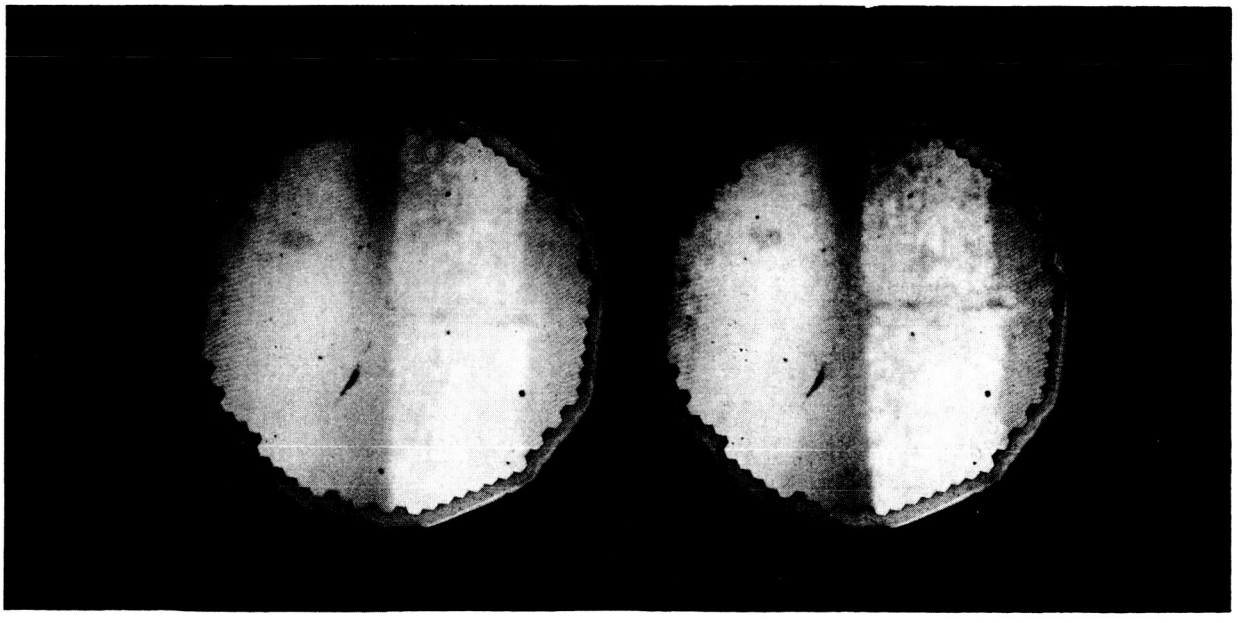

b) COMBUSTOR ON LEAN

one picture independently. The two separate views must be merged together to form one stereoscopic view. At the point of merger one will note that the surface defects and pixel array on the end of the image conduit including a scratch appear on an elevated plane above the liner surface. One can also easily see that the left hand liner hoop lies below the right hand lip section. The actual depth is 3.3 mm. A calculation based on equation 6 gives the depth resolution to be about 1 mm in this case. It appears, however, that one can also see the crack depth and the fact that the lower side of the crack is higher than the upper side. This depth is about .3 mm at the left hand side of the crack and diminishes to zero at about half way to the right hand side of the crack. In this case the shading may help in the depth perception. The length of the crack from the left hand edge of the lip to the right hand side of the picture is about 12 mm.

The stereo photo pair in Fig. 49a was taken with lamp illumination and the burner off. In Fig. 49b the burner was in operation. As noted previously, the presence of the flame between the viewing probe and lens significantly reduces the contrast and also reduces one's ability to see depth.

We decided to build a monoscopic instead of a stereoscopic viewing probe at this time for several reasons. The principal reason was the large probe size required for stereoscopic viewing (it might be better to use two separate probes). To obtain the .25 mm depth resolution with the narrow FOV would require a probe of at least 25 mm diameter. This size would not be convenient to use for an engine test and may significantly perturb the combustor aerodynamics. The depth resolution for crack measurements would be marginal and probably insufficient during combustor operation when optical distortion from the hot gases would be present. The distortion is especially strong for the narrow FOV case required for good depth resolution.

Looking at depth resolution in the flame itself with the wide FOV probe may be inaccurate since the flame is partially transparent at many locations, especially in the downstream portion of the flame that is consuming the luminous soot. We also may have to remotely tilt the angle between the lenses to keep the same object in view. Basically, we felt that it was not worth the additional size and complexity at this time until we can learn more about the viewing and operating conditions of a probe in a combustor.

5.0 COMBUSTOR RIG TESTS

5.1 Combustor Facility - The combustor viewing system was tested on a high pressure combustor rig at UTRC's Jet Burner Test Stand (JBTS) facility. The JBTS is a self-contained facility with four test cells suited for high-pressure combustion tests. In addition to the test cells with control rooms, the JBTS provides assembly areas, automatic data acquisition systems and air, gaseous nitrogen, water and fuel (liquid and gaseous) supply systems. In particular, air is supplied to the JBTS through the system depicted in Fig. 50. The multi-staged reciprocating compressors are capable of delivering a combined continuous flow-rate of 4.5 kg/s at pressures up to 2.7 MPa. The airflow can be heated by use of either an indirect-fired burner, a 720 kW electrical resistance heater, or both. Large-quantity distillate fuel storage is available at the JBTS; a positive displacement pumping system is capable of delivering fuel flowrates in excess of 25 ℓ/min at pressures up to 10 MPa to each test cell.

The electric heater both with and without the indirect fired heater was used for the tests. At full operating conditions of 15 atmospheres, 1.9 kg/sec gas flow and combustor inlet temperatures of 426°C, both heaters are required. A calibrated venturi, located in the delivery system upstream of the electrical heater was used to monitor the air flow, with appropriate measurements of the pressure and temperature performed upstream and at the throat of the device. A plenum was used at the heater exit to establish reference airflow velocity and temperature conditions.

A schematic of the test facility is shown in Fig. 51. The test section houses the combustor liner and provides appropriate access for spark ignitor, fuel injector support, and the viewing probe at multipile locations. Commercially available pipe with an inside diameter of 15.2 cm was used for the fabrication of the test section. The 1.3 cm annular gap between the housing and the 12.6 cm diameter liner permits adequate backside convective cooling of the liner louvers. The fuel injector/swirler assembly supports the liner by use of a clamp ring to a liner dome flange; and an aft sliding seal permits axial thermal growth.

The combustor uses a modified JT-12 liner that has a 12.6 cm inside diameter and an overall length of 41 cm. The modified liner consists of a dome constructed from a frustrum of a 90-deg cone and six conventional sheet metal louvers. The material of construction is 0.6-mm thick Hastelloy. A flange on the dome provides access to mount a central fuel injector-swirler combination. The swirler is the principle air supply source for the primary zone; four of the louvers contain six 12.7 mm holes each to admit combustion air to the burner. There are three probe mounting ports along the top of the housing pipe. The ports are placed along the axis of the combustor at distances of 8.6 cm, 14.3 cm and 19.9 cm downstream from the fuel nozzle. The mounting pieces on the ports

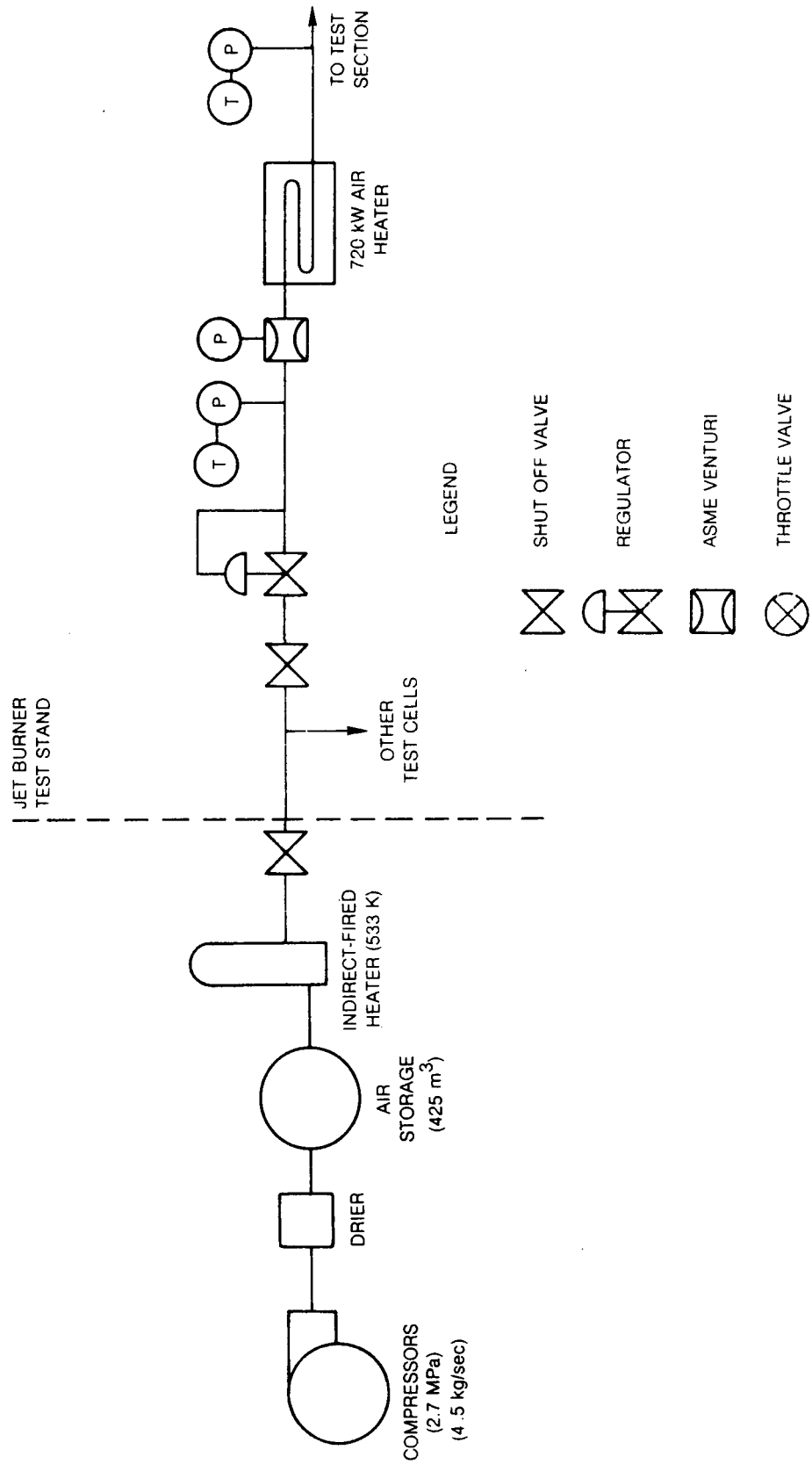

FIG. 50 GAS SUPPLY SYSTEM

81-6-64-7

FIG. 51 GENERIC COMBUSTOR TEST FACILITY

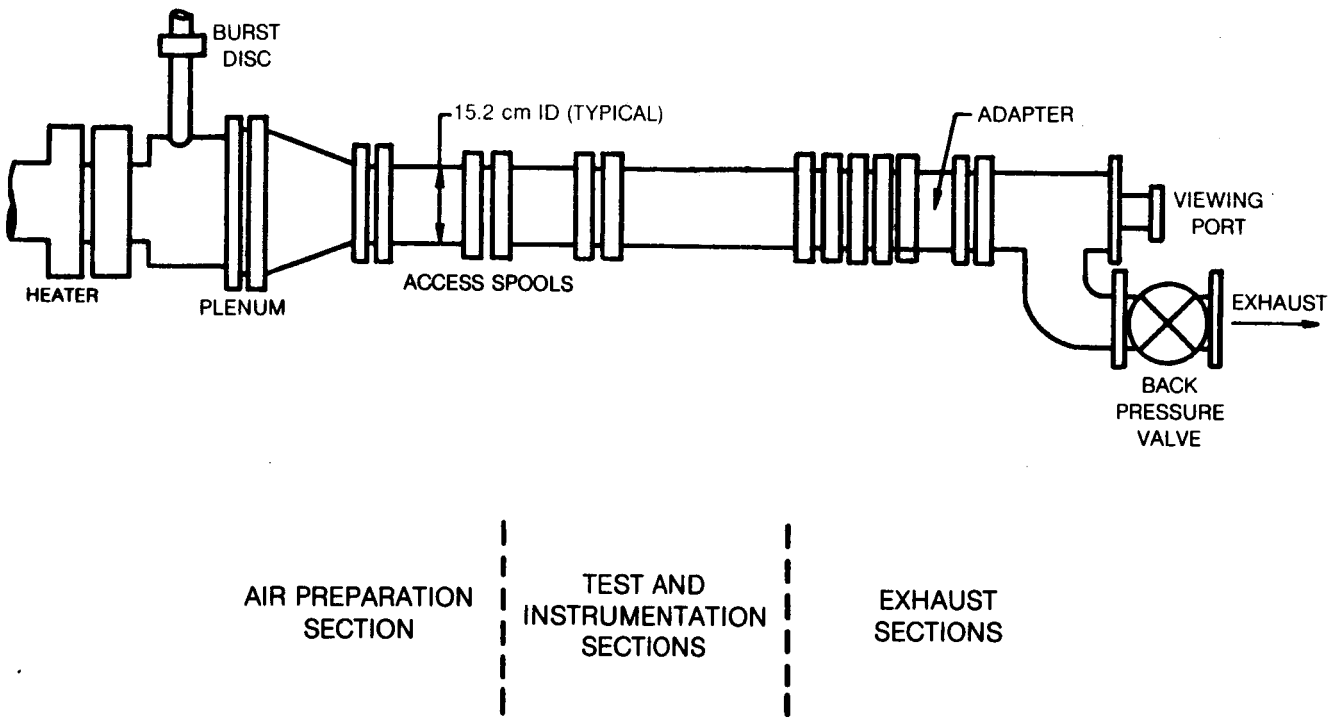

81-6-64-5

are 2.54 cm Swagelok fittings. The first and third ports at 8.6 cm and 19.9 cm are in line along the combustor axis. The middle port, however, is staggered at 60° from the in-line ports. The probe mounting ports are aligned on the 12.7 mm diameter dilution holes in the combustor liner. These holes were enlarged and extended slightly upstream to assure probe clearance under thermal growth between the housing and liner. A schematic showing part of the liner inside the test rig pipe and two viewing ports is given in Fig. 52.

The exhaust section of the test facility (cf. Fig. 51) consists of a water cooled T-section and a backpressure value. There was a 7.6 cm diameter viewport on the T-section as shown in Fig. 51 for observation of the combustor exit plane with CCTV. This feature was not needed during the tests. The remotely operated backpressure valve controlled the test section pressure. A water quench upstream of the valve reduced the rig exhaust gas temperature to less than 400°C.

5.2 Test Program - The purpose of the test program was to demonstrate the capability of the viewing system on a high pressure (HP) combustor rig whose operating conditions simulate those of a gas turbine engine. The probe was to be capable of being traversed directly into the center of the primary combustion zone. Both probes, each with two different fields-of-view, were to be tested. Clean images were to be made of inside liner surfaces during operation, and application of wide latitude photography and digital image analysis techniques were to be applied for enhancement of the images. Data were to be taken and analyzed to determine how well the probe and viewing system performed mechanically and optically as compared to the design goals.

Prior to operation on the HP combustor rig, the viewing system was bench tested and adjusted with a series of tests in the laboratory. One important lab test was made on the viewing probe seals with a 30 atmosphere pressure cell. As discussed in Section 3, we found it necessary to provide two sliding seals. We also found that it was desirable to have a lower speed, higher torque drive motor to traverse the probe against the 30 atmosphere pressure. The drive motor was changed later in the program. Cooling water flow rates, alignment of the viewing and illuminating optics, and adjustments with the remote control units were also made during the lab tests. As a final check of the system we used the laboratory combustor (cf. Fig. 31) to test the probe and system in a hot flame. Video and film camera exposure levels were also determined in these tests.

A drawing of the combustor rig with the distal end of the probe protruding into the liner is shown in Fig. 52. The dimensions in the figure are reduced to 80% of full scale. Combustor gas flow is from left to right in the figure. The 2.54 cm fitting that connects the actuator box to the rig pipe is shown at two locations on the top side of the rig. The probe, protruding through the fitting, is shown at ports 1 and 3. Port 2, not shown, is in between ports 1 and 3 and 60° out of the plane of the figure. Also shown is the 7.6 cm insertion range of

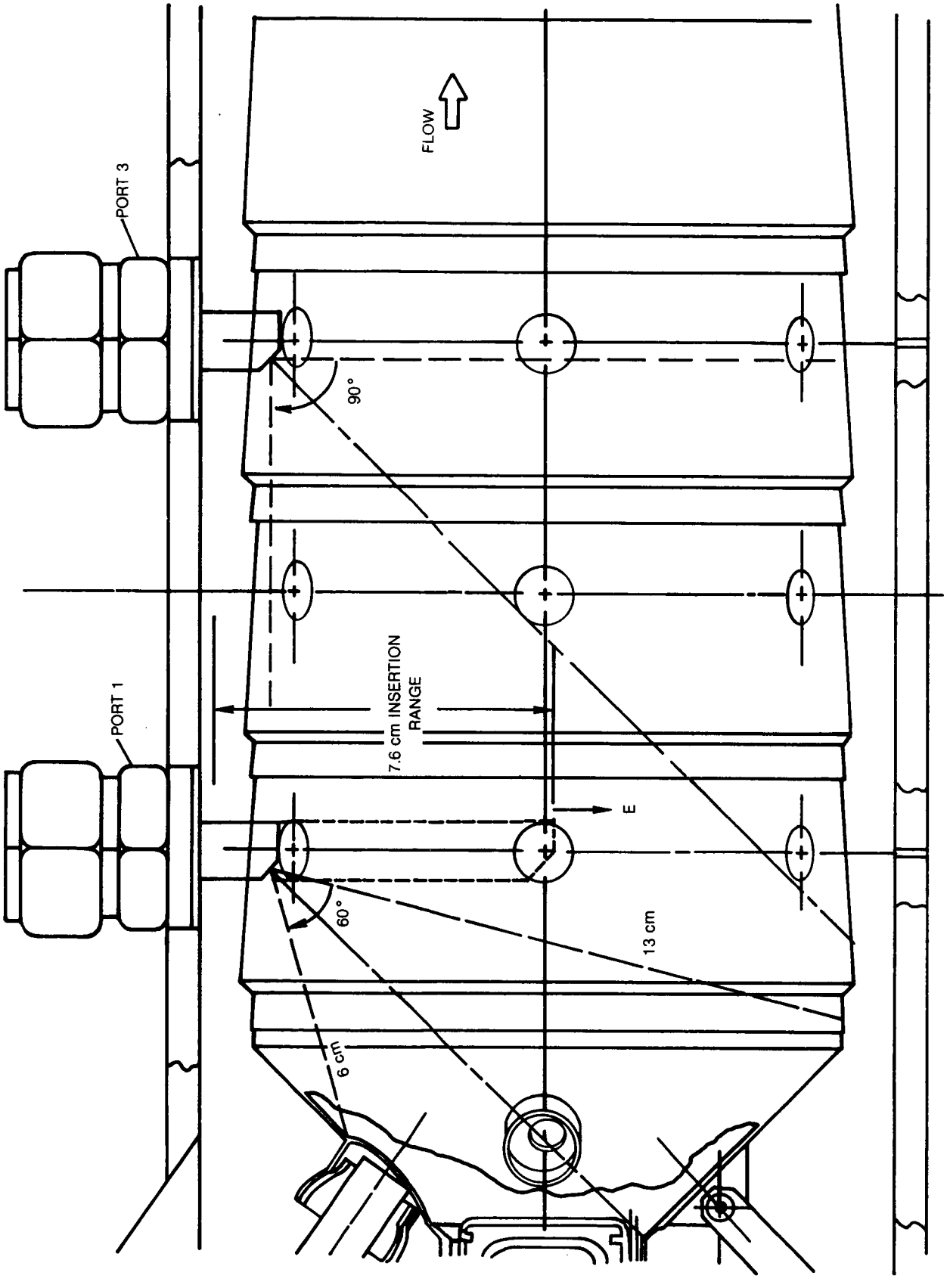

FIG. 52 SIDE VIEW OF COMBUSTOR RIG

83-6-95-7

FIG. 53 VIEWING PROBE MOUNTED IN TEST RIG

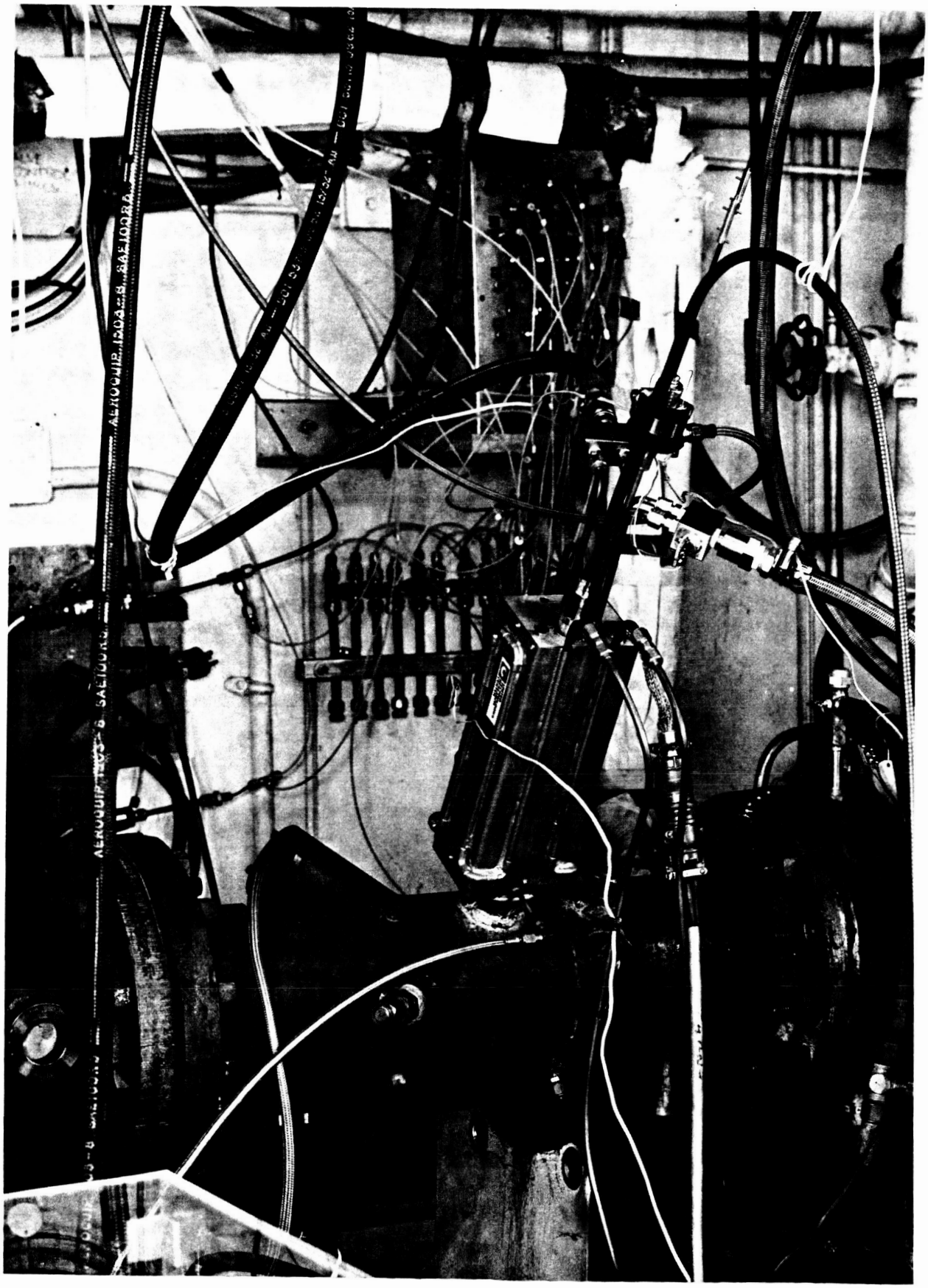

83–303–A

83–10–16–1

FIG. 54 COMBUSTOR VIEWING SYSTEM

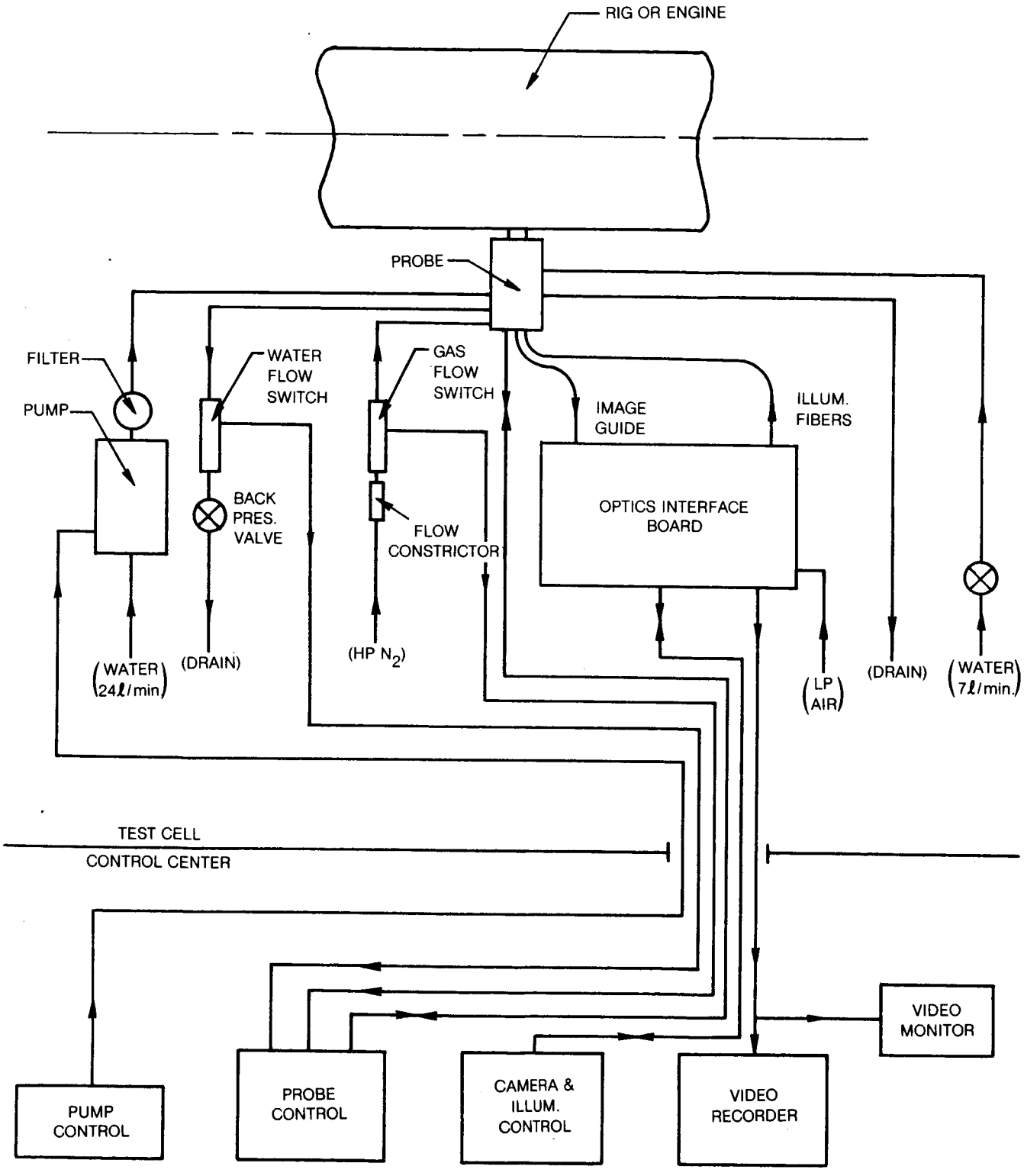

84–7–78–31

the probe (not lined up with the air hole as it should be). In port 1 we have depicted the conical 60° FOV view looking upstream at the igniter and fuel nozzle. In port 3 we show the 90° FOV lens that has views directly along the liner and across the liner. These views at the far field angles, however, are somewhat distorted.

A photograph of the actuator unit mounted to the rig on port 1 is shown in Fig. 53. In this picture the flexible image guide can be seen comming out at the top of the tubing above the actuator box and bending downward along the right hand side of the picture. The probe cooling water lines, one from the pump, enter at right angles to the copper tubes at the top of the actuator and terminate at fittings in the brass adapter blocks shown. The brass blocks divide the water inlet and outlet into the two 6 mm copper tubing for the quadrant sector probe cooling discussed previously. The smaller gas purge line also enters at right angles on the right hand side at the top of the actuator. Two illumination fibers and their connectors can be seen comming straight out the top of the harnessing along the probe axis. The copper tubing for water cooling the actuator case (at line pressure) and boss mounting plate along with the electrical cable harness and connector can also be seen just to the right of the actuator box.

Care had to be taken with the support of the flexible water liner to allow for rotation of the probe. The probe could rotate from +165° to -165°. This rotation range was set by the placement of the limit switches in the actuator unit. The hoses were arranged so they would not interfere with the image guide and the sensitive illumination fibers. This problem can be greatly alleviated (as we found out after the tests) by using pairs of swival fittings for connecting the water lines to the probe. The swival fitting pairs give the water lines two degrees of rotational freedom at the connecting joints; thus, greatly reducing the motion of the water lines with the probe is rotated.

Connections of the different viewing system components and the water and gas supply inputs are shown in the system schematic of Fig. 54. The pump on the left hand side of the figure boosts the line water pressure (0.65 MPa) to 0.93 MPa for the probe cooling. Care must be taken that the water supply line can provide at least 24 ℓ/min flow. A valve, placed in the cooling water return line, is set to give a 0.45 MPa backpressure at the probe outlet to increase the boiling temperature. If the water flow falls below about 18 ℓ/min a flow switch sends back a signal to the remote probe control unit.

Purge gas for the probe is obtained from a high pressure nitrogen line. A sonic flow constrictor keeps the mass flow of nitrogen at a constant flow rate determined by the upstream pressure and independent of the downstream (rig) pressure; provided the upstream pressure is initially much greater than the downstream pressure. For the rig test we used 5.6 MPa nitrogen for the inlet

pressure, giving 10 kg/hr flow. During the engine tests, however, we only had 3.9 MPa of nitrogen available. This is only about 0.86 MPa above the engine pressure. Initially the engine is at atmospheric pressure and the flow constrictor throttles the flow to about 6.8 kg/hr. This mass flow should hold up to a point as the discharge pressure rises closer to the inlet pressure.

We also require low pressure air (~0.24 MPa) to operate the pneumatic mirror slides on the optic interface board. In addition to the cooling water for the probe, an additional cooling water line (at line pressure) is used for the actuator case and adapter plate that mounts the probe to the rig. Cooling the adapter plate is very important for the survivability of the sliding seals on the probe.

Ten test runs were made with the HP rig that ran in duration from 15 min to 60 min. Most of the runs were closer to 40 min and the accumulated running time was about 7 hours. Testing in the HP rig took place over a period of 4 weeks.

The first three test runs were made at full rig operating conditions; that is, both the indirect fired and electrical heater were in the air supply line (cf. Fig. 50). In this condition the inlet air can be heated to the required 430°C at air flows of 1.8 kg/sec and pressure at 13 atmospheres. For the last 7 runs the rig was operated at a reduced air flow of 0.8 kg/sec because only the electrical heater was available for the test. At reduced conditions the air inlet temperature is again brought up to 430°C but the flow and pressure are reduced to 0.8 kg/sec and 8.5 atmospheres. The rig was autoignited at the inlet temperature which could momentarily be raised to about 460°C with the exhaust backpressure valve reducing the flow. Jet A was the fuel used for the tests.

Eight of the test runs were made in port 3, the furthest port downstream in the combustor. One run was made in port 1 and one in port 2. During the test runs, probe tip temperatures were monitored. The highest temperature observed was 204°C at a 50% probe insertion. When the probe tip was fully extended and at the center of the combustor (cf. Fig. 52) the temperature fell to 150°C. The highest temperatures were in the 30% to 50% insertion range which indicates that the most intense combustion was taking place a short distance inside the liner.

At full operating conditions and with the probe fully inserted into the combustor the probe cooling water temperature rose about 2.8°C. With 24 ℓ/min flow, this temperature rise corresponds to a heat removal rate of 4700 watts, or an average heat flux of 150 watts/cm^2 (0.92 Btu/sec/in^2) in the probe. For comparison, under a previous program maximum heat fluxes at the liner surface were measured with a calorimeter to be 90 W/cm^2. The average heat flux is greater on the immersed probe because of additional convective heating, and the probe surface probably has more radiant heat loading than the liner since each elemental surface area sees the flame from a greater angular distribution (viz. 2π steradian).

Twelve rolls of 35 mm film (20 and 36 exposures) were taken inside the combustor rig. Five of the rolls were made with black and white tri-X film of which one roll was developed using a wide latitude developer (POTA). Another roll used was a special EG&G extended range film which was supplied by NASA personnel. Six rolls of color film, ektachrome 400, were also exposed in the combustor. In addition to photography, about two hours of video tape were recorded with views in the combustor rig.

Views are scanned in all directions from about -165° to +165° and over the full range of probe depth. With the probe fully withdrawn we could view the outside surface of the liner and the space between the liner and rig wall. At port 3 we appeared to be near the end of the luminous flame zone. At ports 1 and 2, however, the probe was almost completely immersed in the flame when inserted in the combustor. Very clean views of the liner walls could be observed when the combustor operation was reduced to typically idle conditions. At full power operations, however, the heavy and luminous particulate (soot) ladened environment reduced the clarity of the view in most instances. With high speed photography (1/200 to 1/1000 sec exposures) the view improved somewhat with the high variability of the flame position. Photographs show the flame burning downstream from liner holes and around the end of the probe, both possibly acting as flame holders. Views of liner holes and louver lips could be seen in many cases through regions of the luminous flame.

Pictures and video images were recorded with the arc and laser illuminating sources prior to the combustor operation. Film exposure times required were on the order of 1/2 to 1 sec with the arc lamp source and the two large core illuminating fibers. Exposure with the flame present in the picture could vary from 2 to 3 orders of magnitude less than required with the arc illuminator. As a consequence, the arc illuminator is only useful with the combustor off. Pulsed laser illumination can overcome this problem by allowing exposures to be taken that are too short for flame exposures. The fastest sync. speed for our camera (Nikon FM-2) was 1/200 sec, and this was not sufficient for discrimination of the flame with the pulsed laser illumination. A 100 μsec electronic shutter would have been sufficient in this case, but was not available.

The exposed surfaces of the viewing lenses remained soot-free even when the probe view was turned upstream in the primary combustion zone. The mirror on the narrow field probe obtained some sooting deposits in certain instances, particularly on the outer edges. The sooting never obstructed the view since only a portion of the center of the mirror is in the field-of-view. On the other hand, except on a couple of occasions, the ends of the illuminating fibers would accumulate soot deposits and block the illuminating light. On one test run with the narrow field probe, no sooting was observed on the fiber ends; and after the final run a protruding fiber in the wide field probe was also clean. The protruding fiber end was most likely kept clean by a pyrolytic heating effect.

Six figures (viz. 35, 42, 43, 46, 47, and 48), discussed previously in conjunction with other topics, have shown views inside the operating combustor rig. Figures 55a through 55f shows six more views inside the combustor. In Fig. 55a we have a clean view of the liner wall and hole illuminated by the flame upstream (to the left) of the view. In this case the combustor was reduced to idle conditions and there was no flame to partially obscure the view. Details on the order of 1 mm can be seen. The probe was in port 2 with the 90° FOV lens. The views from Figs. 55a through 55e were taken on Ektachrome 400 film (color transparencies). Muitiple processing necessary to produce the report figures reduced the original quality of the pictures somewhat. From Figs. 55a through 55d the camera exposures were set for 1/200 sec at F/4.

In contrast to Fig. 55a, Fig. 55b shows a view of the liner surface through partially transparent flame. In this case the combustor was in full operation (but at the reduced inlet air conditions discussed before); and the 60° FOV probe was in port 3. The camera settings were the same as before. We also had a neutral density ND 0.6 filter in the optical path, making the exposure of Fig. 55b four times less than Fig. 55a. In Fig. 55b the flame partially obscures the liner air mixing hole and the lower lip. The image conduit was chipped forming the non circular outline and crack on the right hand side of the picture. As discussed previously, the liner view like that shown in Fig. 55b can be improved with the use of wide latitude photography and pulsed laser illumination. Unfortunately the laser illumination could not be demonstrated in the HP combustor rig due to the unavailability of a high speed shutter. Digital image analysis is somewhat limited on a picture like Fig. 55b since much of the information on the surface detail of the hole and louver lip is not present. The flame background could be suppressed and the hole and louver lip contrast improved some; however, spatial noise will increase to obscure the details.

Figure 55c shows a view across the combustor taken with the 60° FOV lens and the probe only slightly extended into port 3 of the liner. The flame has saturated the lower portion of the picture but the liner surface in the upper part of the figure can be clearly seen. The camera settings were again 1/200 sec at F/4 for Fig. 55c, but this time we had a ND 1.0 filter in the path, making the exposure 10 times less than in Fig. 55a.

For Fig. 55d we extended the probe (60° FOV, port 3) to 50% of its full insertion depth and turned the view downstream. Here we can see pieces of the flame downstream of the probe. No filter was in the optical path and the camera settings were the same as before.

FIG. 55 COMBUSTOR RIG VIEWS

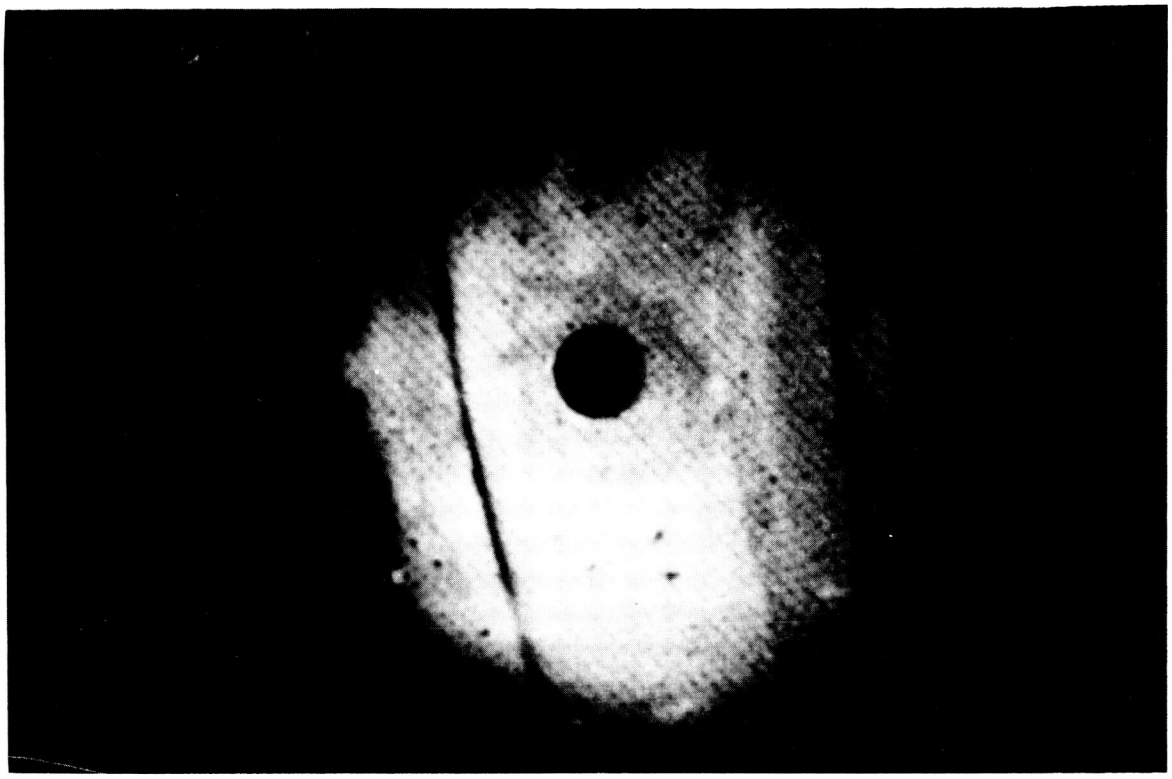

a) COMBUSTOR AT IDLE

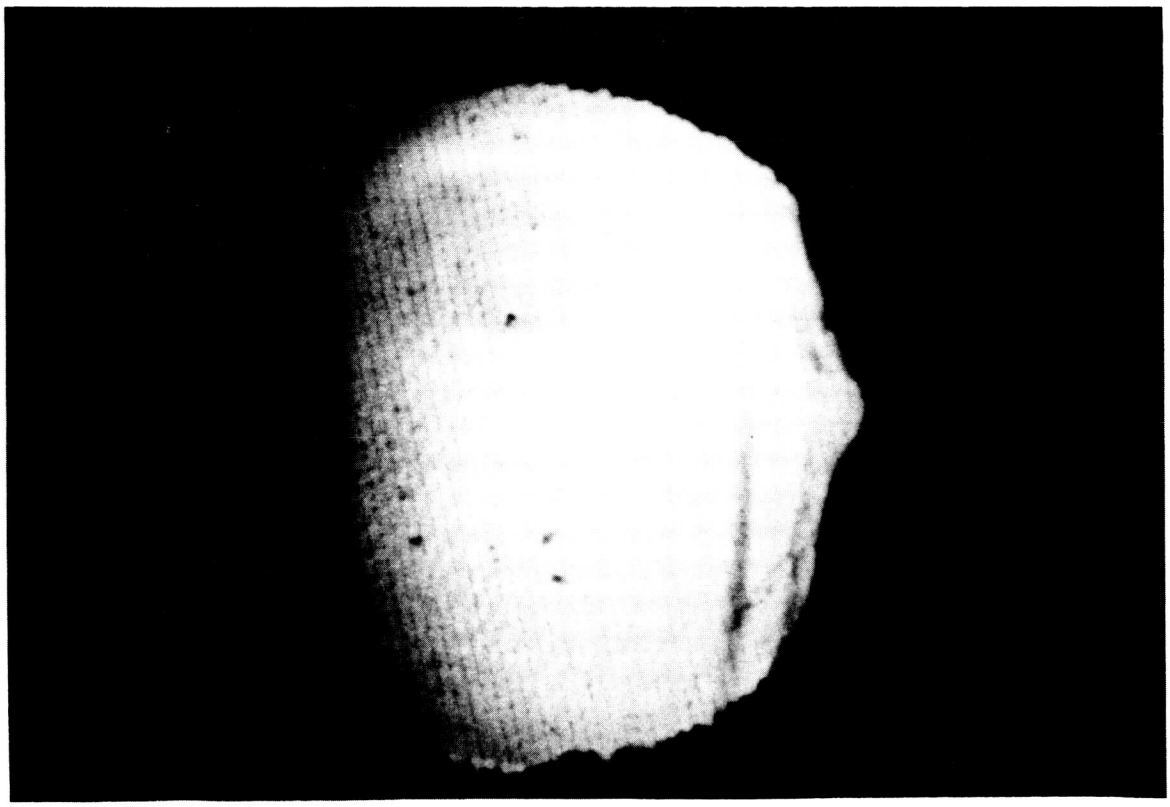

b) COMBUSTOR ON FULL

84-7-78-32

FIG. 55(CONT'D) COMBUSTOR RIG VIEWS

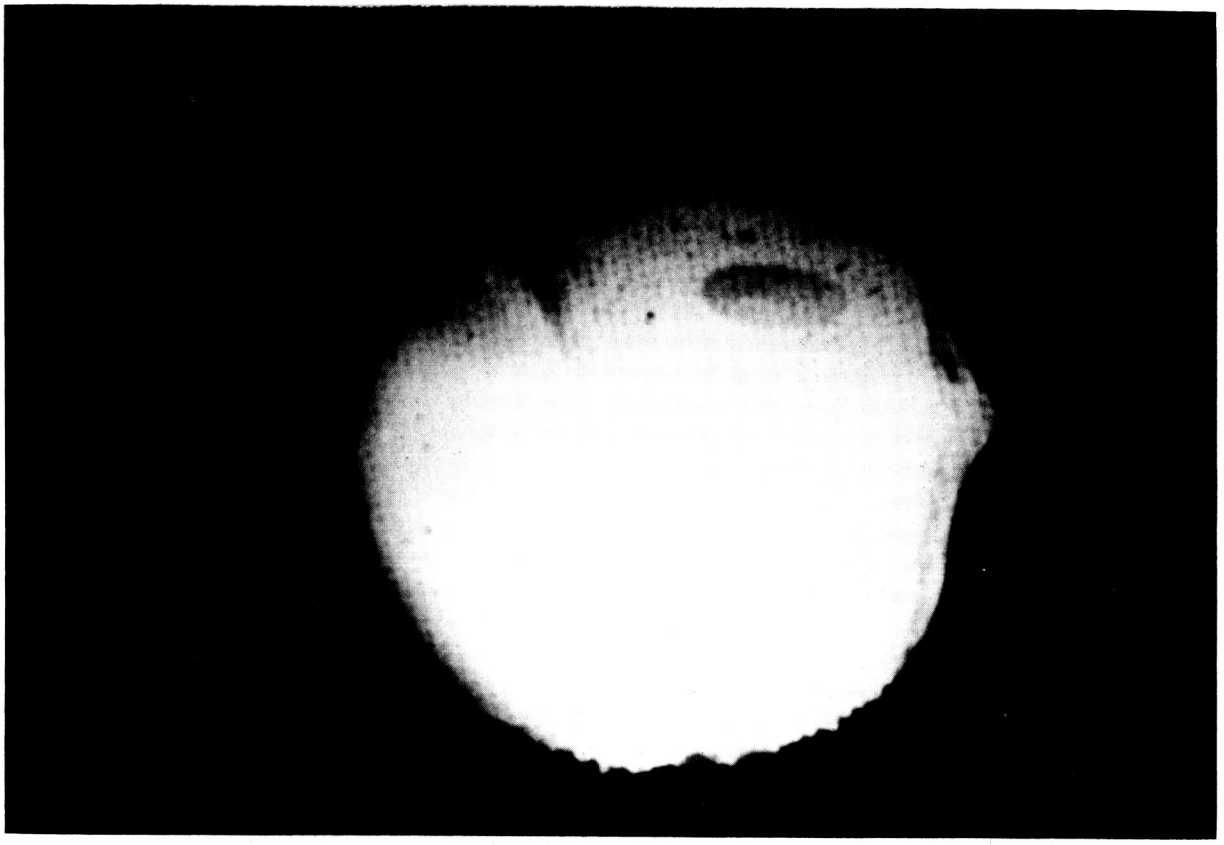

c) VIEW ACROSS LINER

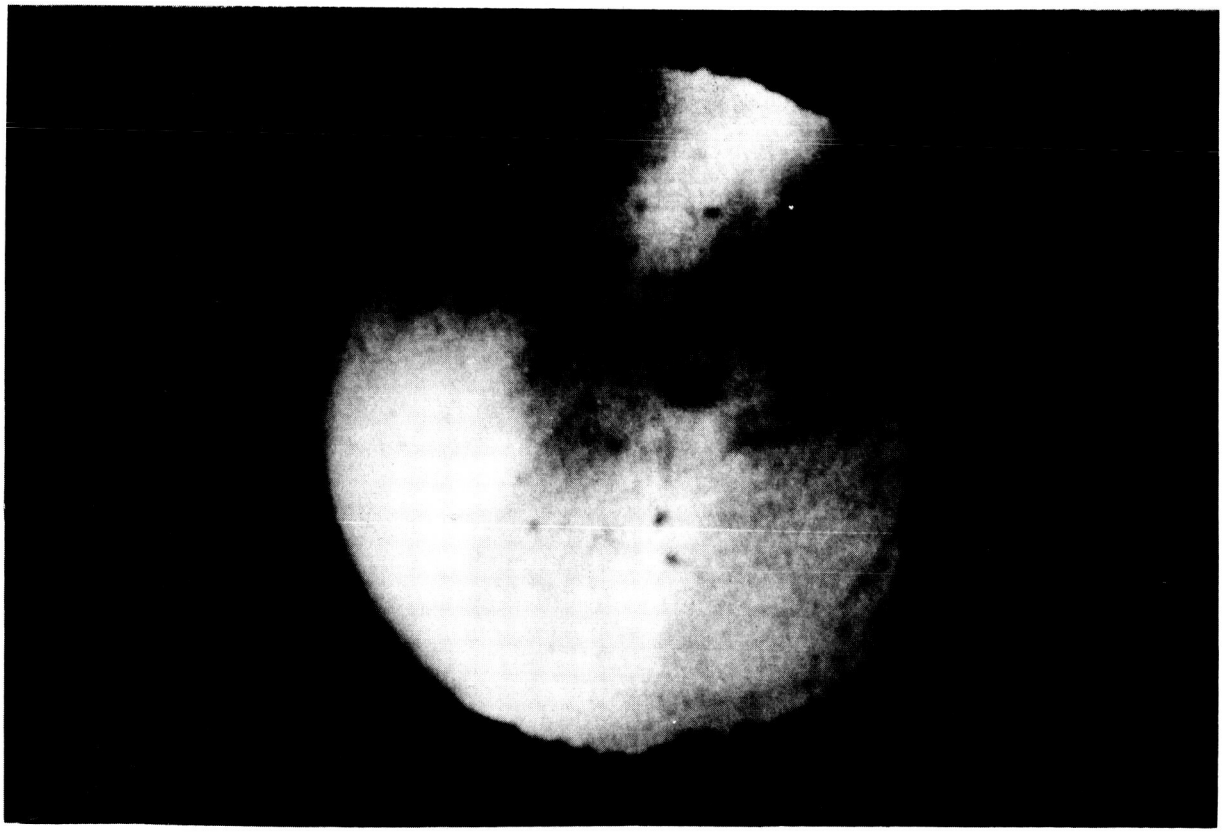

d) VIEW DOWNSTREAM

FIG. 55(CONT'D) COMBUSTOR RIG VIEWS

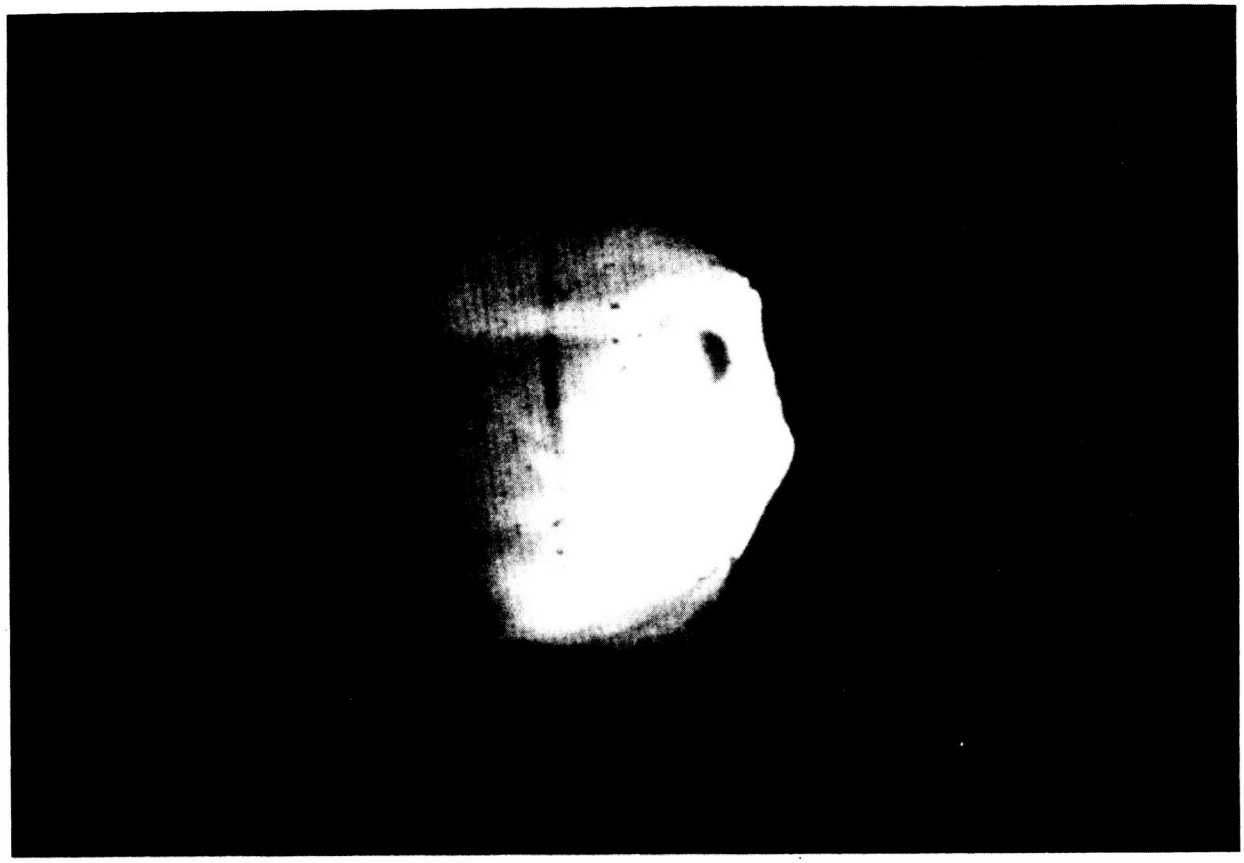

e) COMBUSTION AT UPSTREAM AIR MIXING HOLE

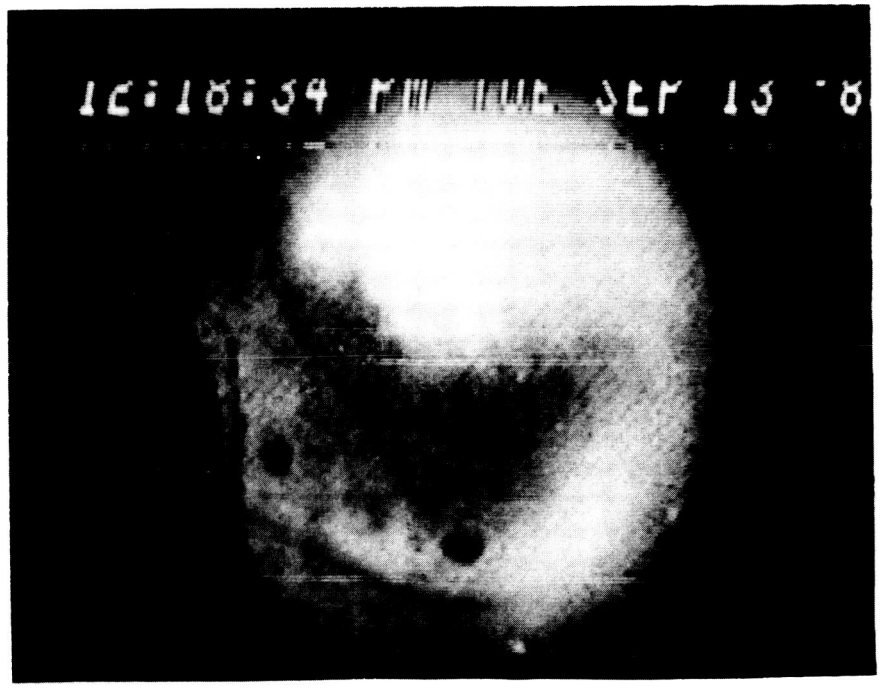

f) COMBUSTION AROUND END OF PROBE

Figure 55e shows an internal view across the combustor with the flame near the liner wall and around an air mixing hole. For this figure the 90° FOV probe was fully inserted in port 3 and turned to view slightly upstream (114° clockwise from the downstream axis). In this case the camera exposure time was decreased to 1/1000 sec at F/4 and a ND 0.6 filter was in the path. The flame intensity has saturated part of the picture, but the louver lip can be seen with only a few mm resolution at those locations where the flame is absent. A series of 5 pictures were taken at this position at 1/1000 sec. The pictures were taken within a couple sec of each other. Figure 55e is one of the pictures. The other four pictures also show the flame by the liner wall but in different intensities and locations. In one of the pictures the liner wall is completely obscured by the flame, and only a small cresent shaped portion of the air mixing hole is visible.

Figure 55f shows a video picture of the 90° FOV probe just barely inserted into port 2. The video framing rate gives an exposure of 1/30 sec. In this view the combustor was being operated at reduced input conditions of pressure and flow (idle). Here we can clearly see a rotation of the flame about the liner hole and just beyond the end of the probe. Whether this flame rotation is caused by the tip of the probe protruding into the combustor, by the air streaming into the liner through the hole, or a combination of both is uncertain. We could observe a similar effect on a mixing hole across the liner where the probe had no effect (cf. Section 4), and the combustor was operating under normal conditions.

6.0 ENGINE TEST

After the HP rig tests at the Research Center and prior to the completion of the contract program, we held discussions with Pratt & Whitney (P&W) engineering personnel on the possibility of testing the combustor viewing system, under their sponsorship, on an engine test run. This test would allow us to further evaluate the system on an even higher pressure combustor (30 atm. vs. 13 atm.) and give the P&W engineers an opportunity to evaluate this type of instrumentation for their future use in engine development. Pratt & Whitney agreed to support a test of the viewing system, and the period of performance of the contract was extended by NASA to allow enough time to schedule the test.

The viewing system was scheduled to run on an experimental PW2037 engine at a sea level jet engine test stand at the P&W Wilgoos turbine facility in East Hartford. The viewing probe test was to be run in conjunction with other tests being performed on the engine. As a consequence, a test run had to be chosen such that the viewing probe would not interface with the other tests being conducted. The viewing probe was to be mounted on an unused igniter boss and view the operation of the fuel nozzles during engine operation. The PW 2037 is a high bypass ratio unducted fan engine. For the engine test, however, large ducts are placed behind the engine fan casing to route the bypass air around the instrumentation on the engine.

Prior to operation on the engine, the viewing probe was tested for modal vibrations at the P&W vibration laboratory. Here the viewing probe was mounted at an igniter boss in the diffuser case of a PW 2037 engine shell. The entire engine shell was vibrated over a range of 20 to 250 Hz. The maximum vibration displacement was .125 mm (commercial specifications). During the vibration tests the probe was actuated in and out and rotated over its angular range. Views of the fuel nozzles and inside the engine shell could be observed with flood lamps lighting the inside of the engine shell. At no time during the tests did the probe view on the video monitor appear to vibrate or distort.

Using a strobe lamp we could observe the modal frequencies of the actuator unit, which is cantilevered from the engine case. At 28 to 30 Hz a tangental (or circumferential) motion of the actuator could be observed. At 45 Hz an axial motion changing to a circular motion at 50 Hz was observed. The 45 Hz frequency gave the maximum acceleration and displacements of 6.2 g's and 1.5 mm. The two copper cooling water tubes connecting the actuator enclosure cooling to the mounting adapter plate cooling vibrated axially at 122 Hz. This vibration was damped significantly by the addition of cross supports to the two tubes. We also expected that the probe water cooling lines and purge air line, which were not connected during the vibration test, would provide additional damping and amplitude attenuation to the actuator case. Several additional, but small, vibration peaks at higher frequencies were observed by an accelerometer pick-up on the actuator housing. These additional peaks were probably due to internal components in the probe actuator.

A strain gauge was placed at the actuator-boss connector where the stress from the vibrating actuator unit would be the greatest. A plot of the dynamic stress amplitude, computed from the gauge reading, from 30 to 270 Hz is shown in Fig. 56. The maximum stress at the connector was 4.6 ksi (31.7 MPa) at 45 Hz. This was an acceptable stress level for the engine test.

Two major changes were made to the viewing system for the engine test. The clear plastic dust cover for the optics interface board was replaced with a sturdy aluminum frame and enclosure, and a new adapter plate for mounting the actuator to the engine was fabricated. The copper tube for cooling the sliding probe seals was imbedded in the new adapter plate around the seals. This construction gave better cooling for the seals and more space for mounting the probe. Besides these changes, the actuator drive motor currents were monitored with separate meters. The currents are related to the torque experienced by the motor so that we could be warned of an impending stall on probe rotation and insertion. Also a new lens barrel was made for the probe that had a 0.5 mm aperture instead of the previous 1 mm aperture for better resolution and depth of field.

A schematic showing the bottom end of the actuator mounted to the engine case, the connector fitting, and the probe extending into the linear is given in Fig. 57. The range of insertion of the probe is indicated with the two short broken lines. The approximate location to which the probe was positioned during the engine test is shown in the figure. We chose the 60°FOV viewing lens with a 0.5 mm aperture (F/6) for the test, because of the better resolution we could achieve compared to the 90° FOV lens. At the 0° position the probe views directly at one of the fuel nozzles. The cooling water hoses placed next to the engine would allow a $\pm$ 90° rotation so that we could also view across the annular liner in both directions.

The probe was mounted on the engine during assembly when the turbine casings were removed. At this time we checked the probe to liner hole clearance to determine if there was enough clearance to allow for thermal growth of the liner relative to the probe. Bending or scraping of the probe from lack of sufficient clearance could restrict the cooling water flow or cause a leak leading to severe damage of the probe. The engine liner hole was enlarged slightly on the upstream side to give a clearance of 1.25 mm which we estimated was adequate in this instance.

At this time we illuminated the inside of the liner with a flood lamp and made video recordings for comparison of the same view during the engine run. Figure 58 shows two photographs taken from the video monitor of the digital image analysis system. The liner inside surface was painted with a dark thermal indicating paint making it hard to see. The discs seen around the fuel nozzles in Fig. 58 were painted with white diamond shaped squares.

FIG. 56 STRESS RESPONSE PLOT OF VIEWING PROBE ON DIFFUSER CASE FITTING

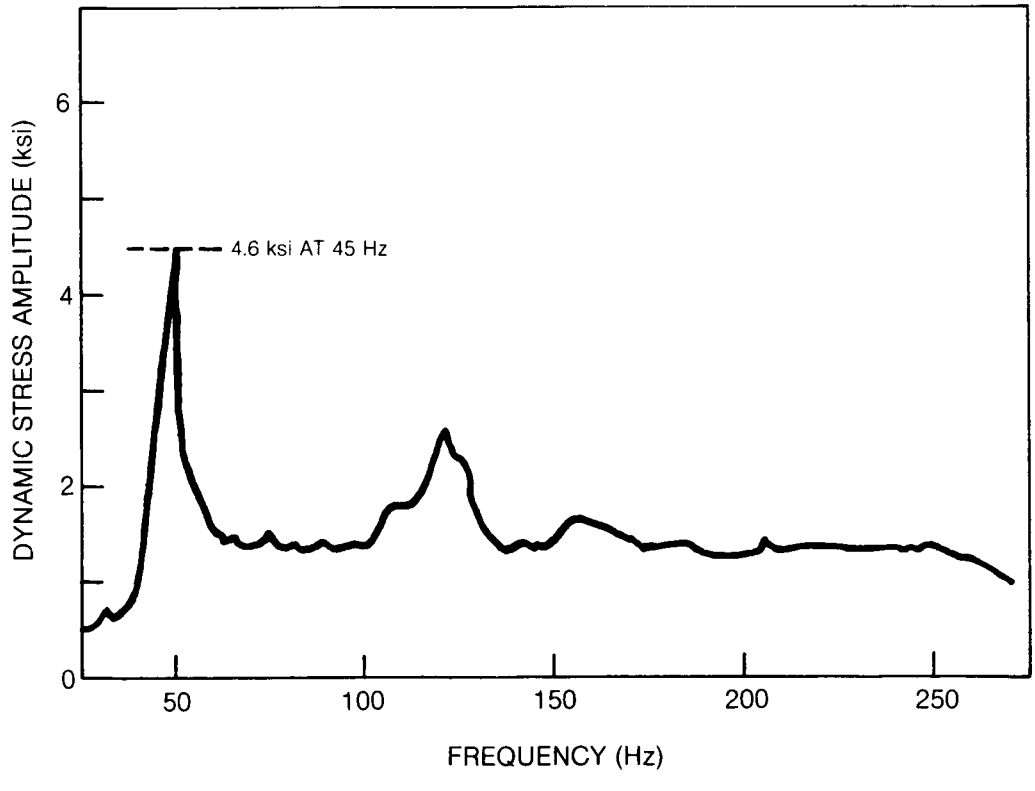

84-7-78-35

FIG. 57 VIEWING PROBE MOUNTED ON ENGINE DIFFUSER CASE

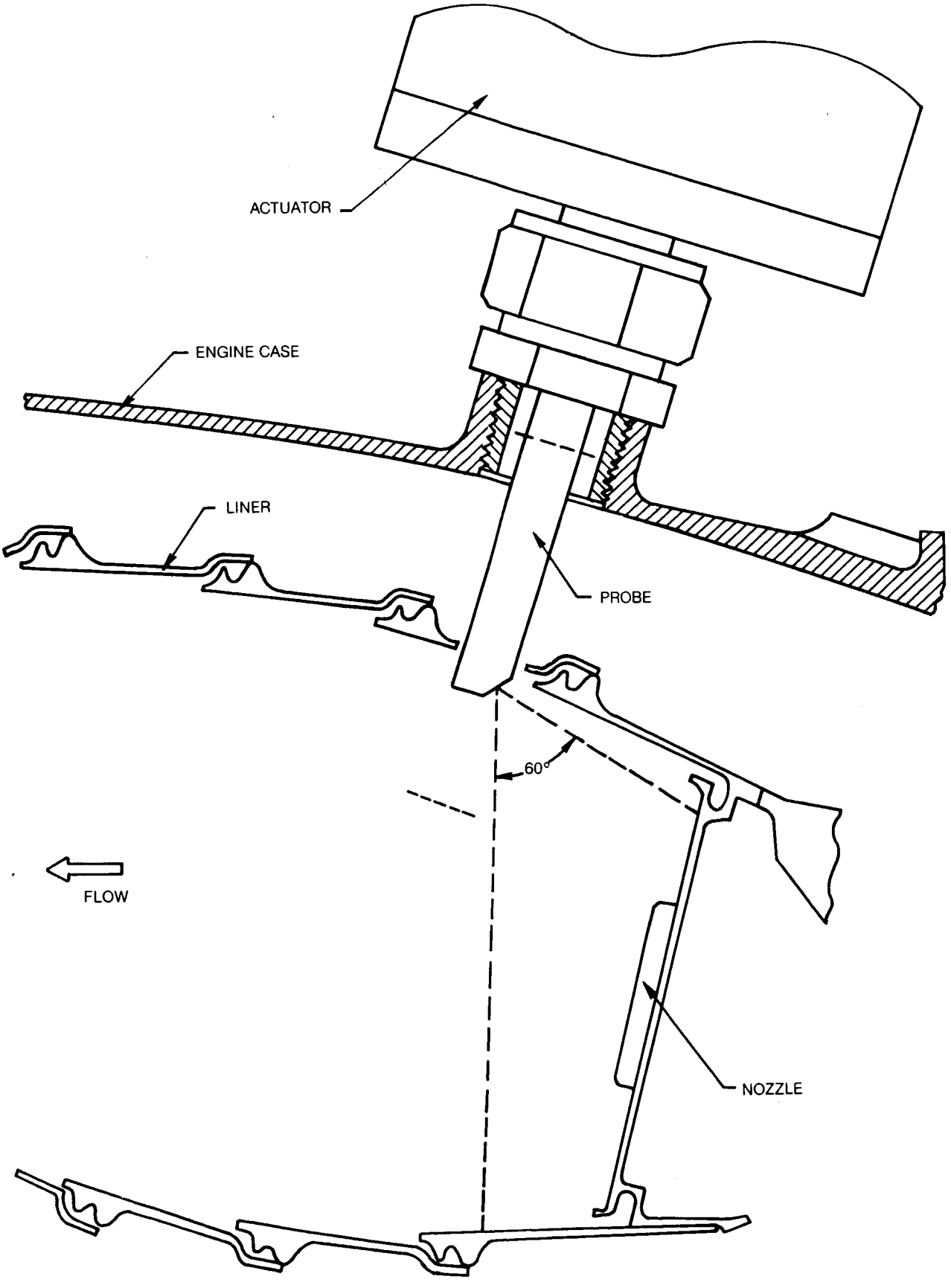

FIG. 58 FLOOD LAMP ILLUMINATED VIEWS INSIDE ENGINE COMBUSTOR LINER

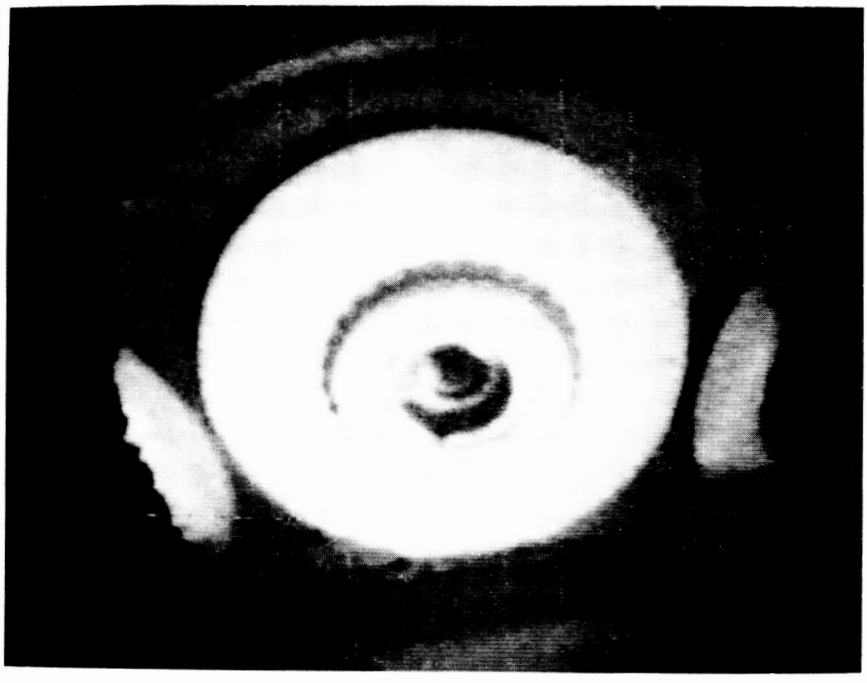

a) DIRECT VIEW OF NOZZLE

b) VIEW AROUND LINER

After the turbine sections were installed and the engine pinned in the test stand, the probe was reinstalled and viewing system was set up and checked out. The illumination fibers were in the probe but not connected to the interface board. External illumination was not used due to the test mentioned above with the flood lamps, the sooting problem, and the extra time needed that was not available in this case. Two accelerometers were also mounted on the actuator box to monitor axial and transverse motion of the unit in the control room.

Two engine runs were made with the viewing probe each lasting about 1 1/2 hr. The probe was fully retracted for a good part of the test while other measurements were being performed. During the viewing probe tests, the probe was inserted to about the position shown in Fig. 57. At full engine power with the probe slightly inserted, probe tip temperatures ranged from 170° to 185°C. With the probe fully retracted the temperatures fell to around 70°C. About an hour of video tape was recorded and 20 film exposures on 35 mm ektachrome 400 were taken.

The accelerometer signals from the actuator box showed no more than .025 mm deflection even though the engine flanges indicated .050 mm of motion. The maximum motion of the actuator during the vibration tests discussed above was 1.5 mm. The water cooling and purge gas lines must be provided the additional dampening as suggested and, of course, the engine vibration was only .050 mm compared to the .125 mm at the vibration lab.

Four pictures from the video tape recordings are shown in Fig. 59. These pictures were made from the digital image analysis system monitor. The reproduced pictures are not quite as good as the original monitor view. Figure 59a and b show two views of the fuel nozzle with the engine running at full power (take-off thrust). For these pictures the video camera lens was set at F/16 and a ND 1.0 filter was in the optical path. The filter reduced the exposure by a factor of 10. Even still, parts of the picture with the flame were saturated. In order to view some of the background we had to overexpose on the flame. With a ND 2.0 filter (100 times attenuation) the flame could be seen but not the background. In Fig. 59c we show a view with the engine at idle. In this case the video camera lens was at F/16 without a neutral density filter. At idle we see the spray or flame from the nozzle is more spread out and thinner. The most luminuous flame occurs near the inside radius of the liner (lower part in the picture). Figure 59d is another view across the liner at full engine power.

Two views inside the engine combustor, taken from the 35 mm color film exposures, are shown in Fig. 60. The camera lens in this case was set on F/4 at 1/1000 sec. No filter was used for the camera shots. Again we have the flame region overexposed and the background, especially above the nozzle, underexposed. The wide latitude photography would be helpful here, but may not be available in color. On many of the views from the video recordings and the photographs, we can see a cone of luminosity emanating from the nozzle. We are not sure if this is the fuel spray being backlighted by the flame or if it is part of the flame itself. That is, we are not sure where the combustion begins.

FIG. 59 ENGINE COMBUSTOR VIEWS FROM VIDEO

a) NOZZLE AT FULL POWER

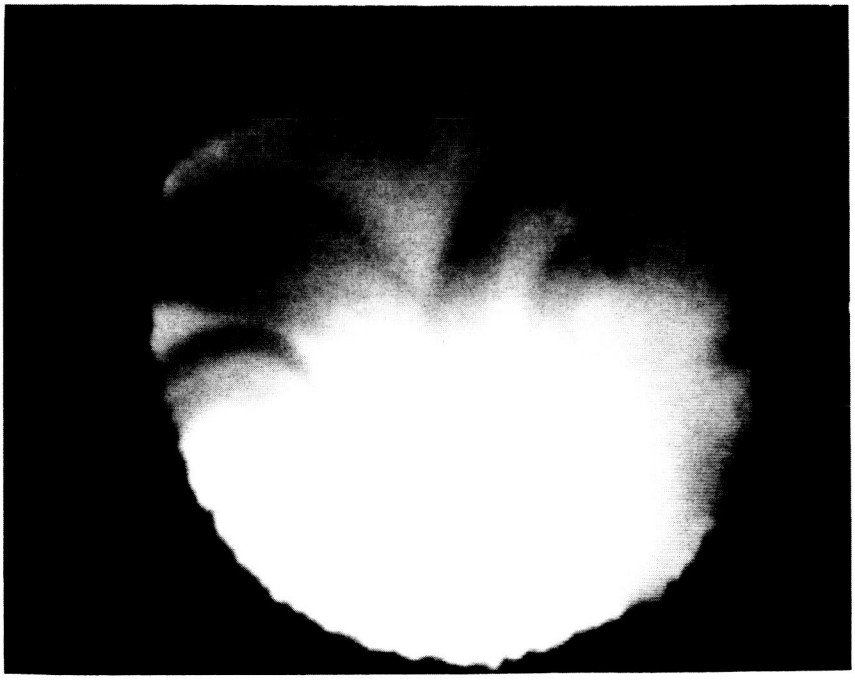

b) TWO NOZZLES AT FULL POWER

FIG. 59(CONT'D) ENGINE COMBUSTOR VIEWS FROM VIDEO

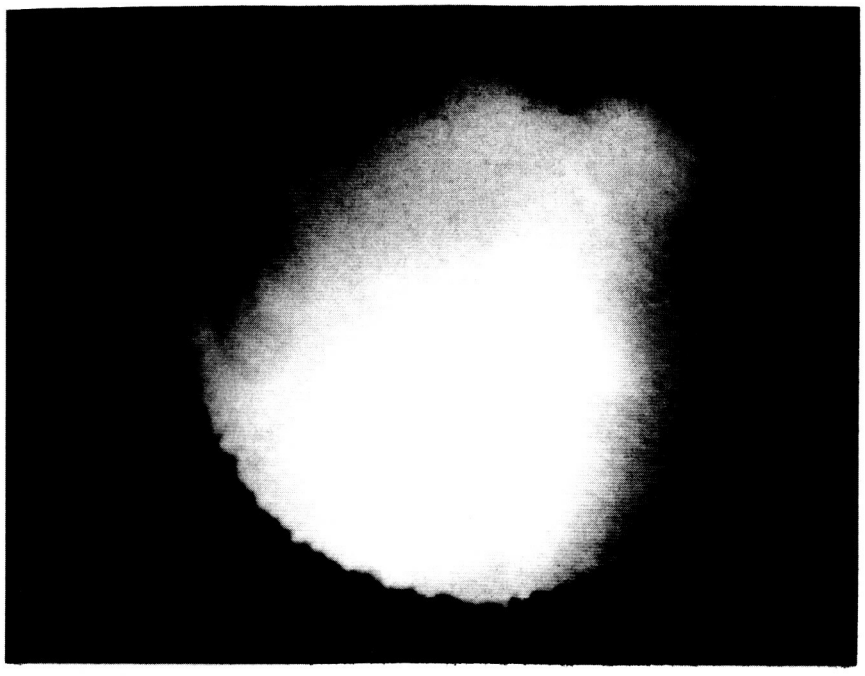

c) IDLE

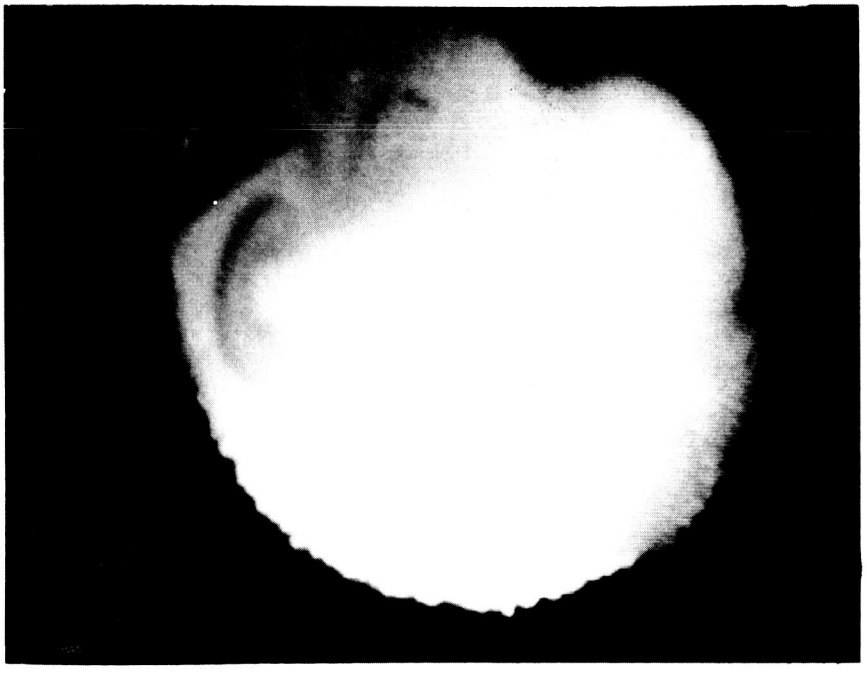

d) FULL POWER

FIG. 60 ENGINE COMBUSTOR VIEWS FROM PHOTOGRAPHS

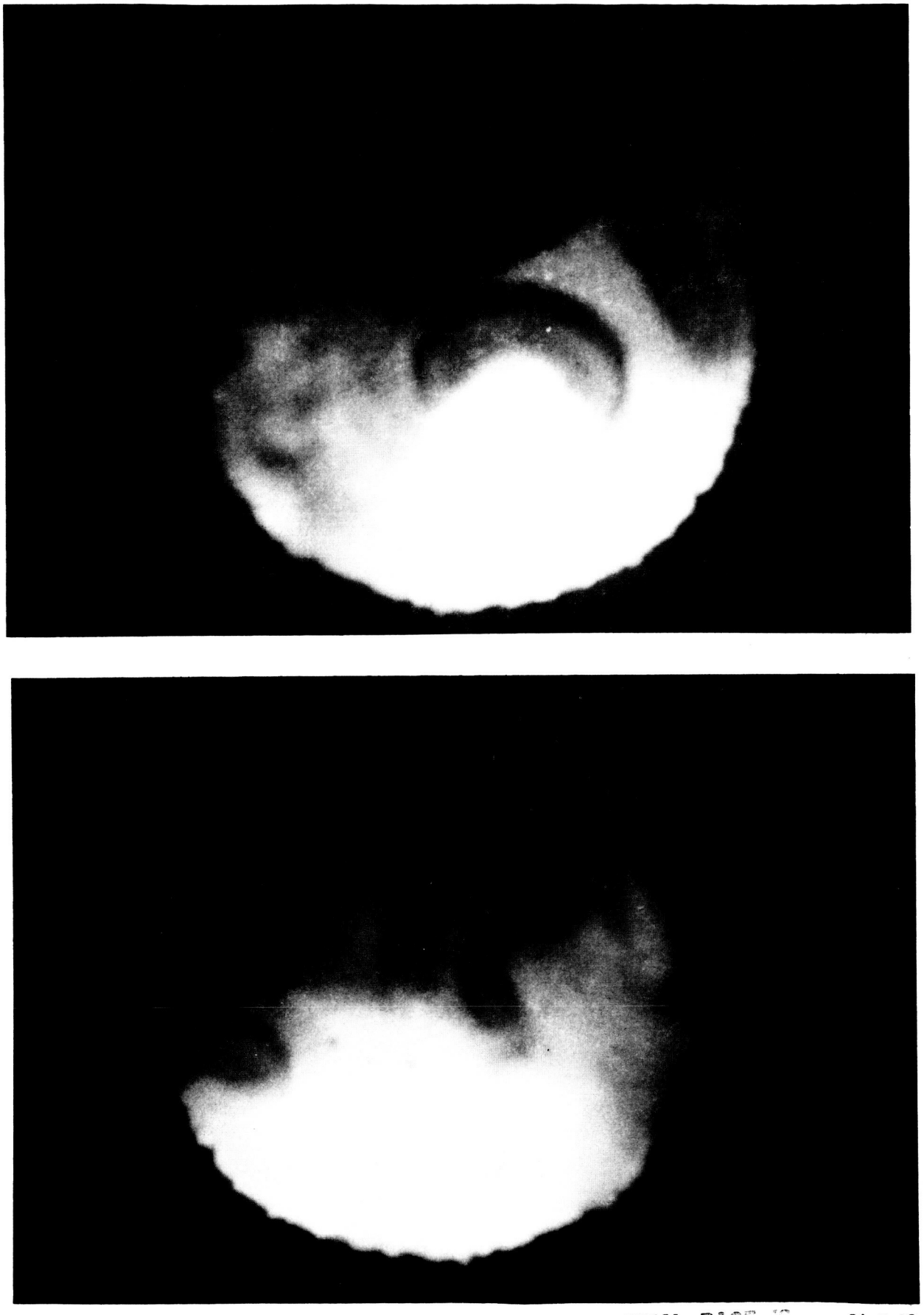

84-7-78-40

7.0 DISCUSSION OF RESULTS

Several design goals and guidelines for the prototype viewing system were laid out in the beginning of the program. In this section we will discuss and compare our results with those goals. We will also discuss some of the problems that arose and corrections that were or could be taken to improve the results. In addition, we will discuss new ideas that could be implemented in future designs.

A major goal of the program was to design a system for continuous viewing inside an operating gas turbine combustor to examine liner surfaces, fuel nozzles, flame holders, and the combustor zone itself. We met this goal with the design of a water cooled cylindrical probe with an external actuator for rotation and linear motion. We demonstrated that the probe could operate safely when fully actuated to the center of the primary combustion zone of a 13 atmosphere combustor. The probe was also operated safely on a 30 atmosphere jet engine combustor where it was positioned a few mm into the liner for best views of the nozzles.

One desired feature of the viewing system was to allow interchangeable probes with the same actuator. Moreover, the distal end section of each probe was to have interchangeable objective optics for different magnifications, view angles and depth of fields. Our system allows interchangeable probes and each probe has provisions for changing the objective lenses to give different fields of view or magnifications. In order to cover a wide range of magnifications, two probes were required - one for the narrow fields-of-view (high magnification and one for the wide fields-of-view (low magnification). The angle of view for the wide field probe is fixed at 45°. For the narrow field probe one could change the view angle with replacement mirrors. Only a 60° view angle mirror was used, however. One of the features we would recommend for a second generation design would be to include a remotely adjustable tilt to the view turning mirror on the narrow field probe. This could be accomplished, for example, using a small flexible shaft with a screw on the distal-end that advances a spring loaded tilting mirror device. The view from the narrow field probe with a fixed direction of view extends around a annulus as the probe is scanned in rotation. With the remote tilt on the mirror one could extend the coverage of the narrow field probe enormously.

This brings us to another problem with the narrow field probe and that is its small depth of field. In fact, the higher the magnification, the more restricted the depth of field becomes. As a consequence, for the second generation probe we would also want a remote focus adjust on the objective lens. This adjustment involves the separation between the objective lens and the image guide. Again, this feature might be accomplished with small flexible shafts that turn screw positioning, spring loaded devices.

The wide field probe, on the other hand, has a view that encompasses a large area and has a large depth-of-field (e.g., 3 cm to infinity). As a consequence the wide field probe does not require the extra adjustments that would be very beneficial for the narrow field probe.

Tests with the image conduit and narrow field viewing lens (13°FOV) showed that we could easily resolve 0.16 mm at a distance of 6 cm from the probe. With the 3 meter flexible image guide coupled to the system the resolution was reduced somewhat giving about the 0.25 mm goal. At further object distances, of course, the resolution would decrease.

Stereoscopic viewing was another desired feature of the probe. We tested stereoviewing in the laboratory combustor with a single probe by taking two separate pictures (c.f. Sec. 4.7). The two pictures were taken with the end of the probe shifted 1 cm and rotated 2.6° to keep the same view in each picture. While we could clearly resolve depth of liner cracks to within our calculated estimates, steroviewing of the semitransparent flame could be confusing. With steroviewing in the laboratory one could visually separate the pixel screen and any defects on the image guides from the desired image. This separation could also probably be done with a digital image analysis routine to enhance the images. We did not recommend designing the prototype probe with stereoviewing, however, primarily because of the extra probe diameter required for the optics. We would probably need a probe 28 to 32 mm in diameter for stereoviewing. This size is fairly large compared to the 12.7 mm diameter that we used for the prototype probe design. We would also need a larger actuator unit to drive the probe. The increased size for stereoviewing would have perturbed the combustor more severely by requiring a large access hole in the liner; and an engine test, which also has limited access on the combustor case, would have been precluded. We felt that the extra benefit from stereoviewing of liner surfaces would not balance the extra difficulty in the design, and data analysis, and the more severe perturbation that the system would cause. Besides, many other problems such a distortion and loss of contrast had not been thoroughly investigated in combustors. These additional problems may reduce the depth measuring ability of stereoviewing in combustors.

The viewing system was to have an illumination source for cold inspection of liner surfaces before and after combustor operation. The illuminator was also to be an aid in viewing liner surfaces when the combustor was operating. We recommended and tested two illumination sources: an arc lamp for a broad spectrum source for cold inspection, and a pulsed laser source for inspection during combustor operation. We demonstrated the usefulness of the pulsed laser system for viewing liner surfaces in the presence of a flame. This demonstration was in a laboratory combustor test. In the high pressure combustor the illumination fiber ends became sooted; and more importantly, we did not have the capability of making short enough exposure times to take advantage of the pulsed laser illumination. The sooting problem was solved by letting the illumination fiber extend from the probe slightly for pyrolytic heating. Exposure times required

for the pulsed laser source could be obtained with a synchronized electronic image intensifier system, or possibly with a synchronized high speed rotating disc with an aperture. Application of these later two techniques was beyond the scope and time scale of the program.

The fiber optics used to deliver illumination light to the distal end of the probe was chosen to handle the pulsed laser source as well as provide as much continuous broadband visible light from the arc lamp source as possible. An obvious choice seemed to be a large diameter fused quartz fiber. The large diameter fiber could provide 0.6 watts of arc lamp light at the distal end of the probe, and also handle sufficient pulsed laser energy without surface breakdown and damage to the end of the fiber. The small radius bend in the fiber required at the end of the probe, however, gave us a problem. A fraction of the illumination power would leak out of the bend in the fiber. The light loss created a shadow in the middle of the illumination pattern, and in addition, could create glare in the image on back scattering from lens surfaces at the probe end. Reflecting or absorbing paint placed on the fiber bend to prevent the glare could burnoff from the continuous, high intensity arc illumination or from a continuous laser source (e.g., Ar ion laser) with powers greater than 1 watt. The solution to this problem may be to use a bundle of much smaller diameter quartz fibers. With the bundle of fibers we will suffer a packing fraction loss from the space between the fiber cores. This loss may amount to 50% of the input light. Besides the packing loss, one would have to determine how to support the fiber bundle. The pulsed laser input end requires cleaved fibers free of epoxy bonding materials. The distal end of the illuminating fibers would also have to be epoxy free if pyrolytic heating is used to keep the ends soot free. One would also have to hold the flexible fiber bundle, possibly in a metal tube, for insertion into the probe.

Another important aspect of the program was to obtain clear images inside the combustor. We showed that optical distortion from thermal gradients can visibly degrade the image to a certain extent, especially in a high pressure combustor, if we view with good resolution. A digital image program to correct for distortion requires information on the distortion itself. This information could be obtained from a liner hole or louver lip edge that we know is well defined. One could experiment with different distortion functions to find one that sharpens the edges. This function could then be applied in the local area to sharpen the image of a crack that opens during combustor operation, for instance. The application of digital techniques for distortion correction requires two dimensional Fourier plane analysis and large amounts of computation. Experimentation with these procedures was well beyond the scope of the program. Digital image enhancement techniques including contrast modification, broken fiber removal, pseudocolor, and cross section plots were applied successfully to video images from the combustor. One cannot expect the modified image to improve drastically, however, if information is lost in the original image from over or under exposure.

We would recommend that pulsed laser illumination be used to view liner problems that develop during operation of the combustor. In this case, the flame exposure is discriminated against with a combination of wavelength filtering and ultrashort exposures. An optically dense flame will appear as a dark cloud; and if the flame is fairly transparent one can view through it. It would be feasible to operate a repetitively pulsed laser at 30 Hz that would be in synchronization with the video frame signal. The video camera would also have a synchronously operating shutter (possibly a rotating aperture or electronic shutter) to capture the short pulsed laser illumination. Exposure times required may be on the order of 1/10,000 sec or less. In this manner, one could continuously view the liner without interference from the luminous flame. The development of such a system would require state-of-the-art pulsed lasers and cameras.

We feel that most of the goals and guidelines for the prototype viewing probe were met, and with some modifications the probe could exceed those goals. Advanced techniques were presented for image analysis and for viewing through the flame onto liner surfaces. The system could be used, for example, in long duration engine tests to observe the formation of damage in combustor liners.

8.0 CONCLUSIONS

Prior to this program there had been some doubt raised as to the possibility of building a probe that could be inserted into the primary combustion zone of a gas turbine combustor for viewing purposes. The extremely hostile environment in the combustor with temperatures up to 2400K, very turbulent and soot ladened gases, a high speed gas flow giving high heat transfer, and high vibration level over a wide frequency range may be prohibitive for a viewing probe. This program addressed these problems and a prototype viewing system was developed and successfully tested in a high pressure combustor rig and on a Pratt & Whitney PW 2037 engine.

The viewing probe, which was 12.7 mm in diameter and water cooled, was positioned with an actuator that was mounted on the combustor case. With remote controls the probe could be traversed in and out through a hole in the combustor liner and rotated 330° to scan the view inside the combustor. Fiber optics were used to transfer the image from the distal end of the probe to a nearby pallet that contained recording video and film cameras. An arc lamp illumination system was also contained in the pallet and provisions were made for switching to laser illumination. The illumination sources were coupled to fiber optics that carry the light to the distal end of the probe. The cameras and instruments on the pallet were remotely controlled.

Most of the design goals were met during the program including interchangeable viewing lenses with the probes, an illuminator system for viewing the combustor when cold and for viewing when in operation, the ability to monitor and record images from inside the combustor, and remote operation of the system. These goals were achieved with pressure seals, water cooling, and gas purging that allowed the probe to be operational inside the combustor. Two probes were designed and constructed. By interchanging lenses one probe can have fields-of-view from 0° to 45° and the other probe from 45° to 120°. The narrow field probe has a turning mirror to set the direction of view at 60°; and the wide field probe has its viewing optics oriented at 45°.

A problem was experienced with the large diameter illuminator fibers used in the probe. Light would leak from the fiber bend at the distal end of the probe. Replacement of the two large diameter fibers with a multifiber bundle may improve the illumination system. The smaller fibers in the bundles will not lose illumination light like the large fibers at the bend required at the end of the probe. Other improvements recommended for the system include making the view turning mirror and focus at the distal end of the narrow field probe adjustable, using double swivel connectors at the cooling water lines connecting to the probe, and current meters to monitor the torque on the probe actuator motors.

Besides the development of a workable combustor viewing system, another achievement of the program was the demonstration of pulsed laser illumination to view liner surfaces in the presence of a flame and to allow one to see through semitransparent flames. This result was demonstrated in the laboratory combustor rig. We could not demonstrate this result in the high pressure combustor principally because of the lack of an electronic or rotating disc shutter that would give shynchronized exposure times on the order of 1/10,000 sec. This exposure time would be required to discriminate against the flame illumination.

The use of digital image analysis techniques, especially contrast modification and removing broken fiber elements, was also demonstrated during the program. Pseudocolor images that show contours of combustion taking place around and behind air mixing holes was demonstrated with pictures made from sequential video frames. Air streaming in the liner holes may be creating a flame holder effect on the combustion gas moving downstream. A low pressure area may be created near the holes where the higher velocity air is streaming inward causing the combustion gases to be pulled in behind the holes. We also estimated the optical distortion in the high pressure combustor from image cross section profiles of liner holes taken before and during operation of the combustor.

Another important achievement was the successful operation of the system on a PW 2037 engine. The probe was mounted and operated on one of the engines unused igniter ports. Prior to operation on the engine, the probe passed a vibration test at a Pratt & Whitney vibration test facility. During operation of the probe on the engine, views were observed and recorded on video tape of the fuel nozzles before and during full power operation of the engine. The nozzles, spray, and flame could clearly be seen.

The combustor viewing system represents a new instrumentation device that was demonstrated to be a useful tool for combustor development. Full use of the probe has hardly been made at this time. An important thrust of this program was to build an instrument for observing damage occurring inside combustor liners. This observation could help one understand the damage process, and ultimately be used to design more durable combustors. Our liner for the high pressure rig tests was not operational for a long enough period to generate damage. Engine tests, however, can run for thousands of hours and damage in the form of cracking and buckling inevitably occurs. The feasibility of observing the damage process with a combustor viewing system that would periodically view an engine liner during phases of long term operation was clearly demonstrated.

Future uses of the viewing probe can also involve observations of the location of the combusting flame, build-up of coking deposits, fuel spray patterns, flame transient effects, measure luminous flame temperature patterns,

examination of hot liner spots at engine shutdown, monitor flame instability and turbulence, and examine first stage turbine vanes in operation. With the pulsed laser illumination one can effectively stop the motion of the view and possibly observe the fuel spray droplets. As an engine monitor one could also use a simplified viewing system to record certain functions as a flame signature to warn of impending engine problems. Many aspects of the viewing system have not been explored, and even new uses and techniques for visualization of problems may be found in the future.

APPENDIX 1

Derivation for illumination light backscattered from flame and reflected from liner wall.

Figure 61 illustrates the problem under consideration. An illuminating fiber with emitting area A_i emits light into solid angle Ω_i. The light is backscattered from the flame particles in an elemental volume $\Omega_i R^2 dx$ at position x in the flame zone from 0 to L. The light is backscattered into the receiver aperture (a pixel element or group of pixel elements) of area A_r and solid angle Ω_r.

The illumination intensity at position x from the illuminating fiber is

$$I_x = \tau A_i I_o / (\Omega_i R^2) \qquad (1)$$

where I_o is the illuminating intensity (watt/cm^2) at A_i and τ is the wavelength dependent transmission through a distance x of the flame.

The intensity at the receiver from element dx is

$$dI_{scatt} = (\tau\, n\, Q_{scatt}\, A_p\, \Omega_i\, R^2 dx)\; I_x\; (A_r/4\pi R^2)\; (1/A_r)$$

where n is the number density of scattering particles, A_p the average particle area, and Q_{scatt} the scattering efficiency of the average particle. The first factor times I_x represents the optical power scattered back toward the receiver. The $(A_r/4\pi R^2)$ factor gives the fraction scattered into the receiver aperture (assuming equal scattering in all directions), and the last factor converts power into an intensity at the receiver. We also assume that R is much greater than L.

The total intensity of the scattered light at the receiver is then given by

$$I_{scatt} = [A_i A_p\, N\, Q_{scatt}\, I_o/(4\pi R^2)] \int_0^L \tau^2\, dx$$

FIG. 61 BACKSCATTERED ILLUMINATION

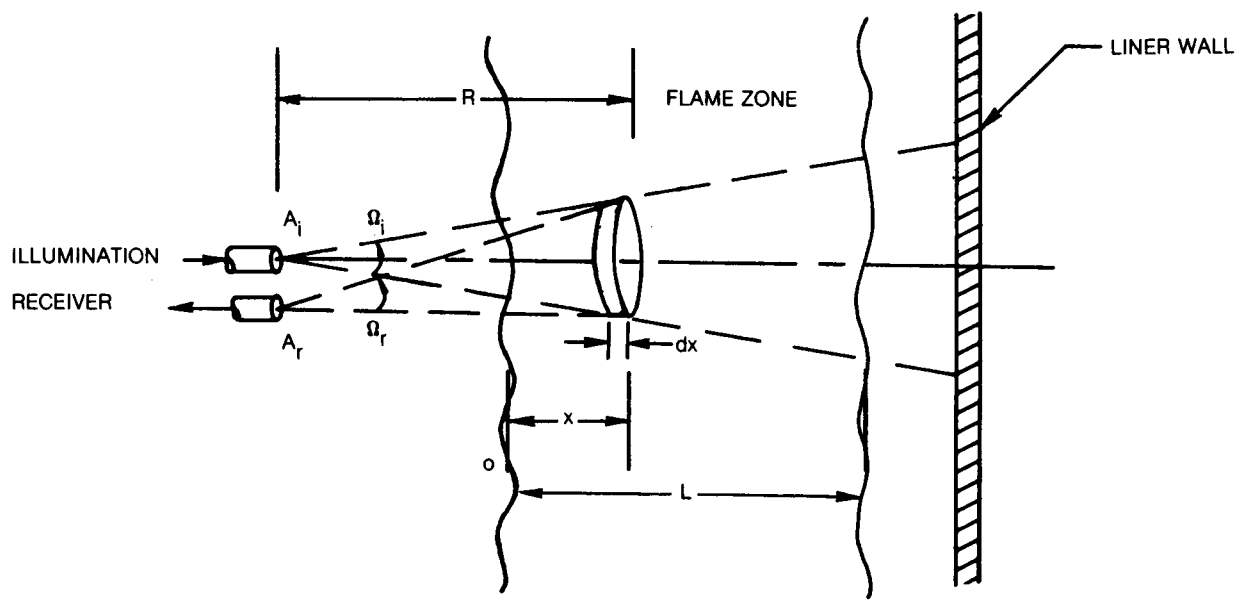

84–7–78–42

The transmission function τ is given by

$$\tau = \exp\ (-n\ Q_{ext}\ A_p\ x)$$

where Q_{ext} is the extinction efficiency.

The integral from o to L of the function τ^2

$$\int_o^L \tau^2\ dx = (1-\tau^2)/(2nQ_{ext}A_p)$$

where we redefine τ to be taken over the flame zone path L

$$\tau = \exp\ (-nQ_{ext}A_pL)$$

We thus have,

$$I_{scatt} = (\Omega_i'/8\pi)\ (Q_{scatt}/Q_{ext})\ (1-\tau^2)\ I_o$$

where $\Omega_i' = A_i/R^2$

To compute the illumination light intensity reflected from the liner wall and picked up at the receiver we refer to Fig. 62. In this case the illumination power at the liner wall is given by the product $I_o\ A_i\ \tau$. The illumination power is reflected at the wall that has a reflectivity coefficient r. We take the reflection to be Lambertian, that is diffuse and obeying the cosine law. Therefore, the fraction reflected towards the receiver (approx. at right angles to the reflecting wall) would be given by the factor $(A_r/\pi R^2)$. Again we divide by the area of the receiver to convert back to intensity to get the final result

$$I_{refl} = (\Omega_i'/\pi)\ r\ \tau^2\ I_o$$

FIG. 62 ILLUMINATION REFLECTED FROM LINER WALL

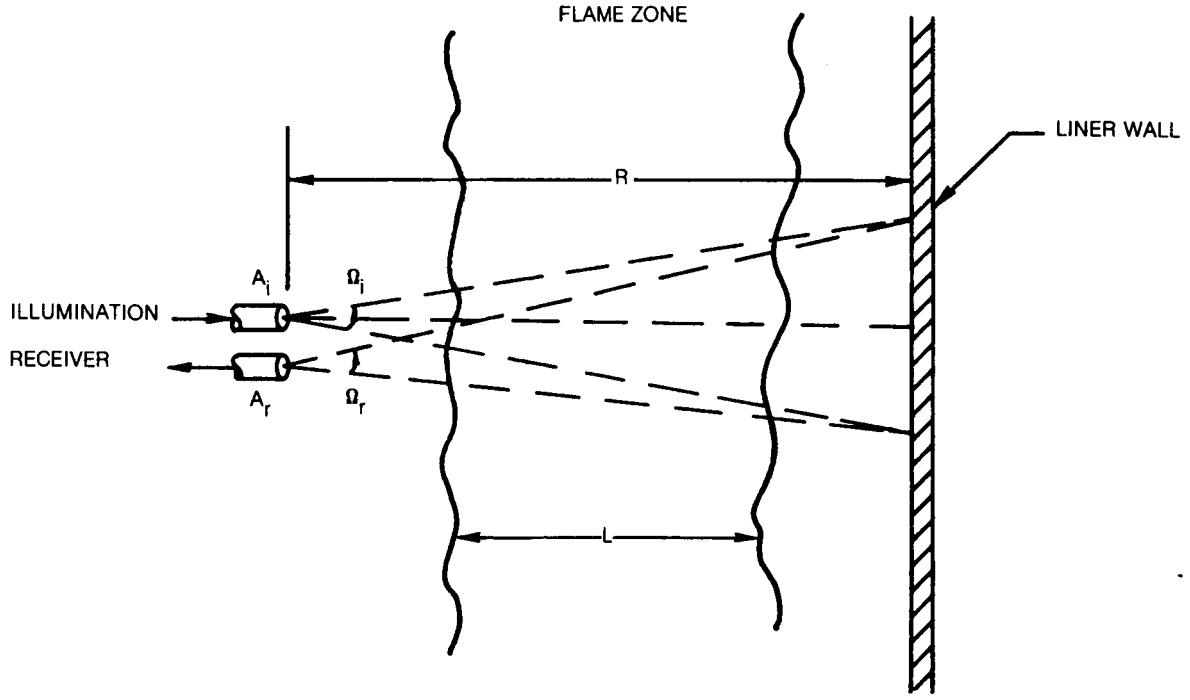

84-7-78-43

APPENDIX 2

Derivation for flame light intensity at the receiver aperture.

The transmission function of an optical signal through the flame is given by τ as defined in Appendix 1. The loss in the optical signal would be $1-\tau$. If practically all this loss is due to absorption then the emissivity of the radiating flame is also approximately $1-\tau$. If the temperature of the flame (i.e., luminous particles) is given by T_F, then the flame radiation at the receiver can simply be represented by

$$I_f = \Omega_r \, (1-\tau) \, N(T_F) \, \Delta\lambda$$

where $N(T_F)$ is the blackbody radiance function at temperature T_F in watts/ (cm^2 • Ster • nm) and is given by Planck's law. Using Wein's approximation for Planck's law (valid in our wavelength range)

$$N(T) = (C_1/\lambda^5) \exp \left[(-c_2/(\lambda T)\right]$$

The wavelength passband of the system in nm is given by $\Delta\lambda$.

REFERENCES

1. McCord, R. M.: Fiber Optic Probes Monitor Engine Condition. Mech. Eng., pp. 36-40, January 1981.

2. Drinkuth, W., W. G. Alwang, and R. House: Laser Proximity Probes for the Measurement of Turbine Blade Tip Running Clearances. ISA ASI 74228 (130-140), 1974.

3. Atkinson, W. H., R. R. Strange: Pyrometer Temperature Measurements in the Presence of Reflected Radiation. ASME Publication 76-HT-74.

4. Morey, W. W.: Investigation of Combustion Process Using Fiber Optics. Final Technical Report R81-925172-4, for Naval Air Systems Command, Contract N00019-80-C-0331, 14 June 1981.

5. Morey, W. W.: Investigation of Combustion Process Using Fiber Optics. Final Technical Report R83-926083-5, for Naval Air Systems Command, Contract N00019-82-C-0131, 21 December 1983.

6. Kapany, N. S.: Fiber Optics, Principles and Applications, Academic Press, N.Y., N.Y., 1967.

7. Ed Niester, Phase R Co., Durham, N.H., Private Communication.

8. A. Coppalle and P. Vervisch, The Total Emissivities of High-Temperature Flames, Comb. and Flame, 49 101-108 (1983).

9. F. Kreith, Principles of Heat Transfer, 2nd ed., Chap. 9, International Textbook Co., Scranton, PA.

10. Copper and Copper Alloy data from AMAX Copper, Inc., 1270 Avenue of the Americas N.Y., N.Y.

11. Discussions with W. Drinkuth and G. Smith of Pratt & Whitney Aircraft.

12. H. H. Barrett, A. F. Garritro, M. Y. Chiu, "Use of an Image Orthicon as an Array of Lock-in Amplifiers," Opt. Lett. 6, 1 (1981).

13. P. J. Foster, "Calculation of the Optical Properties of Dispersed Phases," Combust. Flame 7, 277 (1963).

14. W. H. Dalzell and A. F. Sarofim, "Optical Constants of Soot and their Application to Heat-Flux Calculations," ASME Jour. of Heat Transfer p. 100, Feb. 1969.

REFERENCES (Cont'd)

15. J. J. Sangiovanni and A. S. Kesten, paper presented at the 2nd world Congress of Chem. Eng. Montreal, Oct. 1981.

16. G. D. Gilbert and J. C. Perrnicka, "Improvement of Underwater Visibility by Reduction of Backscatter with a Circular Polarization Technique," Appl. Opt. 6, 741 (1967).

17. Marilyn Levy, "Wide Latitude Photography," Photographic Science and Engineering Vol. 11, No. 1, Jan./Feb. 1967.

18. T. Peli and J. Linn, "Adaptive Filtering for Image Enhancement," Optical Engineering Vol. 21, No. 1 Jan./Feb. 1982, pp. 108.

1. Report No. NASA-CR 174773	2. Government Accession No.	3. Recipient's Catalog No.
4. Title and Subtitle HOT SECTION VIEWING SYSTEM		5. Report Date September 1984 6. Performing Organization Code
7. Author(s) William W. Morey		8. Performing Organization Report No. R84-925830-33 10. Work Unit No. 533-04-1A
9. Performing Organization Name and Address United Technologies Research Center Silver Lane East Hartford, CT 06108		11. Contract or Grant No. NAS3-23156 13. Type of Report and Period Covered Contractor Report
12. Sponsoring Agency Name and Address National Aeronautics and Space Adminstration Washington, DC 20546		14. Sponsoring Agency Code

15. Supplementary Notes

Project Manager, Frank G. Pollack, Research Sensor Technology Section,
NASA Lewis Research Center, Cleveland, Ohio

16. Abstract

This report covers the development and testing of a prototype combustor viewing system. The system allows one to see and record images from the inside of an operating gas turbine combustor. The program proceeded through planned phases of conceptual design, preliminary testing to resolve problem areas, prototype design and fabrication, and rig testing. Successful tests were completed with the viewing system in the laboratory, in a high pressure combustor rig, and on a Pratt & Whitney PW20307 jet engine. Both film and video recordings were made during the tests. Digital image analysis techniques were used to enhance images and bring out special effects. The use of pulsed laser illumination was also demonstrated as a means for observing liner surfaces in the presence of luminous flame.

17. Key Words (Suggested by Author(s))

Fiberscope
Combustor
Viewing System

19. Security Classif. (of this report)	20. Security Classif. (of this page)	21. No. of Pages	22. [illegible]
Unclassified	Unclassified		